NASA Technical Memorandum 87632

IMPLEMENTATION AND FLIGHT TESTS FOR THE DIGITAL INTEGRATED AUTOMATIC LANDING SYSTEM (DIALS)

Part 1 - Flight Software Equations, Flight Test Description, and Selected Flight Test Data

Richard M. Hueschen

JULY 1986

National Aeronautics and Space Administration

Langley Research Center
Hampton, Virginia 23665

IMPLEMENTATION AND FLIGHT TESTS FOR DIALS

INTRODUCTION

In the early 70's, LaRC's Terminal Configured Vehicle (TCV) program was formulated with an overall goal of improving the efficiency and capabilities of transport operations (ref. 1). A specific goal, in support of its broader objective, was to increase the capabilities of autoland systems. To achieve this goal, a research effort was begun to design, develop, and flight test an advanced autoland system which eventually became known as the Digital Integrated Landing System (DIALS). This is part one of a report which describes the implementation and flight tests and presents flight test data of the DIALS.

Prior to the design phase, guidelines were formulated to establish the general system architecture for the DIALS and to take advantage of emerging technologies. The first guideline was to design the system using direct-digital design methods. Such a design could be implemented in the digital flight computers (which were to be used in future aircraft) without having to transform the control laws into the digital or discrete domain as is necessary for analog designs. A second guideline was to design an integrated controls system using modern control theory methods as opposed to the classical design methods currently used by the industry. Modern control theory methods provide a means for designing multiple-input, multi-output systems whose control commands are coordinated to assist each other during a flight path maneuver. On the other hand, classical methods are restricted to single-input, single-output methods. A typical problem of classical designs is that the individual controls are not necessarily coordinated and can work against each other to reduce the overall closed-loop system stability and performance and to introduce unnecessary control activity. Another reason for using modern control methods was that these methods had evolved (over a period of 20 years or more) to a level where practical designs were considered to be achievable. However, a successful flight test of such a system had not been achieved. Thus the design, development, and successful flight test of a modern control design was necessary to establish this method as a useful tool for integrated control designs. The last guideline was to use the digital navigation signals of the Microwave Landing System (MLS) in the design rather than the analog signals of the current Instrument Landing System (ILS). The MLS, being developed by the Federal Aviation Administration (FAA), will provide signals with more accuracy and more volume coverage (ref. 2) than that provided by the ILS. Thus, the MLS was to be used to provide better performance and to allow for more flexibility in the final approach-to-landing path.

The design and development of DIALS is covered in references 3, 4, 5, and 6. The basic equations with a general discussion of the DIALS control modes and flight tests with some flight test data are presented in reference 7. The details of the implementation of the DIALS in the flight control computers are not included. Thus, part of this report is to provide the implementation details of the DIALS in the flight control computers and present a more comprehensive selection of the flight test data. Part two of the report presents the data from the last five flight tests of the DIALS (those free of major software errors) and specifies the differences in the software system from flight to flight and run to run.

In this part of the report a general description of the DIALS and the test vehicle will be given. Also, the sensor measurements that were used by DIALS will be described. A discussion of the equations implemented and the modifications of these, which were made during the flight hardware/software implementation process, follows.

Next, a description of the test procedures for a test run will be given. Finally, the results of the flight tests will be presented and discussed followed by some concluding remarks.

SYMBOLS LIST

Measurements

1. Sensors for Control System

ϕ	roll attitude, rad
θ	pitch attitude, rad
ψ_T	yaw or true heading, rad
f_x	body-mounted acceleration specific force along x-body axis, ft/sec
f_y	body-mounted acceleration specific force along y-body axis, ft/sec
f_z	body-mounted acceleration specific force along z-body axis, ft/sec
p	roll rate about aircraft x-body axis, rad/sec
q	pitch rate about aircraft y-body axis, rad/sec
r	yaw rate about aircraft z-body axis, rad/sec
EPR1	engine pressure ratio of the number 1 engine
EPR2	engine pressure ratio of the number 2 engine
h_B	barometric altitude, ft
h_R	radar altitude, ft
$\dot{h}_B$	barometric altitude rate, ft/sec
Th_{RF}	position of the right forward throttle, deg
Th_{LF}	position of the left forward throttle, deg
s	stabilizer position, rad
δ_{es}	elevator servo position, rad
δ_{a_A}	right aileron servo position, rad
δ_{a_B}	left aileron servo position, rad
$\delta_{a_{trim}}$	aileron trim position, rad

Az	MLS azimuth angle, deg
$E\ell$	MLS elevation angle, deg
R_m	MLS range, ft
V_a	calibrated airspeed, ft/sec
δ_R	rudder servo position, rad
$\delta_{R_{trim}}$	rudder trim position, rad

2. Processed

a_{xb}	acceleration along the x-body axis, ft/sec^2
a_{zb}	acceleration along the z-body axis, ft/sec^2
a_{xs}	acceleration along the x-stability axis, ft/sec^2
a_{zs}	acceleration along the z-stability axis, ft/sec^2
T	total thrust of both engines, Klbs
HBC	adjustment term to account for mean-sea-level attitude of runway and the Earth's curvature, ft
x_{cg}	x-coordinate of the aircraft c.g. in the MLS coordinate frame, ft
y_{cg}	y-coordinate of the aircraft c.g. in the MLS coordinate frame, ft
z_{cg}	z-coordinate of the aircraft c.g. in the MLS coordinate frame, ft
$\dot{h}_{CF}$	vertical velocity estimate from the second-order complementary filter or test vehicle, ft/sec
$\dot{h}_{MLS}$	vertical velocity estimate from the third order complementary filter of test vehicle (see appendix B), ft/sec
$x_{E\ell}$	x-ciirdubate if MLS ground elevation antenna in MLS coordinate frame, ft
$y_{E\ell}$	y-ciirdubate if MLS ground elevation antenna in MLS coordinate frame, ft
$z_{E\ell}$	z-ciirdubate if MLS ground elevation antenna in MLS coordinate frame, ft
x_{DME}	x-coordinate of MLS ground DME antenna in the MLS coordinate frame, ft
y_{DME}	y-coordinate of MLS ground DME antenna in the MLS coordinate frame, ft
z_{hR}	z-MLS coordinate computed from radar altitude measurement, ft

3. Constants

h_{R1} constant to incorporate the radar altimeter measurement into MLS processing, non-dimenional

x_{GPIP} x-coordinate of glidepath intercept point in the runway coordinate frame, ft

H_{TDC} distance from aircraft center-of-gravity to bottom of main landing gear wheels with gear struts extended, ft

2KN2 constant to account for Earth's curvature, 1/ft

KZO constant for mean-sea-level atitude of runway, ft

UOI constant equal to 1 divided by desired calibrated airspeed, sec/ft

R_o MLS range measurement processing constant, ft

R_c length of MLS c-band antenna cable to MLS receiver, ft

$\psi_{R/W}$ true heading of runway, rad

4. Additional Sensors and Variables for Plotting and Data Analysis

a_n specific force of normal accelerometer equal to the negative of f_z, ft/sec^2

a_x measured specific force of longitudinal accelerometer equal to f_x, ft/sec^2

EPR average of the engine pressure ratio measurements from each engine (EPR1 and EPR2), non-dimensional

β measured aerodynamic sideslip, deg

δ_e elevator surface position relative to stabilizer chord plane, deg

δ_{th} the average of the left and right forward flight deck throttle positions (Th_{RF} and Th_{LF}), deg

$\delta_{Th_{EST}}$ estimate of the throttle position equal to $z_{L8} + Th_o$, deg

$\delta_{Th_{AFT}}$ the measured position of the aft flight deck throttle position, deg

Δh the estimated altitude deviation from the desired glideslope equal to the negative of $e_{Lx6}U_o$, ft

Δy estimated distance from runway centerline equal to x_6U_o, ft

$\Delta\psi$ yaw deviation from runway centerline equal to $\psi_T - \psi_{R/W}$, deg

$\Delta\psi_{EST}$ estimated yaw deviation from runway centerline equal to $x_2(57.3)$, deg

$\Delta\psi_{TK}$ aircraft ground track angle deviation from runway centerline equal to measured track angle from inertial navigation system minus $\phi_{R/W}$, deg

Filter Variables and Parameters

1. Longitudinal

b_{L31} constant gain on elevator servo position for vertical acceleration innovation, 1/sec

$f_{Lx_{ij}}$ the i^{th} row j^{th} column filter gain element for the aircraft state estimation

x_{L1} perturbed pitch estimate, rad

x_{L2} perturbed normalized inertial speed component along the the x-stability axis, non-dimensional

x_{L3} perturbed inertial alpha, rad

x_{L4} perturbed pitch rate, rad/sec

x_{L5} normalized inertial runway x-axis component, sec

x_{L6} normalized inertial runway z-axis component, sec

x_{L7} perturbed thrust, Klbs

x_{L8} perturbed throttle position, deg

x_{L9} perturbed stabilizer position, rad

$f_{LW_{ij}}$ the i^{th} row j^{th} column filter gain element for wind state estimation

w_{L1} normalized wind gust component along the z-body axis, non-dimensional

w_{L2} wind gust state, non-dimensional

w_{L3} wind gust state, non-dimensional

w_{L4} normalized wind gust compinent along the x-body axis, non-dimensional

w_{L5} normalized steady state wind along the x-body axis, non-dimensional

w_{L6} normalized steady state wind along the z-body axis, non-dimensional

w_{L7} normalized shear wind component along the x-body axis, sec^{-1}

ν_{L1} pitch innovation, rad

ν_{L3} x position innovation, sec

ν_{L4} z position innovation, sec

ν_{L5} barometric altitude innovation, sec

ν_{L6} vertical velocity innovation, non-dimensional

ν_{L7} vertical acceleration innovation, sec^{-1}

ν_{L8} airspeed innovation, non-dimensional

ν_{L9} longitudinal acceleration innovation, sec^{-1}

y_{L1} incremental pitch measurement, rad

y_{L2} pitch rate measurement, rad/sec

y_{L3} measured x distance from the GPIP normalized by U_o, sec

y_{L4} MLS measured z distance above the touchdown point normalized by U_o, sec

y_{L5} barometric altitude measured z distance above the touchdown point normalized by U_o, sec

y_{L6} processed vertical velocity measurement normalized by U_o, non-dimensional

y_{L7} processed acceleration measurement along the z-stability axis normalized by U_o, sec^{-1}

y_{L8} processed calibrated airspeed measurement normalized by U_o, non-dimensional

y_{L9} acceleration measurement along the x-stability axis normalized by U_o, sec^{-1}

2. Lateral

b_{31} constant gain aileron servo position for lateral acceleration inovation, 1/sec

ν_1 roll innovation, rad

ν_2 yaw innovation, rad

ν_5 y position innovation, sec

ν_6 lateral acceleration innovation, sec^{-1}

y_1 measured roll attitude, rad

y_2 measured yaw from runway heading, rad

y_5 measured y distance from runway centerline, sec

y_6 processed lateral acceleration measurement, sec^{-1}

x_1 estimated roll attitude, rad

x_2 estimated yaw attitude from runway heading, rad

x_3 estimated inertial sideslip, non-dimensional

x_4 estimated roll rate about the x-stability axis, rad/sec

x_5 estimated roll rate about the z-stability axis, rad/sec

x_6 estimated y distance from the runway centerline, sec

x_7 -measured perturbed rudder position, rad

$f_{x_{ij}}$ the i^{th} row j^{th} column filter gain for aircraft state estimation

w_1 estimated normalized gust component about the z-body axis, non-dimensional

w_2 gust state variable, sec^{-1}

w_3 estimated rotational gust component about the z-body axis, rad/sec

w_4 estimated rotational gust component about the x-body axis, rad/sec

w_5 normalized steady state wind along the y-body axis, non-dimensional

w_6 normalized shear wind along the y-body axis, sec

$f_{w_{ij}}$ the i^{th} row j^{th} column filter gain for wind state estimation

3. Euler Transformations

$\bar{\phi}$ estimated roll attitude, rad

$\bar{\theta}$ estimated pitch attitude, rad

$\bar{\psi}$ estimated yaw attitue from runway heading, rad

L_{EB} 3 × 3 Euler transformation matrix, body to Earth axis

$^1EB_{ij}$ the i^{th} row j^{th} column component of the L_{EB} matrix

L_{ES} 3 × 3 Euler transformation matrix, stability to Earth axis

$^1ES_{ij}$ the i^{th} row j^{th} column component of the L_{ES} matrix

4. General

F_x gain matrix for Kalman Filter aircraft states

F_w gain matrix for Kalman Filter wind states

$\hat{X}$ third-order complementary filter estimate of the x-coordinate in the MLS frame, ft

$\hat{Y}$ third-order complementary filter estimate of the y-coordinate in the MLS frame, ft

$\hat{Z}$ third-order complementary filter estimate of the z-coordinate in the MLS frame, ft

α_c, β_c constants for alpha-beta filters used to smooth aircraft rotational body rates, nondimensional

Guidance and Control Variables and Parameters

1. Longitudinal

q_k counter variable for the flare airspeed command easy-on

Δq_k incremental change per iteration of the counter variable for flare airspeed command easy-on

EZ5 flare airspeed command easy-on value, non-dimensional

Δv_F perturbed airspeed command for flare, non-dimensional

EZ3 flare gain increase easy-on value, non-dimensional

h_{Lxf_3} constant flare gain increase factor on inertial alpha or normalized velocity along the z-stability axis

h_{Lxf_4} constant flare gain increase factor on vertical position error

h_{Lxf_6} constant flare gain increase factor on vertical position error

x_a flare x distance argument, sec

$T_{\gamma D}$ tangent of the instantaneous flare flight path angle

h'' desired vertical acceleration along flare trajectory, sec^{-1}

h''' derivative of h'', sec^{-2}

z_e desired perturbed altitude from the glideslope, sec

z_{L1} desired perturbed pitch attitude, rad

z_{L2} desired perturbed inertial speed along the x-stability axis, non-dimensional

z_{L3} desired perturbed inertial alpha, non-dimensional

z_{L4} desired perturbed pitchrate, rad/sec

z_{L6} desired perturbed altitude from the nominal glideslope path (positive down), sec

$\dot{\bar{x}}$ desired perturbed inertial velocity along runway centerline (positive in direction of landing), non-dimensional

η_{L1} command pitch rate due to cross-coupling and second order effects, rad/sec

η_{L2} commanded acceleration along the x-stability axis due to cross-coupling and second order effects, sec^{-1}

η_{L3} commanded acceleration along the z-stability axis, due to cross-coupling and second order effects, sec^{-1}

η_{L5} predicted velocity along runway centerline, non-dimensional

η_{L6} commanded velocity along z-stability axis due to cross-coupling and second order effects and predicted velocity, sec^{-1}

ζ_{L1} commanded pitch rate due to trajectory changes, rad/sec

ζ_{L2} commanded acceleration along x-stability axis due to trajectory changes, sec^{-1}

ζ_{L3} commanded vertical acceleration due to trajectory changes, sec^{-1}

ζ_{L4} -commanded pitch acceleration due to trajectory changes, sec^{-1}

ζ_{L6} commanded vertical velocity (positive down) due to trajectory changes, non-dimensional

EZ7 glideslope easy-on value for vertical velocity command

EZ4 glideslope easy-on value for gain increase

GF3 glideslope gain increase factor

e_{Lx1} error from desired pitch attitude, rad

e_{Lx2} error from desired inertial speed along x-stability axis, non-dimensional

e_{Lx3} error from desired inertial angle of attack, rad

e_{Lx4} error from desired pitchrate, rad/sec

e_{Lx6} vertical position error from desired trajectory (positive down), sec

e_{Lx7} error from trim thrust, K lbs

e_{Lx8} error from trim throttle position, deg

e_{Lx9} error from trim stabilizer position, deg

z_{INT} integral of the vertical error, e_{Lx6}, sec^2

h_{Lxij} feedback gain for the i^{th} control and the j^{th} error signal

h_{Lwij} feedback gain for the i^{th} control and the j^{th} wind estimate component

h_{Lzij} feedback gain for the i^{th} control and the j^{th} desired path state

$h_{L\zeta ij}$ feedback gain for the i^{th} control and the j^{th} commanded rate error state

h_{zTi} feedback gain for the i^{th} control on the vertical path error integrator, z_{INT}

h_{zPi} feedback gain for the i^{th} control on the vertical gain programmed as a function of distance to touchdown

u_{cL1} elevator position command, rad

u_{cL2} stabilizer rate command, rad/sec

u_{cL3} throttle rate command, deg/sec

δ_{ec} elevator servo position command, deg

δ_{Thc} throttle servo rate command, deg/sec

h_f desired altitude to engage flare mode, ft

$h_{Lx3}(i)$ contains initial values of feedback gains, h_{Lxi3}, at start of flare for i = 1, 2, and 3

$h_{Lx4}(i)$ contains initial values of feedback gains, h_{Lxi4}, at start of flare for i = 1, 2, and 3

$h_{Lx6}(i)$ contains initial values of feedback gains, h_{Lxi6}, at start at flare for i = 1, 2, and 3

ΔV_{FR} rate of change of desired airspeed during flare, ft/sec^2

ΔV_{FD} change in desired airspeed per controls update cycle during flare, ft/sec

ΔV_{FL} maximum allowed change to airspeed command during flare, ft/sec

$h_{1/2P}$ 1/2 of the desired x-coordinate distance traveled during the vertical acceleration period during flare, sec

h_{FLR} normalized flare height constant ($HFLR_F/U_o$), sec

$HFLR_F$ selectable flare height trajectory constant, ft

$XFLR_F$ selectable x-coordinate distance from glidepath intercept point (GPIP) to desired touchdown point, ft

x_{FLR} normalized touchdown point distance ($XFLR_F/U_o$), sec

T_{γ_o} tangent of the desired glideslope angle, non-dimensional

$T_{\gamma_{TD}}$ constant equal to the tangent of the desired glideslope angle for touchdown of the final segment of the flare trajectory, non-dimensional

Δx_f a constant flare trajectory distance normalized by $u_o (h_{1/2P} - x_{FLR})$, sec

x_f flare trajectory distance parameter

$CWB_{11}, CWB_{14}, CWB_{15}, CWB_{16}$ constants used to compute desired inertial speed deviation from estimated winds

e_{x5} error in desired yaw rate about the z-stability axis, rad/sec

e_{x6} error in the desired position deviation perpendicular to the runway centerline, sec

e_{x7} rudder position deviation from trim, rad

y_{INT} integral of the error in desired position deviation perpendicular to the runway centerline, sec^2

G_y gain factor on error in desired position deviation perpendicular to runway centerline

ϕ_{INT} integral of the perturbed roll attitude, sec

ψ_{INT} integral of the perturbed yaw attitude, sec

$h_{x_{ij}}$ feedback gain for the i^{th} control and j^{th} error signal

$h_{w_{ij}}$ feedback gain for the i^{th} control and j^{th} estimated wind component

$h_{\zeta_{ij}}$ feedback gain for the i^{th} control and j^{th} command rate error state

$h_{y_{INTi}}$ feedback gain for the i^{th} control on lateral position error integrator

$h_{\phi_{INTi}}$ feedback gain for the i^{th} control on the roll integrator

$h_{\psi_{INT_i}}$ feedback gain for the i^{th} control on the yaw integrator

u_{c1} aileron position command, rad

u_{c2} rudder rate command, rad/sec

δ_{ac} aileron servo position command, deg

$\dot{\delta}_{RC}$ rudder servo rate command, deg/sec

δ_{RC} rudder servo position command, deg

h_{DC} desired altitude to engage decrab mode, ft

DECRAB logical to indicate if decrab mode is engaged

A_{ez} constant gain for decrab easy-on factor EZ1

A_ϕ constant gain factor on desired roll-rate command

$A\psi$ constant gain factor on desired yaw-rate command

a_{xij} constants gains to compute desired rate of change of the i^{th} desired trajectory parameter, ζ_{zi}, from the j^{th} trajectory parameters, z_j

J_{LGN} logical to indicate if localize track mode is engaged

d_{31}, d_{41}, d_{51} constant gains used in computation of desired lateral path trajectory parameters due to wind disturbances

h_{F6} upper limit of localizer gain factor, G_{y_k}

JPHINT logical to indiate if roll integrator is engaged

ϕ_{Lim} maximum commanded bank angle during decrab, rad

α_a constant filter gain for aileron command

u_{imin} mainimum value of i lateral command

u_{imax} maximum value of i lateral command

A1,A2,A3 hysteresis constants used in computation of aileron command

3. General

C_x output aircraft state prediction matrix

C_w output wind state prediction matrix

Γ discrete control transition matrix

H_x feedback gain matrix for aircraft states

H_w feedback gain matrix for wind states

H_z feedback gain matrix for trajectory states

H_ζ feedback gain matrix for prediction states

e_k aircraft state error vector

SWTC one-half second easy-on factor used to turn on elevator or aileron command at glideslope capture or localizer capture

ΔT constant equal to the increment of time between discrete equation updates, sec

Prediction Variables

1. Longitudinal

$\hat{x}_{Li}$ predicted value of the i^{th} state component

ϕ_{Lij} constants used to compute the i^{th} predicted longitudinal aircraft state from the j^{th} estimated aircraft state, x_{Lj}

γ_{Lij} element of the i^{th} row, j^{th} column of the control transition matrix for predicted aircraft state update

γ_{Lwij} element of the i^{th} row, j^{th} column of the wind transition matrix for the predicted aircraft state update

ψ_{Lij} constants used to compute the i^{th} predicted longitudinal aircraft state form the j^{th} cross-coupling and second-order command terms, η_{ij}

$\hat{w}_{Li}$ predicted value of the i^{th} wind state component

$\phi_{Lw_{ij}}$ element of the i^{th} row, j^{th} column of the wind state transition matrix

$\hat{b}_{L1}$ estimate of bias in the barometric altitude measurement, sec

$\hat{b}_{L5}$ estimate of bias in the barometric altitude measurement, sec

$\hat{b}_{L6}$ estimate of the bias in the vertical velocity measurement, non-dimensional

$\hat{b}_{L7}$ estimate of the bias in the normal accelerometer measurement, sec^{-1}

$\hat{b}_{L9}$ estimate of the bias in the longitudinal accelerometer measurement, sec^{-1}

$f_{Lb_{ij}}$ element of the i^{th} row, j^{th} column of the bias estimation matrix

$\hat{y}_{L6}$ predicted vertical velocity measurement, non-dimensional

$\hat{y}_{L7}$ predicted normal accelerometer measurement, sec^{-1}

$\hat{y}_{L8}$ predicted calibrated airspeed measurement, non-dimensional

$\hat{y}_{L9}$ predicted longitudinal accelerometer measurement, sec^{-1}

c_{Lxij} constants used to compute the predicted i^{th} longitudinal measurement from the j predicted longitudinal aircraft state

c_{Lwij} constants used to compute the i^{th} predicted longitudinal measurement from the j^{th} predicted longitudinal wind state

2. Lateral

$\hat{x}_1$ predicted roll attitude, rad

$\hat{x}_2$ predicted yaw deviation from runway heading, rad

$\hat{x}_3$ predicted inertial sideslip, non-dimensional

$\hat{x}_4$ predicted roll rate, rad/sec

$\hat{x}_5$ predicted yaw rate, rad/sec

$\hat{x}_6$ predicted lateral position deviation from runway centerline, sec

$\hat{x}_7$ predicted rudder position from trim

ϕ_{ij} element of the i^{th} row, j^{th} column of the aircraft state transition matrix for the predicted aircraft state update

γ_{ij} element of the i^{th} row, j^{th} column of the control transition matrix for predicted aircraft state update

$\gamma_{w_{ij}}$ element of the i^{th} row, j^{th} column of the wind transition matrix for predicted aircraft state update

ψ_{ij} element of the i^{th} row, j^{th} column of the cross-coupling and second-order effects transition matrix for aircraft predicted state update

$\hat{w}_i$ the i^{th} predicted wind state

$\phi_{w_{ij}}$ element of the i^{th} row, j^{th} column of the wind state transition matrix

$\hat{b}_\phi$ estimated bias in the roll attitude measurement, rad

$\hat{b}_\psi$ estimated bias in the yaw attitude measurement, rad

$\hat{b}_{f_y}$ estimated bias in the lateral accelerometer measurement, sec^{-1}

g_ϕ gain for the roll bias estimate

g_ψ gain for the yaw bias estimate

g_{f_y} gain for the lateral accelerometer bias estimate

$\hat{y}_6$ predicted lateral position deviation from runway centerline, sec

$\hat{\eta}_{L6}$ predicted rate of change altitude due to nonlinear effects, nondimensional

$\bar{H}$ estimated altitude above the touchdown point, ft

$\hat{\beta}$ predicted sideslip parameter, non-dimensional

$\hat{\xi}$ predicted sideslip parameter, non-dimensional

c_{xij} command constants used to compute the predicted i^{th} lateral measurement from the j predicted aircraft lateral state

c_{wij} constants used to compute the i^{th} predicted lateral measurements from the j^{th} lateral predicted wind state

3. General

$\hat{\ell}_{ESij}$ the i j element computed from predicted attitudes $(\hat{\phi},\hat{\theta},\hat{\psi})$ of a matrix to transfer vectors from the stability axes to the Earth reference axes

$\hat{\phi}$ predicted roll attitude, rad

$\hat{\theta}$ predicted pitch attitude, rad

$\hat{\psi}$ predicted yaw deviation from runway centerline, rad

Initialization Parameters

U_o selected reference calibrated airspeed, ft/sec

WEITO aircraft empty fuel weight, lbs/10

γ_o selected glideslope angle, rad

α_o trim angle of attack, rad

θ_o trim pitch attitude, rad

T_o trim engine thrust, K lbs

Th_o trim throttle position, deg

s_o trim stabilizer position, rad

$HFLR_F$ height of flare path above selected touchdown point, ft

$XFLR_F$ distance of selected touchdown point from the glideslope intercept point, ft

$T_{\gamma TD}$ tangent of desired flight path angle at touchdown

h_f calculated desired flare altitude, sec

h'_{GSC} desired altitude to engage glideslope capture mode, sec^{-1}

a_{GSCi} constants used in the computation of h'_{GSC}

Pw_4 selectable constant having a value between 0 and 1 used for initializing predicted wind states w_{L4} and $\hat{w}_{L5}$

Y_{Loc} desired distance from runway centerline to engage localizer capture mode, sec^{-1}

TFQ total fuel quantity, lbs

$a_1, a_2, a_3, b_1, b_2, b_3,$ computed constants ued to determine trim inertial angle of attack, α_o, and trim thrust, T_o

u'_k perturbed inertial velcoity along x-stability axis computed during pre-capture, non-dimensional

β_{I_k} computed inertial sideslope used during pre-capture

α_k computed inertial angle of attack used during pre-capture

GENERAL DESCRIPTION OF SYSTEM AND TEST VEHICLE

The DIALS is a complete digital autoland system consisting of a longitudinal and a lateral control law. The form of each control law is essentially the same and thus the functional blocks shown in figure 1 represent both control laws. Each control law consists of a fixed gain fullstate Kalman filter which processess innovations--the differences between sensor measurements and predicted measurements. Each contains a guidance algorithm which calculates guidance errors from the Kalman filter estimates and desired flight path trajectory commands (e.g., desired glideslope angle, desired calibrated airspeed). Finally, both control laws have a control algorithm which computes the servo commands needed to drive the guidance errors to

zero. The commands of the longitudinal control algorithm are elevator position, δ_{ec}, stabilizer rate, $\dot{\delta}_{sc}$, and throttle rate, $\dot{\delta}_{Thc}$. The commands of the lateral control algorithm are aileron position, δ_{ac}, and rudder rate, $\dot{\delta}_{RC}$.

Each control law was designed independent of the other; but for the implementation some cross coupling of the variables was used for each control law in the processing of the innovations and the desired flight path trajectory commands to account for some second order effects (e.g., the effect of roll on lift).

Each control law has three control modes. Those of the longitudinal law are glideslope capture, glideslope track, and flare. These modes were designed to operate with standard and steeper glideslopes (the pilot selects a glideslope between 2.5 and 5.5 degrees prior to system engagement). The control modes for the lateral law were localizer capture, localizer track, and decrab. The localizer capture mode was designed to provide satisfactory capture for ground intercept track angles between 0 and 60 degrees of runway centerline.

The test vehicle, shown in figure 2, was a small twin-jet commercial-type aircraft (ref. 8). It was especially equipped for flight test research of advanced navigation, guidance, and control laws and advanced displays. The aircraft was equipped with an aft research cockpit slightly forward of midship, triplicate flight control computers, a navigation computer, a display computer to drive electronic attitude and map displays, triplex inertial navigation systems and central air data computers, triplex sensors for the primary control variables, and a data recording system which stored in excess of 200 variables on magnetic tape. Of these variables forty-eight were software selectable internal flight control computer variables. Also located within the vehicle were test stations to monitor the computers, displays, and recording systems during the flight experiment.

CONTROL SYSTEM IMPLEMENTATION

Sensor Measurements

A total of twenty-four sensor measurements were input to the control system. The longitudinal control system used seventeen of these measurements and the lateral used nine. Some signals were used in both systems. The signals input to the system were as follows:

Pitch (θ), roll (ϕ), and yaw (ψ_T) attitudes were obtained from the Inertial Navigation System (INS) gimballed platforms. The pitch and roll were taken directly from the synchro outputs of the INS and thus were actually, respectively, $\sin\theta$ and $\sin\phi$.

Roll rate (p), pitch rate (q), and yaw rate (r) were used from standard rate gyro's.

Specific forces in the aircraft body axes (f_x, f_y, f_z) were obtained from a set of 3 accelerometers mounted near the aircraft's center-of-gravity. The specific force along the x body axis, f_x, was from the longtudinal accelerometer, and the specific force along the y body axis, f_y was from the lateral accelerometer. The output of the normal accelerometer has its output biased so that it has a zero output for steady level flight. In other words, the one g of gravity acting on the accelerometer in level flight was biased out. This accelerometer also gives a positive output for acceleration upward. Thus in order to get a right-handed

coordinate frame of specific forces for rotation to other axes and to properly account for gravity in the rotations, one g was added to the normal accelerometer output and then the negative of that quantity was obtained to give specific force along the z body axis, f_z.

Engine pressure ratios from the right and left engines, EPR1 and EPR2, were obtained from synchro outputs of engine sensors.

Barometric altitude, h_B, altitude rate, $\dot{h}_B$, and calibrated airspeed, V_a, were obtained from the central air data computers (CADC).

Radio altitude, h_R, was input from the radio altimeter.

The elevator servo position, δ_{es}, was taken from the LVDT output of the elevator servo and the stabilizer position, s, was determined from the output of the trim potentiometer used for an autotrim algorithm of the test aircraft.

The left and right throttle positions (Th_{RF}, Th_{LF}) were from outputs of potentiometers mounted on the left and right throttle lever mechanisms.

The right aileron servo position, δ_{a_A}, was taken from the LVDT output of the "A" hydraulic system and the left aileron servo position, δ_{a_B}, was taken from the LVDT output of the "B" hydraulic system.

Three MLS signals--the elevation signal, El, the azimuth signal, Az, and the range or DME signal, R --were used as a position measurement. These signals were not input directly to the DIALS software. Instead, they were transformed to obtain x, y, and z components of a right-handed coordinate frame. These components were then input to the DIALS processing. The details of these transformations are given in appendix B.

For reasons which will be discussed later, filtered vertical velocity from the MLS processing software, $\dot{h}_{MLS}$ was made available to the DIALS software in place of $\dot{h}_B$ by a software switch. The MLS vertical velocity is the output of a third-order complementary filter (see appendix B) which is driven by the z component of the runway coordinate frame, mentioned above, and the vertical acceleration derived from the transformed body-mounted accelerometers.

Discussion of Implemented Equations

The DIALS system of equations (a modern multi-input, multi-output) control theory design) is a set of matrix equations plus the logical expressions required to engage and transition between the various control modes. For the computer simulations used during the DIALS design and development phase, these equations were implemented largely with matrix operation subroutines. However, for the flight test implementation, such an implementation was not possible due to flight computer limitations and real-time constraints. The flight computers were fixed-point 16-bit machines and were not suited to handle matrix operations efficiently. Thus, the matrix equations were broken down into individual element-by-element multiply and add operations. In addition, due to the fixed-point machine, variables were appropriately scaled to meet range and round-off error requirements--the method for determining round-off error requirements is discussed in reference 7.

The specific equations implemented are given in appendix A. The appendix also includes the scaling of the variables, a flow chart of the equations and logic, and tables specifying values of the constants that were used in the test flights. The general equations which summarize the calculations done within the flight control computers are given below and are written in vector and matrix form for conciseness. The calculations were executed once for the lateral control law and once for the longitudinal control law for each DIALS update cycle which was 0.1 seconds. The general equations are:

Measurement Innovation Computations

$$\nu_k = y_k - \hat{y}_k$$

where y_k is a processed measurement vector, $\hat{y}_k$ is a predicted measurement vector, and ν_k is an innovation vector.

Steady-State Kalman Filter Computations

$$x_k = \hat{x}_k + F_x \nu_k$$

$$w_k = \hat{w}_k + F_w \nu_k$$

$$L_{ES} = L_{EB} L_{BS}$$

where x_k and $\hat{x}_k$ are respectively the estimated and predicted aircraft state vectors, w_k and $\hat{w}_k$ are respectively the estimated and predicted wind state vectors, F_x and F_w are constant matrices, L_{ES} is the aircraft stability axis to earth axis (runway frame) transformation matrix, L_{EB} is the aircraft body axis to earth axis transformation matrix, and L_{BS} the aircraft stability axis to aircraft body axis transformation matrix.

Guidance Variables Computations

$$z_k = \phi_z z_{k-1} + \zeta_{k-1}$$

$$\zeta_k = f(x,z)$$

$$\eta_k = f(x)$$

$$e_k = x_k - z_k$$

where z_k and ζ_k are desired path command vectors, ϕ_z is a matrix with time varying terms, η_k is a vector containing non-linear second-order cross-coupling effects, and e_k is the trajectory error vector.

Control Law Command Computations

$$u_k = -H_x e_k - H_w w_k - H_z z_k - H_\zeta (\zeta_k - \eta_k) + \text{added terms}$$

where u_k is the control command vector; the added terms are integrator feedback and flare trajectory terms, and H_x, H_w, H_z and H_ζ are matrices.

Prediction Computations

$$\hat{x}_{k+1} = \phi x_k + \Gamma u_k + \Gamma_w w_k + \psi \eta_k$$

$$\hat{w}_{k+1} = \phi_w w_k$$

$$\hat{b}_{k+1} = \hat{b}_k + F_b \nu_k$$

$$\hat{y}_{k+1} = C_x \hat{x}_{k+1} + C_w \hat{w}_{k+1} \hat{b}_{k+1}$$

where $\hat{x}_k$ and $\hat{w}_k$ are respectively the predicted aircraft state and wind vectors, $\hat{b}_k$ is a vector of measurement bias estimates, and ϕ, Γ, Γ_w, Ψ, ϕ_w, F_b, C_x, and C_w are matrices.

All the DIALS equations were executed during two major frames within the flight computers--filtering and control commands in one frame and aircraft state and measurement predictions in the other. The DIALS was designed to be updated every 100 msec whereas the time for one major flight computer frame was 49.152 msec or 98.304 msec for two major frames. The effects of this time difference from the design time is small and is discussed in reference 7.

Control Law Implementation Modifications

Most of the modifications of the control law required for flight testing and those made to improve performance were accomplished in nonlinear batch simulations which were good representations of the test aircraft, engine dynamics, and control servos. However, one significant modification was made during ground testing of the flight software and another of less significance was made during flight testing. During real-time simulation ground testing in the Experimental Avionics System Integration Laboratory (EASILY), the elevator and servo commands were modified to

make the system insensitive to transport delays encountered in the EASILY. Tests showed that some signals had an average delay of 100 msec with peak delays reaching 200 msec. The delays arose because the digital flight control computers and digital aircraft simulation computer operated asynchronously and could not be synchronized. Although the maximum transport delays on the aircraft were only expected to be 30 msec, the control laws were modified to make them insensitive to 100 msec delays. The insensitivity was achieved by a simple modification of the original elevator and aileron control commands while maintaining system stability (see ref. 7 for analysis) as follows:

$$\delta_{c_k} = \alpha\, \delta_{c_{k-1}} + u_c$$

where u_c is the original unmodified command, $\delta_{c_{k-1}}$ is the previous modified command, δ_{c_k} the current modified command and α is a constant ($\alpha = 0.24758$ for the elevator command and $\alpha = 0.170355$ for the aileron command used for all test flights).

The modification made during flight testing was to replace the barometric sink rate signal (vertical velocity) from the central air data computer with an estimate of vertical velocity from a third-order complementary filter (see appendix B). The modification was necessary because of the poor signal quality of the measured barometric sink rate for the test flights. The peak errors reached 30-40 ft/sec which was at least an order of magnitude higher than that used for design of the DIALS Kalman filter. The noise design values were more appropriate for cruise configuration of the test aircraft. The noise on this signal increases dramatically when the aircraft is in a landing configuration (flaps and gear down) and particularly in turbulent wind conditions. Thus to avoid redesign of the Kalman filter, the barometric sink rate signal was simply replaced with the filtered vertical velocity signal after simulation tests showed satisfactory operation of DIALS with the filtered signal.

During the EASILY tests, second-order digital prefilters described in appendix C were implemented in the flight computers to filter the body-mounted accelerometer measurements. These were implemented to prevent aliasing. In the early EASILY tests, aliasing was considered as a possible contributor to the instabilities which later were found to be caused by the transport delays. However, the prefilters were left in the flight computers and were available upon activation of a software switch. They were activated on one test run which will be discussed later.

First-order low-pass software-selectable digital filters were also coded to remove noise from the body rate measurements during the EASILY tests. However, the filters were not used in the flight tests since the EASILY tests showed that the filters caused a performance degradation after the modification for the transport delay was implemented.

On one run of a flight test, several gains were set to zero in the longitudinal control law. This test was made to verify simulation tests showing that zeroing the gains would not affect performance. The zeroing of the gains would result in elimination of several multiply and add operations reducing code and real-time requirements. These tests supported efforts to develop a "simplified" version of the DIALS.

FLIGHT TEST DESCRIPTION

The flight tests were conducted at Wallops Flight Center (WFC) on Runway 22 (the runway which has an MLS installation). Prior to a DIALS test run, the aircraft first proceeded to a calibration test point on Runway 22 (test point No. 12, 1000 ft from the stop end of Runway 22). The aircraft's vertical stabilizer, which had a laser tracking cube mounted on it, was positioned over this point to calibrate the WFC FPS-16 radar/laser tracking system. After calibration of the tracking system, the aircraft taxied to test point No. 74 for calibration and functional checks of the MLS. The aircraft's cockpit, which had the MLS C-band receiving antenna mounted above it, was positioned over this test point and the MLS signals were observed and recorded. The bias error on the MLS range or DME signal was computed and entered into the flight computer; then, on subsequent flight test runs, the bias was subtracted from the DME measurements. After the calibrations, the aircraft flew to the area to begin a DIALS test run. Upon arriving in the test area, the desired glideslope angle was entered into the flight computer (in a fully operational system the pilot would enter or select the desired glideslope). The pilot then positioned the aircraft at the desired flight level and ground track intercept angle specified for the test run using a velocity control-wheel-steering (VCWS) mode of the autopilot. (The general vertical and lateral path profiles for the flight tests are shown in fig. 3.) When the pilot achieved the desired flight level and ground track intercept angle, the pilot selected the desired reference calibrated airspeed for the landing on the mode control panel and, if not already engaged, engaged the calibrated airspeed hold mode. The desired ground track angle and flight level were then automatically maintained by the autopilot engaged in the VCWS made until engagement of the DIALS localizer and glideslope capture modes. After localizer and glideslope engagements, the aircraft flew to touchdown controlled automatically by the DIALS control laws. At touchdown, the system was automatically disengaged and the safety pilots then took control of the flight. The safety pilots then performed a nosewheel letdown and executed a touch-and-go in preparation for a subsequent test run.

FLIGHT TEST RESULTS

Selected time history plots of data from the test runs of the last five DIALS flights (R353, R355, R357, R361, and R364) will be presented in this section to show the performance of each of the control modes of the DIALS--localizer capture, localizer track, decrab, glideslope capture, glideslope track, and flare.

Localizer Capture

The DIALS begins the capture of the localizer (runway centerline) according to its capture criteria logic. The criteria is a function of the distance of the aircraft from the centerline (ΔY), aircraft true heading ($\Delta\psi$), track angle ($\Delta\psi_{TK}$), and estimated winds ($\hat{w}_5$). Localizer captures were performed in various wind conditions and track angles relative to the runway centerline. Figure 4 shows the capture performance for intercept angles from 20 degrees to 50 degrees which were performed on successive runs of test Flight R355. The data for deviation from runway centerline (Δy) shows that the capture overshoot increases with increasing intercept angles from no overshoot for a 20 degree intercept to about 50 feet for a 50 degree intercept. Figure 5 shows a 30 degree intercept angle capture approaching from the left side (facing runway) and figure 6 shows 30 degree intercept angle capture approaching from the right side, both in the presence of a 12 knot crosswind. The overshoot of the runway centerline is small in both cases and the yaw attitude (ψ) achieves the

proper crab angle in a smooth manner (without oscillation) which is attributed to the good estimation of the runway crosswinds.

Localizer Tracking

The localizer tracking mode maintains the aircraft on the runway centerline with the proper crab angle in crosswinds while holding the roll attitude at zero or wings level attitude. The plots of figure 5 illustrate the system's ability to maintain the above conditions and, in addition, show the response to a crosswind shear. The shear begins at 100 seconds into the run, and is characterized by the crosswind decreasing to zero over a small altitude distance (a shear wind of 8 knots/100 ft). A drift off runway centerline was induced by this shear of approximately 30 ft, but the aircraft was corrected back to centerline within 10 seconds after the shear stopped. The good tracking performance of the system in the presence of gust winds is illustrated in the plots of figure 7. In the period of 60 to 95 seconds, the crosswinds magnitude changed four times--each change of approximately 10 knots. The maximum excursion from centerline during these gust encounters was 30 ft.

Decrab

The function of the decrab mode is to align the aircraft's true heading to that of the runway in the presence of crosswinds by performing a sideslip maneuver. Examination of the roll angle, ϕ, and the heading or yaw angle relative to the runway, $\Delta\psi$, (see figs. 4(b), 4(c), and 4(d)) near the end of the runs illustrates the maneuver and the variable, Δy, shows the good tracking performance achieved during the maneuvers for crosswind magnitudes of 6 knots. For high crosswinds of 18 to 20 knots, the DIALS decrabed the aircraft, but limiting occurred on both the aircraft bank angle (limited to 5 degrees for safe clearance of engine pod and wing tip at touchdown) and the rudder position (see figs. 7(a) and 7(b)). The rudder limiting was set on the test vehicle as a function of dynamic pressure sensed in the elevator servo system to a value low enough to permit the safety pilots some remaining authority to override the automatic system commands.

Glideslope Capture

The objective of the glideslope capture mode was to capture the glideslope with low overshoot and low settling time for pilot-selected glideslopes between 2.5 to 5.5 degrees. The last test flight (R364) contained a series of four consecutive runs in which the glideslope was increased from 3 to 5 degrees. The flight test data for 3, 4, 4.5, and 5 degree glideslopes is shown, respectively, in figures 8, 9, 10, and 11. The winds for these runs were high. The steady headwind component was 10 to 12 knots and the steady crosswind component was 18 to 20 knots. In addition to the steady wind, rapidly changing gusts of 8 to 10 knots were encountered (e.g., see the airspeed, V_a, of fig. 8(a) at 110 to 120 seconds).

The start of the capture is shown in the figures when the DIALS elevator command, u_{cL1}, and throttle rate command, u_{cL3}, become active. The capture completion occurs essentially when the glideslope error, Δh, reaches zero for the first time. The capture time for all cases was less than 10 seconds and the maximum value of the first crossover of the glideslope error was 10 feet (see glideslope error, Δh, of figs. 8(b), 9(b), 10(b), and 11(b)).

In a non-gusty wind condition, the glideslope capture is normally initiated by a commanded reduction in throttle and a coordinated small positive commanded elevator deflection for pitchdown; however, in gusty conditions these control commands may change considerably due to the feedback of estimated winds and aircraft states to the control law. For example, note in figure 9, that there was no initial positive elevator deflection and that the throttle rate command became positive after a small initial negative value. In this case, the control law was adjusting for a decreasing headwind condition occurring during the capture (see V_a of fig. 9(a)).

The glideslope capture criteria was designed to adjust for different initial aircraft conditions. Figures 12 and 13 illustrate this adjustment capability. Figure 12 shows the capture of a 3 degree glideslope while the aircraft was descending (approximately 4 ft/sec). Since the throttle was at the position required for the 3 degree glideslope tracking, the control did not command a throttle decrease. Only a small initial positive elevator command was required to initiate the capture which was completed smoothly without overshoot. Figure 13 shows a 4.5 degree glideslope capture for the aircraft climbing (approximately 12 ft/sec) at capture initiation. For this case, a large throttle decrease was commanded along with a positive elevator command and, as before, the capture was completed smoothly with low overshoot.

Glideslope Tracking

The glideslope tracking mode maintains the aircraft along the selected glideslope while controlling the calibrated airspeed to the chosen reference speed. The DIALS achieves airspeed control indirectly by commanding a desired inertial speed which is computed by subtracting the estimated headwind from the selected reference airspeed. The control is illustrated in the plots of calibrated airspeed, V_a, and desired inertial speed, $U_o + z_{L2}$, of figure 11. At 73 seconds, a headwind gust occurs increasing the airspeed while, at the same time, the desired inertial speed begins to decrease. At 78 seconds, the throttle rate command responds to the decreasing desired inertial speed. Examination of the airspeed data in figures 8 through 11 shows that its nominal value was 4 to 5 knots above the reference speed (the middle value on the y-axis for airspeed, V_a, is the desired reference airspeed) with peak deviations from the nominal of $\pm$5 knots.

Glideslope tracking performance in wind gusts of 8 to 10 knots is shown in the plot of glideslope error, Δh, of figures 8 through 13. These plots can be compared to the plot of Δh in figure 14 which is typical of the glideslope performance for mild wind conditions. For the gusty wind conditions, the peak glideslope error deviations generally do not exceed 10 feet; but, in the data of figure 8, a peak glideslope error of 20 feet occurred around 90 seconds apparently due to strong vertical up and down wind gusts that began around 90 seconds. Note that at 80 seconds, the aircraft is rising above the glideslope while both controls are in a direction to reduce the glideslope error. The elevator is going positive to pitch the aircraft down while the throttle is reducing. The airspeed, V_a, does not show a signiicant increase at that point, but the normal acceleration signal, a_n, does show an upward acceleration indicating the presence of a vertical gust. Some sensitivity of the elevator command to certain gusts is shown in figure 8. At around 95 to 105 seconds, sharp headwind gusts were encountered (see V_a of fig. 8) which induced some oscillatory behaviour in the elevator command for 3 to 5 seconds.

For mild wind conditions (relatively steady winds and low frequency gusts), represented by the plots of figure 14, peak glideslope errors do not exceed 5 feet

(see the plot Δh). The wind conditions for the data of figure 14 consisted of a 6 knot headwind component and an initial 12-13 knot crosswind component which gradually reduced to zero at low altitude (350 to 400 feet). Note that, similar to the gusty wind conditions, the airspeed control for mild wind conditions also has about a 5 knot positive bias.

The glideslope performance may have been affected by a lag in the throttle response to the throttle command. The lag which was identified in the flight data but not included in the design or simulation development occurred between the forward throttles, which directly drive the engine fuel flow valves, and the aft throttles which drive the forward throttles. The aft throttles are driven by the integrated throttle rate command, u_{cL3}. An examination of $\delta_{th_{EST}}$ of figure 14(c), which is the average position of the forward throttles, and the aft throttle position, $\delta_{Th_{AFT}}$, shows lags between the respective peaks and valleys of this data. For some peaks and valleys, the lag can be characterized as a pure lag and for others it appears more like hysteresis. This lag can also be identified in figure 14(b) by examination of the throttle rate command, u_{CL3}, and the throttle position, δ_{Th}. At 120 seconds u_{CL3} is negative, but δ_{Th} does not move in the negative direction until at least a 1-second delay. The lag, in general, could be characterized as a one second lag. The slow oscilatory motion of the throttle in figure 14(b) ($\approx$20 second time period) may be due to this unmodeled lag. Simulation studies which could quantify the effects of the lag have not been performed.

The elevator activity before the DIALS glideslope capture (control by non-DIALS commands) and its activity immediately after capture appears to be about the same for the data of figures 8(b), 9(b), 10(b), 11(b), and 14(b) (see plot); but in the data of figures 12 and 13, more elevator activity occurs immediately after glideslope capture. Figures 12 and 13 represent data from an earlier flight (Flight R357, runs 7R and 8R) than the data of the figures discussed above. On the earlier flight, the gain on pitch rate feedback (h_{Lx14}) was -2.0 compared to -2.2 for the later flights. The lower gain may have caused increased elevator activity; but the possibility of an unintentional increase in the glideslope tracking gains by an erroneous easy-on function seems more likely to have caused the increased activity.

Flare

The general objective of the flare mode is to transition the aircraft from the selected glideslope condition, whether a standard or steep one, to an acceptable touchdown condition. The DIALS flare mode achieves this condition by following a flare path from the glideslope to a specified touchdown point (a selectable parameter) on the runway. Upon selection of the desired glideslope, flare path parameters are set to generate a desired vertical path profile (altitude versus distance) during the flare maneuver. During the maneuver, the flare control law commands the aircraft to pitch up to keep the nosewheel clear of the runway upon main gear touchdown; it also slowly commands a reduction in the airspeed rather than a reduction in the throttle as is done for existing flare laws.

The performance of the flare law for mild wind conditions is illustrated in the data plots of figure 14 which shows a flare from a 4.5 degree glideslope. The plots of pitch, θ, and vertical velocity, $\dot{h}_{MLS}$, show a smooth flare maneuver which was engaged at 180 seconds. At touchdown, the pitch attitude is a positive 2 degrees and the vertical velocity is -2 ft/sec while the deviation from the flare path, Δh, is nearly zero. The commanded reduction of airspeed during flare is achieved by

reducing the desired inertial speed, $U_o + z_{L2}$, and the resulting airspeed decrease can be seen in the plot of V_a.

The performance of the flare law for gusty wind conditions is partially illustrated by the plots of figures 8, 9, 10, and 11; these are partial results since no landings were made for the runs of these figures because of lateral drifting due to high crosswinds and rudder limiting. However, prior to the go-around maneuver, the flare control, executing the flare from different glideslope angles, had established a positive pitch attitude and reducing vertical velocity for each glideslope angle. A significant vertical deviation from the flare path is shown by the Δh plot of figure 8 which was induced in part by gusty conditions and in part by abnormal lateral control maneuvers due to the high cross winds and rudder limiting.

Ten completely "hands-off" automatic landings were performed during the flight tests. For these landings, the mean touchdown point was 1164 feet from the glideslope intercept point compared to a commanded value of 1300 feet (see ref. 7). The standard deviation from the mean touchdown point was 244 feet. The mean touchdown vertical velocity was 2.4 ft/sec with a standard deviation of 0.74 ft/sec. The commanded touchdown vertical velocity is a function of the ground speed which for a 125 knot ground speed is -2.2 ft/sec.

CONCLUDING REMARKS

The implementation of a modern control theory, direct-digital designed, full-state feedback autoland system on a 16-bit fixed-point flight computer was achieved and was successfully flight tested. The DIALS thus became the first modern control theory autoland design to be successfully flight tested on a small commercial type jet aircraft. The tests demonstrated that the methods used are a viable approach to the design of multiple-input multiple-output systems which can provide increased performance through the coordination of the multiple control commands. The system also demonstrated expanded capabilities over current systems. The expanded capabilities include the capture of glideslopes and localizers with lower overshoot and settling time, the capture of steeper glideslopes, and the ability to perform the flare maneuver from various glideslopes.

The DIALS achieved low overshoot captures (average value of 24 ft with standard deviation of 26 feet) of the runway centerline for capture angles of 20 degrees through 50 degrees. The aircraft was generally settled and tracking the runway centerline less than 40 seconds after capture initiation which is a factor of 3 less than current autoland systems.

The DIALS maintained small glideslope and localizer tracking errors for mild wind conditions--steady winds of 10 knots and gusts of 3 to 5 knots. For these winds, the glideslope and localizer errors did not exceed, respectively, ±5 feet and ±20 feet.

For gusty wind conditions, steady winds 20 to 25 knots and gusts 8 to 10 knots, glideslope and localizer tracking errors generally did not exceed, respectively, ±10 feet and ±30 feet. However, on some occasions, the longitudinal control law exhibited an oversensitivity to gust wind conditions resulting in oscillatory behavior. Pitch changes of 8 degrees within 5 seconds and glideslope errors of 20 feet occurred. Of course, the aircraft must make pitch changes, in the absence of direct-lift control, to tightly track the glideslope in gusty wind conditions. The pitch changes that did occur were in the right direction to correct the glideslope

errors, but appeared to be too large or, in other words, an over correction. Another factor that contributed to the pitch behavior in these gust conditions was a significant lag of approximately one second in the response of the throttle to a command which was not accounted for in the system design nor in non-linear simulation development.

The DIALS performed successful decrab maneuvers in crosswinds up to 6 knots. Decrab maneuvers in crosswinds of 18 to 20 knots were performed but lateral drifting occurred due to rudder and bank angle limiting. (Rudder limiting occured at approximately 10 degrees for approach condition on the research system to permit safety pilot override.) Crosswinds between 6 and 18 knots were not encountered in the tests.

The longitudinal capture criteria and capture control mode demonstrated an insensitivity to initial conditions and the selected glideslope angle. Various glideslopes--3 degrees to 5 degrees--were successfully captured with low overshoot (typically less than 5 feet) without system gain changes from descending, level, and climbing initial flight conditions.

The flare mode successfully flared the aircraft from 3, 4, 4.5, and 5 degree glideslopes with automatic landings resulting for 3 and 4.5 degree glideslopes. Successful landings for the other glideslope angles would have been achieved (pitch attitude and vertical touchdown velocity were acceptable), but due to lateral drift in high crosswinds, go-around maneuvers were executed.

In general, the flight tests demonstrated that each of the six control modes successfully performed its intended function. Improvements to the performance of each could most likely have been achieved given additional flight tests and data analysis time. For instance, no tests were performed for different flare trajectories; that is, different selectable trajectory parameters in the flare control law such as the desired touchdown point were not tested. No time was spent to fine tune these parameters to the aircraft from values set during the non-linear simulation development.

The implementation and flight tests of the DIALS illustrated the importance of accounting for system transport delays and lags. The transport delays encountered during the EASILY ground tests required a modification to the DIALS before the ground tests could be successfully completed. The modification may not have been required for the flight tests since the average transport delay on the aircraft was estimated to be a factor of 3 less than that measured in the EASILY tests. Thus, the message is that the ground test facility should have transport delays which are on the order of that of the flight system. The lags encountered between the aft throttle position and the forward throttle position, which were on the order of 1 second, may have contributed to some throttle instability, especially in gusty wind conditions. The message in this case which is not new, but which was illustrated in the data, is to make sure that all significant lags are accounted for in the design and particularly, in simulation testing and development.

REFERENCES

1. Reeder, J. P., Taylor, R. T., and Walsh, T. M., "New Designs and Operating Techniques for Improved Terminal Area Compatibility," SAE, Air Transportation Meeting, Dallas, Texas, April 30, 1974.

2. Anon., "A New Guidance System for Approach and Landing," Vol. 2, Radio Technical Commission for Aeronautics, 1717 H Street N.W., Washington, DC. Document DO-148, December 18, 1970.

3. Halyo, N., "Development of an Optimal Automatic Control Law and Filter Algorithm for Steep Glideslope Capture and Glideslope Tracking," NASA CR-2720, August 1976.

4. Halyo, N., "Development of a Digital Automatic Control Law for Steep Glideslope Capture and Flare," NASA CR-2834, June 1977.

5. Halyo, N., "Development of a Digital Guidance and Control Law for Steep Approach Automatic Landings Using Modern Control Techniques," NASA CR-3074, Feb. 1979.

6. Halyo, N., "Terminal Area Automatic Navigation, Guidance, and Control Research Using the Microwave Landing System (MLS), Part 5--Design and Development of a Digital Integrated Automatic Landing System (DIALS) for Steep Final Approach Using Modern Control Techniques," NASA CR-3681, April 1983.

7. Halyo, N., "Flight Tests of the Digital Integrated Automatic Landing System (DIALS)," NASA CR-3859, December 1984.

8. Staff of NASA Langley Research Center and Boeing Commercial Airplane Company, "Terminal configured Vehicle Program--Test Facilities Guide," NASA SP-435, 1980.

9. Pines, S., Schmidt, S. F., Mann, F., "Automated Landing, Rollout, and Turnoff Using MLS and Magnetic Cable Sensors", NASA CR-2907, October 1977.

APPENDIX A

DIALS SOFTWARE EQUATIONS 7 SYSTEM FLOWCHART

1. Software Equations

The following equations were implemented in the flight control computers of the test aircraft. For each equation and above each variable in the equation, there is the letter "B" followed by an integer number which specifies the scaling of the variable in the computer. For example, B-2 means that the maximum value of the variable is 2^{-2} or 0.25 or B6 means that the maximum value of the variable is 2^{6} or 64. From this scaling specification, the resolution of the variable can be found given that the computer was a 16-bit machine (one bit for sign). For the above examples the resolutions are, respectively, 0.25/32768 or 7.6294×10^{-6} and 64/32768 or 1.9531×10^{-3} ($2^{15} = 32768$). For some variables double precision was used and this is indicated by DP enclosed in parentheses following the scaling specification (e.g., B18 (DP). For this example, the maximum variable value is 2^{18} or 262144 and the resolution is $2^{18}/2^{31}$ or 1.2207×10^{-4}.

The values of the gains and constants used for runs 4, 6, and 7 of the last test flight are given in the last section of this appendix.

I. PRE-PROCESSOR EQUATIONS

A. Accelerations

$$\theta^{B-2} = \mathrm{ASIN}(\mathrm{SIN}\theta)^{B0}$$

$$\phi^{B0} = \mathrm{ASIN}(\mathrm{SIN}\phi)^{B0}$$

$$a_{xb}^{B6} = f_x^{B8} - g\sin(\theta - \hat{b}_{L1_k})^{B6\ B-2\ B-2}$$

$$a_{zb}^{B6} = f_z^{B8} + g\cos(\theta - \hat{b}_{\phi_k})\cos(\theta - \hat{b}_{L1_k})^{B6\ B0\ B0\ B-2\ B-2}$$

$$a_{zs}^{B6} = C_{\alpha_o}\, a_{xb}^{B0\ B6} + S_{\alpha_o}\, a_{zb}^{B0\ B6}$$

$$a_{zs}^{B6} = -S_{\alpha_o}\, a_{xb}^{B0\ B6} + C_{\alpha_o}\, a_{zb}^{B0\ B6}$$

B. Thrust Computations

$$T = \frac{(EPR1 + EPR2)}{2}^{B5} \; 26.7878^{B3} - 25.9395^{B5}, \quad 1000^{B8} \text{ lbs.}$$

II. FILTERING

A. Longitudinal Innovations

$$y_{L1_k} = \theta^{B-2} - \theta_o^{B-2}$$

$$\nu_{L1_k}^{B-2} = y_{L1_k}^{B-2(DP)} - \hat{x}_{L1_k}^{B-2(DP)} - \hat{b}_{L1_k}^{B-2(DP)} \quad \text{,rad}$$

$$x_{L4}^{B-1} = y_{L2_k}^{B-1} = q \quad \text{rad,sec}$$

$$y_{L3_k}^{B10} = (x_{GPIP}^{B25(DP)} - x_{cg}^{B18(DP)})/U_o^{B8}$$

$$\nu_{L3_k}^{B4} = y_{L3_k}^{B10(DP)} - \hat{x}_{L5_k}^{B10(DP)} \quad \text{,sec}$$

$$y_{L4_k}^{B6} = -(z_{cg}^{B18(DP)} + H_{TDC}^{B27(DP)})/U_o^{B8}$$

$$\nu_{L4_k}^{B4} = y_{L4_k}^{B6(DP)} - \hat{x}_{L6}^{B6(DP)} \quad \text{,sec}$$

$$y_{L5_k}^{B6} = (HBC^{B25(DP)} - h_B^{B16(DP)} - H_{TDC}^{B27(DP)})/U_o^{B8}$$

WHERE: $HBC = KZ0 + 2KN2(\hat{x}^2 + \hat{y}^2)$

B4 B6(DP) B6(DP) B4(DP)

$$\nu_{L5_k} = y_{L5_k} - \hat{x}_{L6_k} - b_{L5_k} \quad ,\text{sec}$$

B-2 B9 B-7 B0

$$y_{L6_k} = -(\dot{h}_B \text{ UOI} + \hat{n}_{L6_k}) \qquad \text{(See NOTE)}$$

B-2 B-2(DP) B-2(DP)

$$\nu_{L6_k} = y_{L6_k} - \hat{y}_{L6_k} \quad ,\text{non-dimensional}$$

B-2 B6 B-7 B0 102.4 mu/deg

$$y_{L7_k} = a_{zs} \text{ UOI} - b_{L31} \delta_{es_k}$$

NOTE: $\dot{h}_B$ may be replaced by $\dot{h}_{CF}$ or $\dot{h}_{MLS}$ by changing the selection index, HDSEL.

B-2 B-2 B-2

$$\nu_{L7_k} = y_{L7_k} - \hat{y}_{L7_k} \quad ,\text{sec}$$

B-1 B9 B-7 B-2 B0 B-1 B1 B-1

$$y_{L8_k} = \text{SQRT}[(V_a \text{ UOI})^2 - \hat{x}^2_{L3_k} - (\hat{x}_{3_k} + \beta_k)^2] - 1 - \hat{y}_{L8_k}$$

B-1 B-1(DP) B-1(DP)

$$\nu_{L8_k} = y_{L8_k} - \hat{y}_{L8_k} \quad ,\text{sec}^{-1}$$

B-2 B6 B-7

$$y_{L9_k} = a_{xs} \text{ UOI}$$

B-2 B-2(DP) B-2(DP)

$$\nu_{L9_k} = y_{L9_k} - \hat{y}_{L9_k} \quad ,\text{sec}^{-1}$$

B. Filtered Longitudinal State Vector

$$x_{L1_k}^{B-2} = \hat{x}_{L1_k}^{B-2} + f_{Lx_{11}}^{B0}\,\nu_{L1_k}^{B-2} + f_{Lx_{13}}^{B-6}\,\nu_{L3_k}^{B4}$$

$$+ f_{Lx_{14}}^{B-6}\,\nu_{L4_k}^{B4} + f_{Lx_{15}}^{B-6}\,\nu_{L5_k}^{B4} + f_{Lx_{16}}^{B0}\,\nu_{L6_k}^{B-2}$$

$$+ f_{Lx_{17}}^{B0}\,\nu_{L7_k}^{B-2} + f_{Lx_{18}}^{B-1}\,\nu_{L8_k}^{B-1} + f_{Lx_{19}}^{B0}\,\nu_{L9_k}^{B-2} \quad \text{,rad}$$

$$\bar{\theta}^{B-2} = x_{L1_k}^{B-2} + \theta_o^{B-2}$$

$$x_{L2_k}^{B-1} = \hat{x}_{L2_k}^{B-1} + f_{Lx_{21}}^{B1}\,\nu_{L1_k}^{B-2} + f_{Lx_{23}}^{B-5}\,\nu_{L3_k}^{B4}$$

$$+ f_{Lx_{24}}^{B-5}\,\nu_{L4_k}^{B4} + f_{Lx_{25}}^{B-5}\,\nu_{L5_k}^{B4} + f_{Lx_{26}}^{B1}\,\nu_{L6_k}^{B-2}$$

$$+ f_{Lx_{27}}^{B1}\,\nu_{L7_k}^{B-2} + f_{Lx_{28}}^{B0}\,\nu_{L8_k}^{B-1} + f_{Lx_{29}}^{B1}\,\nu_{L9_k}^{B-2} \quad \text{,non-dimensional}$$

$$x_{L3_k}^{B-2} = \hat{x}_{L3_k}^{B-2} + f_{Lx_{31}}^{B0}\,\nu_{L1_k}^{B-2} + f_{Lx_{33}}^{B-6}\,\nu_{L3_k}^{B4}$$

$$+ f_{Lx_{34}}^{B-6}\,\nu_{L4_k}^{B4} + f_{Lx_{35}}^{B-6}\,\nu_{L5_k}^{B4} + f_{Lx_{36}}^{B0}\,\nu_{L6_k}^{B-2}$$

$$+ f_{Lx_{37}}^{B0}\,\nu_{L7_k}^{B-2} + f_{Lx_{38}}^{B-1}\,\nu_{L8_k}^{B-1} + f_{Lx_{39}}^{B0}\,\nu_{L9_k}^{B-2} \quad \text{,rad}$$

$$x_{L5_k}^{B10(DP)} = \hat{x}_{L5_k}^{B10(DP)} + f_{Lx_{51}}^{B4}\, \nu_{L1_k}^{B-2} + f_{Lx_{53}}^{B-2}\, \nu_{L3_k}^{B4}$$

$$+ f_{Lx_{54}}^{B-2}\, \nu_{L4_k}^{B4} + f_{Lx_{55}}^{B-2}\, \nu_{L5_k}^{B4} + f_{Lx_{56}}^{B4}\, \nu_{L6_k}^{B-2}$$

$$+ f_{Lx_{57}}^{B4}\, \nu_{L7_k}^{B-2} + f_{Lx_{58}}^{B3}\, \nu_{L8_k}^{B-1} + f_{Lx_{59}}^{B4}\, \nu_{L9_k}^{B-2} \quad ,sec^{-1}$$

$$x_{L6_k}^{B6(DP)} = \hat{x}_{L6_k}^{B6(DP)} + f_{Lx_{61}}^{B2}\, \nu_{L1_k}^{B-2} + f_{Lx_{63}}^{B-4}\, \nu_{L3_k}^{B4}$$

$$+ f_{Lx_{64}}^{B-4}\, \nu_{L4_k}^{B4} + f_{Lx_{65}}^{B-4}\, \nu_{L5_k}^{B4} + f_{Lx_{66}}^{B2}\, \nu_{L6_k}^{B-2}$$

$$+ f_{Lx_{67}}^{B2}\, \nu_{L7_k}^{B-2} + f_{Lx_{68}}^{B1}\, \nu_{L8_k}^{B-1} + f_{Lx_{69}}^{B2}\, \nu_{L9_k}^{B-2} \quad ,\text{non-dimensional}$$

$$x_{L7_k}^{B5} = T^{B5} - T_o^{B5} \qquad (1000 \text{ lbs})$$

$$x_{L8_k}^{B6} = \frac{Th_{LF}^{B5} + Th_{RF}^{B5}}{2} - Th_o^{B6} \qquad (deg)$$

$$x_{L9_k}^{B-2} = s^{B-2} - s_o^{B-2} \qquad (rad)$$

C. Filtered Longitudinal Wind Vector

$$w_{L1_k}^{B-2} = \hat{w}_{L1_k}^{B-2} + f_{Lw_{11}}^{B0}\, v_{L1_k}^{B-2} + f_{LW_{13}}^{B-6}\, v_{L3_k}^{B4}$$

$$+ f_{Lw_{14}}^{B-6}\, v_{L4_k}^{B4} + f_{Lw_{15}}^{B-6}\, v_{L5_k}^{B4} + f_{Lw_{16}}^{B0}\, v_{L6_k}^{B-2}$$

$$+ f_{Lw_{17}}^{B0}\, v_{L7_k}^{B-2} + f_{Lw_{18}}^{B-1}\, v_{L8_k}^{B-1} + f_{Lw_{19}}^{B0}\, v_{L9_k}^{B-2}$$

$$w_{L2_k}^{B-2} = \hat{w}_{L2_k}^{B-2} + f_{Lw_{21}}^{B0}\, v_{L1_k}^{B-2} + f_{Lw_{23}}^{B-6}\, v_{L3_k}^{B4}$$

$$+ f_{Lw_{24}}^{B-6}\, v_{L4_k}^{B4} + f_{Lw_{25}}^{B-6}\, v_{L5_k}^{B4} + f_{Lw_{26}}^{B0}\, v_{L6_k}^{B-2}$$

$$+ f_{Lw_{27}}^{B0}\, v_{L7_k}^{B-2} + f_{Lw_{28}}^{B-1}\, v_{L8_k}^{B-1} + f_{Lw_{29}}^{B0}\, v_{L9_k}^{B-2}$$

$$w_{L3_k}^{B-2} = \hat{w}_{L3_k}^{B-2} + f_{Lw_{31}}^{B0}\, v_{L1_k}^{B-2} + f_{Lw_{33}}^{B-6}\, v_{L3_k}^{B4}$$

$$+ f_{Lw_{34}}^{B-6}\, v_{L4_k}^{B4} + f_{Lw_{35}}^{B-6}\, v_{L5_k}^{B4} + f_{Lw_{36}}^{B0}\, v_{L6_k}^{B-2}$$

$$+ f_{Lw_{37}}^{B0}\, v_{L7_k}^{B-2} f_{Lw_{38}}^{B-1}\, v_{L8_k}^{B-1} + f_{Lw_{39}}^{B-}\, v_{L9_k}^{B-2}$$

$$w_{L4_k}^{B-1} = \hat{w}_{L4_k}^{B-1} + f_{Lw_{41}}^{B1} v_{L1_k}^{B-2} + f_{Lw_{43}}^{B-5} v_{L3_k}^{B4}$$

$$+ f_{Lw_{44}}^{B-5} v_{L4_k}^{B4} + f_{Lw_{45}}^{B-5} v_{L5_k}^{B4} + f_{Lw_{46}}^{B1} v_{L6_k}^{B-2}$$

$$+ f_{Lw_{47}}^{B1} v_{L7_k}^{B-2} + f_{Lw_{48}}^{B0} v_{L8_k}^{B-1} + f_{Lw_{49}}^{B1} v_{L9_k}^{B-2}$$

$$w_{L5_k}^{B-2} = \hat{w}_{L5_k}^{B-2} + f_{Lw_{51}}^{B0} v_{L1_k}^{B-2} + f_{Lw_{53}}^{B-6} v_{L3_k}^{B4}$$

$$+ f_{Lw_{54}}^{B-5} v_{L4_k}^{B4} + f_{Lw_{55}}^{B-5} v_{L5_k}^{B4} + f_{Lw_{56}}^{B1} v_{L6_k}^{B-2}$$

$$+ f_{Lw_{57}}^{B1} v_{L7_k}^{B-2} + f_{Lw_{58}}^{B0} v_{L8_k}^{B-1} + f_{Lw_{59}}^{B1} v_{L9_k}^{B-2}$$

$$w_{L6_k}^{B-2} = \hat{w}_{L6_k}^{B-2} + f_{Lw_{61}}^{B0} v_{L1_k}^{B-2} + f_{Lw_{63}}^{B-6} v_{L3_k}^{B4}$$

$$+ f_{Lw_{64}}^{B-6} v_{L4_k}^{B4} + f_{Lw_{65}}^{B-6} v_{L5_k}^{B4} + f_{Lw_{66}}^{B0} v_{L3_k}^{B-2}$$

$$+ f_{Lw_{67}}^{B0} v_{L7_k}^{B-2} + f_{Lw_{68}}^{B-1} v_{L8_k}^{B-1} + f_{Lw_{69}}^{B0} v_{L9_k}^{B-2}$$

$$w_{L7_k}^{B-2} = \hat{w}_{L7_k}^{B-2} + f_{Lw_{71}}^{B0}\, \nu_{L1_k}^{B-2} + f_{Lw_{73}}^{B-6}\, \nu_{L3_k}^{B4}$$

$$+ f_{Lw_{74}}^{B-6}\, \nu_{L4_k}^{B-4} + f_{Lw_{75}}^{B-6}\, \nu_{L5_k}^{B-4} + f_{Lw_{76}}^{B0}\, \nu_{L6_k}^{B-2}$$

$$+ f_{Lw_{77}}^{B0}\, \nu_{L7_k}^{B-2} + f_{Lw_{78}}^{B-1}\, \nu_{L8_k}^{B-1} + f_{Lw_{79}}^{B0}\, \nu_{L9_k}^{B0}$$

D. Lateral Innovations

$$y_{1_k}^{B0} = \phi^{B0}$$

$$\nu_{1_k}^{B0} = y_{1_k}^{B0} - \hat{b}_{\phi_k}^{B0(DP)} - \hat{x}_{1_k}^{B0(DP)} \quad ,\text{rad}$$

$$y_{2_k}^{B2} = (\psi_T - \psi_{R/W})^{B2}$$

$$\nu_{2_k}^{B2} = y_{2_k}^{B2} - \hat{b}_{\psi_k}^{B2(DP)} - \hat{x}_{2_k}^{B2(DP)} \quad ,\text{rad}$$

$$y_{5_k}^{B6} = y_{cg}/U_o^{B18(DP)\ B8}$$

$$\nu_{5_k}^{B2} = y_{5_k}^{B6(DP)} - \hat{x}_{6_k}^{B5(DP)} \quad ,\text{sec}$$

$$y_{6_k}^{B-3} = f_y^{B8}\,UOI^{B-1} - b_{31}^{B-1}\left[-\delta_{a_{trim}} - \frac{\delta_{a_A} + \delta_{a_B}}{2}\right]^{102.4\ mu/deg} - d_{31}^{B-1}\,\hat{\xi}_k^{B-1} - \left(\hat{x}_{L2_k}^{B-1}\,\hat{x}_{5_k}^{B-1} - \hat{x}_{L3_k}^{B-2}\,\hat{x}_{4_k}^{B-2}\right)$$

$$\nu_{6_k}^{B-3} = y_{6_k}^{B-3(DP)} - \hat{y}_{6_k}^{B-3(DP)} \quad ,sec^{-1}$$

E. Filtered Lateral State Vector

$$x_{1_k}^{B0} = \bar{\phi}^{B0} = \hat{x}_{1_k}^{B0} + f_{x_{11}}^{B0}\,\nu_{1_k}^{B0} \quad ,rad$$

$$x_{2_k}^{B2} = \bar{\psi}^{B2} = \hat{x}_{2_k}^{B2} + f_{x_{22}}^{B0}\,\nu_{2_k}^{B2} \quad ,rad$$

$$x_{3_k}^{B0} = \hat{x}_{3_k}^{B0} + f_{x_{31}}^{B0}\,\nu_{1_k}^{B0} + f_{x_{32}}^{B-2}\,\nu_{2_k}^{B2} + f_{x_{35}}^{B-2}\,\nu_{5_k}^{B2} + f_{x_{36}}^{B3}\,\nu_{6_k}^{B-3} \quad ,rad$$

If (ACCFLG > 2):

$$r_k^{B-1} = \alpha_c^{B0}\,r_{k-1}^{B-1} + \beta_c^{B0}\,r^{B-1}$$

$$p_k^{B-1} = \alpha_c^{B0}\,p_{k-1}^{B-1} \quad \beta_c^{B0}\,p^{B-1}$$

Else:

$$r_k^{B1} = r^{B-1}$$

$$P_k^{B-1} = P^{B-1}$$

$$x_{4_k}^{B-1} = C_{\alpha_o}^{B0}\, p_k^{B-1} + S_{\alpha_o}^{B0}\, r_k^{B-1} \quad \text{,rad/sec}$$

$$x_{5_k}^{B-1} = -S_{\alpha_o}^{B0}\, p_k^{B-1} + C_{\alpha_o}^{B0}\, r_k^{B-1} \quad \text{,rad/sec}$$

$$x_{6_k}^{B6(DP)} = \hat{x}_{6_k}^{B6(DP)} + f_{x_{61}}^{B2}\, \nu_{1_k}^{B0} + f_{x_{62}}^{B0}\, \nu_{2_k}^{B2} + f_{x_{65}}^{B0}\, \nu_{5_k}^{B2} + f_{x_{66}}^{B5}\, \nu_{6_k}^{B-3}$$

$$x_{7_k}^{B-1} = (\delta_R - \delta_{R_{trim}})^{B-1}$$

F. Filtered Lateral Wind Vector

$$w_{1_k}^{B-1} = \hat{w}_{1_k}^{B-1} + f_{w_{11}}^{B-1}\, \nu_{1_k}^{B0} + f_{w_{12}}^{B-3}\, \nu_{2_k}^{B2} + f_{w_{15}}^{B-3}\, \nu_{5_k}^{B2} + f_{w_{16}}^{B2}\, \nu_{6_k}^{B-3}$$

$$w_{2_k}^{B-2} = \hat{w}_{2_k}^{B-2} + f_{w_{21}}^{B-2}\, \nu_{1_k}^{B0} + f_{w_{22}}^{B-4}\, \nu_{2_k}^{B2} + f_{w_{25}}^{B-4}\, \nu_{5_k}^{B2} + f_{w_{26}}^{B1}\, \nu_{6_k}^{B-3}$$

$$w_{3_k}^{B-2} = \hat{w}_{3_k}^{B-2} + f_{w_{31}}^{B-2}\, \nu_{1_k}^{B0} + f_{w_{32}}^{B-4}\, \nu_{2_k}^{B2} + f_{w_{35}}^{B-4}\, \nu_{5_k}^{B2} + f_{w_{36}}^{B1}\, \nu_{6_k}^{B-3}$$

$$w_{4_k}^{B-2} = \hat{w}_{4_k}^{B-2} + f_{w_{41}}^{B-2,B0}\nu_{1_k} + f_{w_{42}}^{B-3,B2}\nu_{2_k} + f_{w_{45}}^{B-3,B2}\nu_{5_k} + f_{w_{46}}^{B1,B-3}\nu_{6_k}$$

$$w_{5_k}^{B-1} = \hat{w}_{5_k}^{B-1} + f_{w_{51}}^{B-1,B0}\nu_{1_k} + f_{w_{52}}^{B-3,B2}\nu_{2_k} + f_{w_{55}}^{B-3,B2}\nu_{5_k} + f_{w_{56}}^{B2,B-3}\nu_{6_k}$$

$$w_{6_k}^{B-2} = \hat{w}_{6_k}^{B-2} + f_{w_{61}}^{B-2,B0}\nu_{1_k} + f_{w_{62}}^{B-4,B2}\nu_{2_k} + f_{w_{65}}^{B-4,B2}\nu_{5_k} + f_{w_{66}}^{B1,B-3}\nu_{6_k}$$

G. Filtered Euler Transformation Matrix, L_{EB}

$$L_{EB} = \begin{bmatrix} c\bar{\theta}c\bar{\psi} & s\bar{\phi}s\bar{\theta}c\bar{\psi}-c\bar{\phi}s\bar{\psi} & c\bar{\phi}s\bar{\theta}c\bar{\psi}+s\bar{\phi}s\bar{\psi} \\ c\bar{\theta}s\bar{\psi} & s\bar{\phi}s\bar{\theta}s\bar{\psi}+c\bar{\phi}c\bar{\psi} & c\bar{\phi}s\bar{\theta}s\bar{\psi}-s\bar{\phi}c\bar{\psi} \\ -s\bar{\theta} & s\bar{\phi}c\bar{\theta} & c\bar{\phi}c\bar{\theta} \end{bmatrix}$$

where

$$c\bar{\theta}^{B-2} = \cos(\bar{\theta}), \qquad c\bar{\phi}^{B0} = \cos(\bar{\phi}), \qquad c\bar{\psi}^{B2} = \cos(\bar{\psi})$$

$$s\bar{\theta}^{B-2} = \sin(\bar{\theta}), \qquad s\bar{\phi}^{B0} = \sin(\bar{\phi}), \qquad s\bar{\psi}^{B2} = \sin(\bar{\psi})$$

H. Filtered Transformation Matrix, L_{ES}

$$L_{ES} = \begin{bmatrix} {}^{1}_{ES11} & {}^{1}_{ES12} & {}^{1}_{ES13} \\ {}^{1}_{ES21} & {}^{1}_{ES22} & {}^{1}_{ES23} \\ {}^{1}_{ES31} & {}^{1}_{ES32} & {}^{1}_{ES33} \end{bmatrix}$$

$${}^{1}_{ES11} = {}^{1}_{EB11} C_{\alpha_o} + {}^{1}_{EB13} S_{\alpha_o}$$

$${}^{1}_{ES12} = {}^{1}_{EB12}$$

$$^{1}_{ES13} = -^{1}_{EB11} -S_{\alpha_o} + {}^{1}_{EB13} C_{\alpha_o}$$

$$^{1}_{ES21} = {}^{1}_{EB21} C_{\alpha_o} + {}^{1}_{EB23} S_{\alpha_o}$$

$$^{1}_{ES22} = {}^{1}_{EB22}$$

$$^{1}_{ES23} = -^{1}_{EB21} -S_{\alpha_o} + {}^{1}_{EB23} C_{\alpha_o}$$

$$^{1}_{ES31} = {}^{1}_{EB31} C_{\alpha_o} + {}^{1}_{EB33} S_{\alpha_o}$$

$$^{1}_{ES32} = {}^{1}_{EB32}$$

$$^{1}_{ES33} = -^{1}_{EB31} -S_{\alpha_o} + {}^{1}_{EB33} C_{\alpha_o}$$

III. GUIDANCE AND CONTROL

A. Longitudinal Control

1. Flare Engage Logic

If $J_{Flare} = 1$, then skip to Flare Airspeed Command (2.)

If $-x^{B6}_{L6_k} > h^{B6}_{f}$ Go to Desired Altitutde (4.), else

$$h_{Lx_3}(i) = h_{Lxi3}$$

$$h_{Lx_4}(i) = h_{Lxi4} \qquad \text{for } i = 1,2,3$$

$$h_{Lx_6}(i) = h_{Lxi6}$$

$$J_{Flare} = 1$$

2. Flare Airspeed Command

If $g_k < \pi$, then $g_k = g_k + \Delta g_k$ and

$$EZ5_k^{B0} = \frac{1}{2}\left[\cos\left(g_k - \pi\right)\right] + \frac{1}{2}$$

$$EZ5_{k+1}^{B-2} = \Delta V_{FR}^{B-2}\, EZ5_k^{B0}$$

$$\Delta V_{F_k}^{B-1} = \begin{cases} \Delta V_{F_k}^{B-1} - \Delta V_{FD}^{B-1} & \text{for } \Delta V_{F_k} > \Delta V_{FL} \\ \Delta V_{F_k} & \text{for } \Delta V_{F_k} \leq \Delta V_{FL} \end{cases}$$

3. Easy-On Flare Gains

If $EZ3^{B1} = 1$ Go To Desired Altitude (4.)

$$EZ3_k^{B1} = EZ3_{k-1}^{B1} + .05^{B1}$$

If $EZ3 > 1$ then $EZ3 = 1$

$$\left.\begin{aligned} h_{Lxi3} &= h_{Lx_3}(i)\left[1 + (h_{Lxf_3}^{B2} - 1)\, EZ3_k^{B1}\right] \\ h_{Lxi4} &= h_{Lx_4}(i)\left[1 + (h_{Lxf_4}^{B2} - 1)\, EZ3_k^{B1}\right] \\ h_{Lxi6} &= h_{Lx_6}(i)\left[1 + (h_{Lxf_6}^{B2} - 1)\, EZ3_k^{B1}\right] \end{aligned}\right\} \quad i = 1,2,3$$

4. Desired Altitude

$$x_{L5_s}^{B6} = x_{L5_k}^{B10(DP)}$$

$$x_f^{B6} = x_{L5_s}^{B6} + \Delta x_f^{B6}$$

If $x_f^{B6} > h_{1/2\,p}^{B6}$, Go to 5.

If $-x_f^{B6} > h_{1/2\,p}^{B6}$, Go to 7.

Go to 6.

5. Last Flare Segment Desired Altitude

$$z_e^{B6(DP)} = h_{fLR}^{B6} + T_{\gamma TD}^{B0} \left(x_f^{B6} - h_{1/2\,p}^{B6}\right)$$

$$z_{L6}^{B2} = T_{\gamma_o}^{B0} x_{L5_s}^{B6} - z_e$$

and $h'' = 0$, $h''' = 0$, $T_{\gamma D} = T_{\gamma TD}$ Go to B.

6. Flare (1-cos) Trajectory

$$z_e = h_f + \frac{(T_{\gamma_o} + T_{\gamma TD})\,(x_f + h_{1/2\,p})}{2} + \frac{(T_{\gamma TD} - T_{\gamma_o})\,(x_f^2 - h^2_{1/2\,p})}{4h_{1/2\,p}} - \frac{h_{1/2\,p}(T_{\gamma TD} - T_{\gamma})\left(\cos\left(\frac{\pi x_f}{h_{1/2\,p}}\right) + 1\right)}{2\pi^2}$$

$$z_{L6_k} = -z_e + T_{\gamma_o}\, x_{L5_s}$$

$$\text{and } h''' = \left[\frac{-\pi(T_{\gamma TD} - T_{\gamma_o})\left(\cos\left(\frac{\pi x_f}{h_{1/2\,p}}\right) + 1\right)}{2h^2_{1/2\,p}}\, U_o\right] / \cos(\alpha_o - \bar{\theta})$$

$$\text{and } h''' = \left[\frac{-\pi(T_{\gamma TD} - T_{\gamma_o})\sin\left(\frac{\pi x_f}{h_{1/2\,p}}\right)}{2h_{1/2\,p}}\right] / \cos(\alpha_o - \bar{\theta})$$

$$\text{and } T_{\gamma D} = \frac{(T_{\gamma TD} + T_{\gamma_o})}{2} + \frac{(T_{\gamma TD} - T_{\gamma_o})\,x_f}{2h_{1/2\,p}} + \frac{(T_{\gamma TD} - T_{\gamma_o})\sin\left(\frac{\pi x_f}{h_{1/2\,p}}\right)}{2\pi}$$

7. Glideslope Trajectory

$$z_{L1_k}^{B-2} = z_{L1_{k-1}}^{B-2} + \Delta T \; z_{L4_{k-1}}^{B-3}$$

$$z_{L2_k}^{B-1} = -CWB_{11}^{B1} \; w_{L1_k}^{B-2} - CWB_{14}^{B0} \; w_{L4_k}^{B-1} - CWB_{15}^{B0} w_{L5_k}^{B-1}$$

$$- CWB_{16}^{B1} \; w_{L6_k}^{B-2} + \Delta V_{F_k}^{B-1(DP)}$$

$$z_{L3_k}^{B0} = -\left[\left(1_{ES31}^{B0} + T_{YD} \; 1_{ES11}^{B0} \right) \left(1 + z_{L2_k}^{B1} \right) \right.$$

$$\left. + \left(1_{ES32} + T_{YD} \; 1_{ES12} \right) x_{3_k}^{B0} \right] / \left(1_{ES33} + T_{YD} \; 1_{ES13} \right)$$

If $J_{Flare} = 0$, then

$$\dot{\bar{x}}^{B0} = 1_{ES11}^{B0} \left(1 + z_{L2_k}^{B1} \right) + 1_{ES13}^{B0} \; z_{L3_k}^{B-2} + 1_{ES12}^{B0} \; x_{3_k}^{B0}$$

Else $\dot{\bar{x}} = 0$

$$z_{L4_k}^{B-1} = h'' \; \dot{\bar{x}}^{B-2 \; B2}$$

$$\zeta_{L2_k}^{B-2} = - DT(2)^{B0} \; w_{L2_k}^{B-2} - DT(4)^{B-1} \; w_{L4_k}^{B-1} - CWB_{15}^{B0} \; w_{L7_k}^{B-2} - EZ5^{B-2(DP)}$$

$$\zeta_{L4_k}^{B-3} = G_{\zeta 4}^{B0} \; \dot{\bar{x}}^{B3} \; h'''^{B-8}$$

$$\zeta_{L6_k}^{B1} = z_{L1_k}^{B-2} - SCY_o\, z_{L3_k}^{B-2} + (T_{Y_o} - T_{YD})\, \dot{\bar{x}}^{B1}$$

Notes: 1. $G_{\zeta_4} = 0$ for all flights

2. CWB15 should have been CWB14; the values for CWB14 & CWB15 are, respectively, 0.99758 and 0.99452 (software specification error).

$$\eta_{L1_k}^{B-2} = x_{L4_k}^{B-1}\,(\cos(\bar{\phi}) - 1) - x_{5_k}^{B0} \sin \bar{\phi}$$

$$\zeta_{L1_k}^{B-2} = -\eta_{L1_k}^{B-2}$$

$$\eta_{L2_k}^{B-2} = -x_{L3_k}^{B-2}\, x_{L4_k}^{B-1} + x_{3_k}^{B0}\, x_{5_k}^{B-1}$$

$$\zeta_{L2_k}^{B-2} = \zeta_{L2_k}^{B-2} - \eta_{L2_k}^{B-2}$$

$$\eta_{L3_k}^{B-2} = x_{L2_k}^{B-1}\, x_{L4_k}^{B-1} - x_{3_k}^{B0}\, x_{4_k}^{B-1}$$

$$\zeta_{L3_k}^{B-2} = -\eta_{L3_k}^{B-2}$$

$$\eta^{B1}_{L6_k} = ({}^{B0}1_{ES31} + T_{\gamma_o}\,{}^{B0}1_{ES11})\,(1 + x^{B-1}_{L2_k})$$

$$+ ({}^{B0}1_{ES33} + T_{\gamma_o}\,{}^{B0}1_{ES13})\,x^{B-2}_{L3_k}$$

$$+ ({}^{B0}1_{ES32} + T_{\gamma_o}\,{}^{B0}1_{ES12})\,x^{B0}_{3_k} + x^{B-2}_{L1_k} - x^{B-2}_{L3_k}\,SC\gamma^{B1}_{o}$$

$$\zeta^{B1}_{L6_k} = \zeta^{B1}_{L6_k} - \eta^{B1}_{L6_k}$$

If $EZ7 < 1$

$$EZ7^{B1(DP)} = EZ7^{B1(DP)} + \Delta EZ7^{B1(DP)}$$

and

$$\zeta^{B1(DP)}_{L6_k} = \zeta^{B1(DP)}_{L6_k} * EZ7^{B1(DP)}$$

8. Glideslope Track Engage Logic

If $J_{GSC} = 1$, then Go to 9.

If $U^{B8}_{o}\,|e^{B2}_{Lx6_k}| > 15^{B10}$, then Go to 10.

$J_{GSC} = 1$ which means glideslope track engage

9. Easy-On Glideslope Gains

If $EZ4^{B1}_{k-1} > 1$, then Go to 10.

$$EZ4^{B1}_{k} = EZ4^{B1(DP)}_{k-1} + \Delta EZ4^{B1(DP)}$$

$$DFGT^{B2} = \left[1 + (GF3^{B2} - 1)\ EZ4^{B1}_{k}\right]^{B1}$$

$$\left.\begin{aligned} h^{B2}_{Lxi3} &= h^{DFGT}_{Lxoi3} \\ h^{B2}_{Lxi6} &= h^{DFGT}_{Lxoi6} \end{aligned}\right\} \quad \text{for } i = 1,2,3$$

10. Trajectory Errors

$$e^{B-2}_{Lx1} = x^{B-2}_{L1_k} - z^{B-2}_{L1_k}$$

$$e^{B-1}_{Lx2_k} = x^{B-1}_{L2_k} - z^{B-1}_{L2_k}$$

$$e^{B-2}_{Lx3_k} = x^{B-2}_{L3_k} - z^{B-2}_{L3_k}$$

$$e^{B-1}_{Lx4_k} = x^{B-1}_{L4_k} - z^{B-1}_{L4_k}$$

$$e^{B2}_{Lx6_k} = x^{B6(DP)}_{L6_k} + T^{B0}_{\gamma_o}\ x^{B10(DP)}_{L5_k} - z^{B6(DP)}_{L6_k}$$

$$e_{Lx7_k}^{B5} = x_{L7_k}^{B5}$$

$$e_{Lx8_k}^{B6} = x_{L8_k}^{B6}$$

$$e_{Lx9_k}^{B-2} = x_{L9_k}^{B-2}$$

11. Altitude Error Integrator Logic

If $K_{FL} = 1$ skip to 12.

If $e_{Lx_6}^{B2} U_o^{B8} < Z_{Lim}^{B10}$ then $K_{FL} = 1$

Else

KFLC = KFLC - 1 and if KFLC < 0 then $K_{FL} = 1$

Else Go to 13.

12. Altitude Error Integrator

$$z_{INT}^{B4(DP)} = z_{INT}^{B4(DP)} + e_{Lx6}^{B2(DP)} \Delta T^{B-3}$$

13. Flare Touchdown Parameters

If $J_{Flare} = 0$, then Go to 14.

$$x_{Lim}^{B5} = x_{FLR}^{B10(DP)} - x_{L5_k}^{B10(DP)}$$

If $x_{Lim}^{B5} < 0.5$, then $x_{Lim}^{B5} = 0.5$

$$FL_{ELX}^{B0} = \frac{(2)\, e_{Lx_6}^{B2(DP)}}{x_{Lim}^{B5}}$$

14. Longitudinal Commands

$$u_{CL1_k}^{B7} = -h_{Lx11}^{B9}\, e_{Lx1_k}^{B-2} - h_{Lx12}^{B8}\, e_{Lx2_k}^{B-1} - h_{Lx13}^{B9}\, e_{Lx3_k}^{B-2}$$

$$-h_{Lx14}^{B8}\, e_{Lx4_k}^{B-1} - h_{Lx16}^{B5}\, e_{Lx6_k}^{B2} - h_{Lx17}^{B2}\, e_{Lx7_k}^{B5} - h_{Lx18}^{B1}\, e_{Lx8_k}^{B6}$$

$$-h_{Lx19}^{B9}\, e_{Lx9_k}^{B-2} - h_{Lw11}^{B9}\, w_{L1_k}^{B-2} - h_{Lw12}^{B9}\, w_{L2_k}^{B-2} - h_{Lw13}^{B9}\, w_{L3_k}^{B-2}$$

$$-h_{Lw14}^{B8}\, w_{L4_k}^{B-1} - h_{Lw15}^{B8}\, w_{L5_k}^{B-1} - h_{Lw16}^{B9}\, w_{L6_k}^{B-2} - h_{Lw17}^{B9}\, w_{L7_k}^{B-2}$$

$$-h_{Lz11}^{B9}\, z_{L1_k}^{B-2} - h_{Lz12}^{B8}\, z_{L2_k}^{B-1} - h_{Lz13}^{B9}\, z_{L3_k}^{B-2} - h_{Lz14}^{B8}\, z_{L4_k}^{B-1} - h_{Lz16}^{B5}\, z_{L6_k}^{B2}$$

$$-h_{L\zeta 11}^{B9}\ \zeta_{L1_k}^{B-2}\ -h_{L\zeta 12}^{B9}\ \zeta_{L2_k}^{B-2}\ -h_{L\zeta 13}^{B9}\ \zeta_{L3_k}^{B-2}$$

$$-h_{L\zeta 14}^{B10}\ \zeta_{L4_k}^{B-3}\ -h_{L\zeta 16}^{B6}\ \zeta_{L6_k}^{B1}\ -h_{zT1}^{B3}\ z_{INT}^{B4}\ -f_c h_{zP1}^{B7} FL_{ELX}^{B0}$$

$$u_{CL1_k}^{B7} = \begin{cases} u_{Lmin1} & \text{for } u_{CL1_k} < u_{Lmin1} \\ u_{CL1_k} & \text{for } u_{Lmin1} \leq u_{CL1_k} \leq u_{Lmax1} \\ u_{Lmax1} & \text{for } u_{CL1_k} > u_{Lmax1} \end{cases}$$

$$u_{CL1_k}^{B2} = \alpha_e^{B0}\ u_{CL1_{k-1}}^{B2} + u_{CL1_k}^{B2}$$

$$u_{CL2_k}^{B2} = -h_{Lx21}^{B4}\ e_{Lx1_k}^{B-2}\ -h_{Lx22}^{B3}\ e_{Lx2_k}^{B-1}\ -h_{Lx23}^{B4}\ e_{Lx3_k}^{B-2}\ -h_{Lx24}^{B3}\ e_{Lx4_k}^{B-1}$$

$$-h_{Lx26}^{B0}\ e_{Lx6_k}^{B2}\ -h_{Lx27}^{B-3}\ e_{Lx7_k}^{B5}\ -h_{Lx28}^{B-4}\ e_{Lx8_k}^{B6}\ -h_{Lx29}^{B4}\ e_{Lx9_k}^{B-2}$$

$$-h_{Lw21}^{B4}\ w_{L1_k}^{B-2}\ -h_{Lw22}^{B4}\ w_{L2_k}^{B-2}\ -h_{Lw23}^{B4}\ w_{L3_k}^{B-2}\ -h_{Lw24}^{B3}\ w_{L4_k}^{B-1}$$

$$-h_{Lw25}^{B3}\ w_{L5_k}^{B-1}\ -h_{Lw26}^{B4}\ w_{L6_k}^{B-2}\ -h_{Lw27}^{B4}\ w_{L7_k}^{B-2}\ -h_{Lz21}^{B4}\ z_{L1_k}^{B-2}\ -h_{Lz22}^{B3}\ z_{L2_k}^{B-1}$$

$$-h_{Lz23}^{B4}\ z_{L3_k}^{B-2}\ -h_{Lz24}^{B3}\ z_{L4_k}^{B-1}\ -h_{Lz26}^{B0}\ z_{L6_k}^{B2}\ -h_{L\zeta 21}^{B4}\ \zeta_{L1_k}^{B-2}$$

$$
\begin{matrix} \text{B4} & \text{B-2} & \text{B4} & \text{B-2} & \text{B2} & \text{B-3} \\ -h_{L\zeta 22}\ \zeta_{L2_k} & & -h_{L\zeta 23}\ \zeta_{L3_k} & & -h_{L\zeta 24}\ \zeta_{L4_k} & \end{matrix}
$$

$$
\begin{matrix} \text{B1} & \text{B1} & \text{B-2} & \text{B4} & \text{B2} & \text{B0} \\ -h_{L\zeta 26}\ \zeta_{L6_k} & & -h_{zT2}\ z_{INT} & & - f_c h_{zP2} FL_{ELX} & \end{matrix}
$$

$$
\overset{\text{B-4}}{u_{CL2_k}} = \begin{cases} u_{Lmin2} \text{ for } u_{CL2_k} < u_{Lmin2} \\ u_{CL2_k} \text{ for } u_{Lmin2} \leq u_{CL2_k} \leq u_{Lmax2} \\ u_{Lmax2} \text{ for } u_{CL2_k} > u_{Lmax2} \end{cases}
$$

$$
\delta_{e_c} = \text{SWTC } (u_{CL1} + \text{GSTAB } u_{CL2})\ \ 57.3/.86) \ \ \text{(deg)}
$$

where SWTC goes from 0 to 1 in one-half second (Easy-on) at glideslope capture.

$$
\begin{matrix} \text{B8(DP)} & \text{B10} & \text{B-2} & \text{B9} & \text{B-1} & \text{B10} & \text{B-2} & \text{B9} & \text{B-1} \\ u_{CL3_k} = -h_{Lx31}\ e_{Lx1_k} & & -h_{Lx32}\ e_{Lx2_k} & & -h_{Lx33}\ e_{Lx3_k} & & -h_{Lx34}\ e_{Lx4_k} & & \end{matrix}
$$

$$
\begin{matrix} \text{B6} & \text{B2} & \text{B3} & \text{B5} & \text{B2} & \text{B6} & \text{B10} & \text{B-2} \\ -h_{Lx36}\ e_{Lx6_k} & & -h_{Lx37}\ e_{Lx7_k} & & -h_{Lx38}\ e_{Lx8_k} & & -h_{Lx39}\ e_{Lx9_k} & \end{matrix}
$$

$$
\begin{matrix} \text{B10} & \text{B-2} & \text{B10} & \text{B-2} & \text{B10} & \text{B-2} & \text{B9} & \text{B-1} \\ -h_{Lw31}\ w_{L1_k} & & -h_{Lw32}\ w_{L2_k} & & -h_{Lw33}\ w_{L3_k} & & -h_{Lw34}\ w_{L4_k} & \end{matrix}
$$

$$
\begin{matrix} \text{B9} & \text{B-1} & \text{B10} & \text{B-2} & \text{B10} & \text{B-2} & \text{B10} & \text{B-2} \\ -h_{Lw35}\ w_{L5_k} & & -h_{Lw36}\ w_{L6_k} & & -h_{Lw37}\ w_{L7_k} & & -h_{Lz31}\ z_{L1_k} & \end{matrix}
$$

$$
\begin{matrix} \text{B9} & \text{B-1} & \text{B10} & \text{B-2} & \text{B9} & \text{B-1} & \text{B6} & \text{B2} \\ -h_{Lz32}\ z_{L2_k} & & -h_{Lz33}\ z_{L3_k} & & -h_{Lz34}\ z_{L4_k} & & -h_{Lz36}\ z_{L6_k} & \end{matrix}
$$

$$
\begin{matrix} \text{B10} & \text{B-2} & \text{B10} & \text{B-2} & \text{B10} & \text{B-2} \\ -h_{L\zeta 31}\ \zeta_{L1_k} & & -h_{L\zeta 32}\ \zeta_{L2_k} & & -h_{L\zeta 33}\ \zeta_{L3_k} & \end{matrix}
$$

$$-h_{L\zeta 34}^{B11}\ \zeta_{L4_k}^{B-3}\ -h_{L\zeta 36}^{B7}\ \zeta_{L6_k}^{B1}\ -h_{zT3}^{B4}\ z_{INT}^{B4} - f_c\ h_{zP3}^{B2}\ FL_{ELX}^{B0}$$

$$u_{CL3_k}^{B7} = \begin{cases} u_{Lim3} & \text{for } u_{CL3} < u_{Lim3} \\ u_{CL3_k} & \text{for } u_{Lim3} < u_{CL3_k} < u_{Lmax3} \\ u_{Lmax3} & \text{for } u_{CL3_k} > u_{Lmax3} \end{cases}$$

$$\dot{\delta}_{Thc_k}^{B7} = u_{CL3_k}^{B7} = \text{throttle rate command, deg/sec}$$

B. Lateral Control

1. Desired Path

If DECRAB = 1, then Go to 2. Estimated Sideslip Parameters

$$z_{1_k}^{B0} = \phi_{z11}^{B0}\ z_{1_{k-1}}^{B0} + \phi_{z13}^{B0}\ z_{3_{k-1}}^{B0} + \phi_{z14}^{B1}\ z_{4_{k-1}}^{B-1} + \phi_{z15}^{B1}\ z_{5_{k-1}}^{B-1}$$

$$+ \psi_{11}^{B-1}\ \zeta_{z1_{k-1}}^{B1} + \psi_{13}^{B1}\ \zeta_{z3_{k-1}}^{B-1} + \psi_{14}^{B-2}\ \zeta_{z4_{k-1}}^{B2}\ \psi_{15}^{B0}\ \zeta_{z5_{k-1}}^{B0}$$

$$z_{2_k}^{B2} = \phi_{z21}^{B2}\ z_{1_{k-1}}^{B0} + z_{2_{k-1}}^{B2} + \phi_{z23}^{B2}\ z_{3_{k-1}}^{B0} + \phi_{z24}^{B0}\ z_{4_{k-1}}^{B3}$$

$$+ \phi_{z25}^{B3}\ z_{5_{k-1}}^{B-1} + \psi_{21}^{B1}\ \zeta_{z1_{k-1}}^{B1} + \psi_{22}^{B3}\ \zeta_{z2_{k-1}}^{B-1} + \psi_{23}^{B3}\ \zeta_{z3_{k-1}}^{B-1}$$

$$+ \psi_{24}^{B0}\ \zeta_{z4_{k-1}}^{B2} + \psi_{25}^{B2}\ \zeta_{z5_{k-1}}^{B0}$$

$$z_{4_k}^{B-1} = \phi_{z41}^{B-1,B0} z_{1_{k-1}} + \phi_{z43}^{B-1,B0} z_{3_{k-1}} + \phi_{z44}^{B0,B-1} z_{4_{k-1}} + \phi_{z45}^{B0,B-1} z_{5_{k-1}}$$

$$+ \psi_{41}^{B-2,B1} \zeta_{z1_{k-1}} + \psi_{43}^{B0,B-1} \zeta_{z3_{k-1}} + \psi_{44}^{B-3,B2} \zeta_{z4_{k-1}} + \psi_{45}^{B-1,B0} \zeta_{z5_{k-1}}$$

$$z_5^{B-1} = \phi_{z51}^{B-1,B0} z_{1_{k-1}} + \phi_{z53}^{B-1,B0} z_{3_{k-1}} + \phi_{z54}^{B0,B-1} z_{4_{k-1}} + \phi_{z55}^{B0,B-1} z_{5_{k-1}}$$

$$+ \psi_{51}^{B-2,B1} \zeta_{z1_{k-1}} + \psi_{53}^{B0,B-1} \zeta_{z3_{k-1}} + \psi_{54}^{B-3,B2} \zeta_{z4_{k-1}} + \psi_{55}^{B-1,B0} \zeta_{z5_{k-1}}$$

$$z_{6_k}^{B6} = \phi_{z61}^{B6,B0} z_{1_{k-1}} + \phi_{z62}^{B4,B2} z_{2_{k-1}} + \phi_{z63}^{B6,B0} z_{3_{k-1}} + \phi_{z64}^{B7,B-1} z_{4_{k-1}}$$

$$+ \phi_{z65}^{B7,B-1} z_{5_{k-1}} + z_{6_{k-1}}^{B6} + \left(\psi_{61}^{B-1,B1} \zeta_{z1_{k-1}} + \psi_{62}^{B1,B-1} \zeta_{z2_{k-1}} + \psi_{63}^{B1,B-1} \zeta_{z3_{k-1}}\right.$$

$$\left. + \psi_{64}^{B-2,B2} \zeta_{z4_{k-1}} + \psi_{65}^{B0,B0} \zeta_{z5_{k-1}} + \psi_{66}^{B-2,B2} \zeta_{z6_{k-1}}\right) / 2^6$$

2. Estimated Sideslip Parameters

$$\bar{\beta}_k^{B-1} = w_{5_k}^{B-1} / {}^{1}EB22^{B0}$$

$$\bar{\xi}_k^{B-1} = \bar{\beta}_k^{B-1} - w_{1_k}^{B-1} - w_{5_k}^{B-1}$$

$$z_{3_k}^{B0} = -\bar{\beta}_k^{B-1}$$

If DECRAB = 1, Go to 4.

$$\dot{z}_{3_k}^{B-1} = -1_{EB22}^{B0}\, w_{6_k}^{B-2}$$

3. Decrab Engage Logic

If h_{DC} UOI + x_{L6_k} < 0, then skip to 6. (Lateral Path Command).

Else

DECRAB = 1,

EZ1 = 0,

and

$$\dot{z}_{3_k} = 0$$

4. Decrab Roll Limit

If $|x_{1_k}^{B0}| > \phi_{Lim}^{B0}$ Go to 6. otherwise,

5. Decrab Trajectory

$$z_{3_k}^{B0} = z_{3_k}^{B0} + \bar{\beta}_k^{B-1}\, EZ1^{B0}$$

$$EZ1_k^{B1} = A_{ez}^{B0}\, EZ1_{k-1}^{B1} + \Delta EZ1^{B1} \quad \text{where}$$

If $EZ1_k > 1$, then $EZ1_k = 1$.

$$\overset{B1}{\dot{z}_{1k}} = \overset{B0}{A_{\phi}}\ \overset{B2}{x_{2k}}\ \overset{B1}{EZ1_k}$$

$$\overset{B-1}{\dot{z}_{2k}} = \overset{B-2}{A_{\psi}}\ \overset{B2}{x_{2_k}}\ \overset{B1}{EZ1_k}$$

6. Lateral Path Command

$$\overset{B1}{\zeta_{z1_k}} = -\overset{B2}{a_{x14}}\ \overset{B-1}{z_{4_k}} - \overset{B2}{a_{x15}}\ \overset{B-1}{z_{5_k}} + \overset{B1}{\dot{z}_{1_k}}$$

$$\overset{B-1}{\zeta_{z2_k}} = -\overset{B0}{a_{x24}}\ \overset{B-1}{z_{4_k}} - \overset{B1}{a_{x25}}\ \overset{B-1}{z_{5_k}} + \overset{B-1}{\dot{z}_{2_k}}$$

$$\overset{B-1}{\zeta_{z3_k}} = -\overset{B-1}{a_{x31}}\ \overset{B0}{z_{1_k}} - \overset{B-1}{a_{x33}}\ \overset{B0}{z_{3_k}} - \overset{B0}{a_{x34}}\ \overset{B-1}{z_{4_k}} - \overset{B0}{a_{x35}}\ \overset{B-1}{z_{5_k}} + \overset{B-1}{\dot{z}_{3_k}}$$

$$\overset{B0}{\zeta_{z4_k}} = -\overset{B0}{a_{x43}}\ \overset{B0}{z_{3_k}} - \overset{B1}{a_{x44}}\ \overset{B-1}{z_{4_k}} - \overset{B1}{a_{x45}}\ \overset{B-1}{z_{5_k}}$$

$$\overset{B0}{\zeta_{z5_k}} = -\overset{B0}{a_{x53}}\ \overset{B0}{z_{3_k}} - \overset{B1}{a_{x54}}\ \overset{B-1}{z_{4_k}} - \overset{B1}{a_{x55}}\ \overset{B-1}{z_{5_k}}$$

$$\overset{B2}{\zeta_{z6_k}} = -\overset{B2}{a_{x61}}\ \overset{B0}{z_{1_k}}\ \overset{B0}{a_{x62}}\ \overset{B2}{z_{2_k}} - \overset{B2}{a_{x63}}\ \overset{B0}{z_{3_k}}$$

$$\overset{B1}{\zeta_{1_k}} = \left(- \frac{\overset{B0}{c\bar{\phi}s\bar{\theta}}}{\overset{B-1}{c\bar{\theta}}} + \frac{S_{\theta_o}}{C_{\theta_o}} \right) r_k$$

$$\overset{B1}{\zeta_{u1_k}} = \overset{B1}{\zeta_{z1_k}} + \overset{B1}{\zeta_{1_k}}$$

$$\zeta_{2_k}^{B-1} = \left(- \frac{c\bar{\phi}}{c\bar{\theta}} + SC_{\theta_o}^{B0} \right) r_k^{B-1}$$

$$\zeta_{u2_k}^{B-1} = \zeta_{z2_k}^{B-1} + \zeta_{2_k}^{B-1}$$

$$\zeta_{3_k}^{B-1} = -d_{31}^{B0} \bar{\xi}_k^{B-1} + x_{5_k}^{B-1} x_{L2_k}^{B-1} - x_{4_k}^{B-1} x_{L3_k}^{B-2}$$

$$\zeta_{u3_k}^{B-1} = \zeta_{z3_k}^{B-1} + \zeta_{3_k}^{B-1}$$

$$\zeta_{4_k}^{B2} = -d_{41}^{B3} \bar{\xi}_k^{B-1}$$

$$\zeta_{u4_k}^{B2} = \zeta_{z4_k}^{B2} + \zeta_{4_k}^{B2}$$

$$\zeta_{5_k}^{B0} = -d_{51}^{B1} \bar{\xi}_k^{B-1}$$

$$\zeta_{u5_k}^{B0} = \zeta_{z5_k}^{B0} + \zeta_{5_k}^{B0}$$

$$\zeta_{6_k}^{B2} = -(1_{ES22}^{B0} - 1) x_{3_k}^{B0} - 1_{ES21}^{B0} (1 + x_{L2_k}^{B-1}) + x_{2_k}^{B2} CY_o^{B0}$$

$$-1_{ES23}^{B0} x_{L3_k}^{B-2} x_{1_k}^{B0} S_{\alpha_o}^{B0}$$

$$\zeta_{u6_k}^{B2} = \zeta_{z6_k}^{B2} + \zeta_{6_k}^{B2}$$

7. Trajectory Errors

$$e_{x1_k}^{B0} = x_{1_k}^{B0} - z_{1_k}^{B0}$$

$$e_{x2_k}^{B2} = x_{2_k}^{B2} - z_{2_k}^{B2}$$

$$e_{x3_k}^{B0} = x_{3_k}^{B0} - z_{3_k}^{B0}$$

$$e_{x4_k}^{B-1} = x_{4_k}^{B-1} - z_{4_k}^{B-1}$$

$$e_{x5_k}^{B-1} = x_{5_k}^{B-1} - z_{5_k}^{B-1}$$

$$e_{x_k}^{B6(DP)} = x_{6_k}^{B6(DP)} - z_{6_k}^{B6(DP)}$$

$$e_{x7_k}^{B-1} = x_{7_k}^{B-1}$$

8. Localizer Track Engage Logic

If $J_{LGN} = 1$, then skip to 9.

If $(|x_6| * U_o < y_{LIM}$, then $\begin{cases} G_y = 1.0 \\ J_{LGN} = 1 \end{cases}$

Otherwise $C_{LGN} = C_{LGN} - 1$; If $C_{LGN} > 0$, Go to 12.

else $\begin{cases} G_y = 1.0 \\ J_{LGN} = 1 \end{cases}$

9. Cross-Track Error Integrator

$$y_{INT_k}^{B6(DP)} = y_{INT_{k-1}}^{B6(DP)} + e_{x6_k}^{B6(DP)} \Delta T^{B-3}$$

10. Easy-On Cross-Track Error Gain

$$G_{y_k}^{B3} = G_{y_{k-1}}^{B3} + 0.05 \text{ if } G_{y_{k-1}}^{B3} < h_{F6}^{B3}$$

Else $G_{y_k} = h_{F6}$

$$e_{x6_k}^{B6(DP)} = G_{y_k}^{B3} e_{x6_k}^{B3}$$

11. Roll and Yaw Integrators

If (JPHINT = 0 and DECRAB = 0) then

If $|x_1 57.3| < 1.0$ deg then JPHINT = 1

If (JPHINT = 1 and DECRAB = 0) then

$$\phi_{INT_k}^{B2(DP)} = \phi_{INT_{k-1}}^{B2(DP)} + x_{1k}^{B0} \Delta T)^{B-3}$$

If DECRAB = 1 then

$$\psi_{INT_k}^{B2(DP)} = \psi_{INT_{k-1}}^{B2(DP)} + x_{2k}^{B2}\,\Delta T^{B-3}$$

12. Lateral Control Commands

$$u_{cl_k}^{B7(DP)} = -h_{x_{11}}^{B7}\, e_{x1_k}^{B0}\, -h_{x_{12}}^{B5}\, e_{x2_k}^{B2} - h_{x_{13}}^{B7}\, e_{x3_k}^{B0}\, -h_{x14}^{B8}\, e_{x4_k}^{B-1}$$

$$-h_{x_{15}}^{B8}\, e_{x5_k}^{B-1}\, -h_{x_{16}}^{B1}\, e_{x6_k}^{B6}\, -h_{x_{17}}^{B8}\, e_{x7_k}^{B-1}\, -h_{w_{11}}^{B8}\, w_{1_k}^{B-1}$$

$$-h_{w_{12}}^{B9}\, w_{2_k}^{B-2}\, -h_{w_{13}}^{B9}\, w_{3_k}^{B-2}\, -h_{w_{14}}^{B9}\, w_{4_k}^{B-2}\, -h_{w_{15}}^{B8}\, w_{5_k}^{B-1}$$

$$-h_{w_{16}}^{B9}\, w_{6_k}^{B-2}\, -h_{\zeta_{11}}^{B6}\, \zeta_{u1_k}^{B1}\, -h_{\zeta_{12}}^{B8}\, \zeta_{u2_k}^{B-1}\, -h_{\zeta_{13}}^{B8}\, \zeta_{u3_k}^{B-1}$$

$$-h_{\zeta_{14}}^{B5}\, \zeta_{u4_k}^{B2}\, -h_{\zeta_{15}}^{B7}\, \zeta_{u5_k}^{B0}\, -h_{\zeta_{16}}^{B5}\, \zeta_{u6_k}^{B2}\, -h_{y_{INT1}}^{B1}\, y_{INT}^{B6}\, -h_{\phi_{INT1}}^{B5}\, \phi_{INT}^{B2}$$

$$-h_{\psi_{INT1}}^{B5}\, \psi_{INT}^{B2}$$

$$u_{cl_k}^{B2} = \begin{cases} u_{1min} \text{ for } u_{cl_k} < u_{1_{min}} \\ u_{cl_k} \text{ for } u_{1min} \leq u_{cl_k} \leq u_{1max} \\ u_{1max} \text{ for } u_{cl_k} > u_{1max} \end{cases}$$

$$u_{cl_k} = u_{cl_k} + \alpha_a u_{cl_{k-1}}$$

$$\text{TEMP} = u_{cl_k}\, \frac{180}{\pi} + \delta_{a_{trim}}$$

$$\delta_{ac} = SWTC \begin{cases} \dfrac{TEMP}{|TEMP|^{B1} * A1 + A2^{B2}} & \text{If } |TEMP| < A3 \\ TEMP & \text{If } |TEMP| > A3 \end{cases}$$

where SWTC goes from 0 to 1 in one-half second (Easy-on) at localizer capture.

$$\begin{array}{llllllll} B5(DP) & B5 & B0 & B3 & B2 & B5 & B0 & B6 & B-1 \\ u_{c2_k} = & -h_{x_{21}} & e_{x1_k} & -h_{x_{22}} & e_{x2_k} & -h_{x_{23}} & e_{x3_k} & -h_{x_{24}} & e_{x4_k} \end{array}$$

$$\begin{array}{llllllll} B6 & B-1 & B-1 & B6 & B6 & B-1 & B6 & B-1 \\ -h_{x_{25}} & e_{x5_k} & -h_{x_{26}} & e_{x6_k} & -h_{x_{27}} & e_{x7_k} & -h_{w_{21}} & w_{1_k} \end{array}$$

$$\begin{array}{llllllll} B7 & B-2 & B7 & B-2 & B7 & B-2 & B6 & B-1 \\ -h_{w_{22}} & w_{2_k} & -h_{w_{23}} & w_{3_k} & -h_{w_{24}} & w_{4_k} & -h_{w_{25}} & w_{5_k} \end{array}$$

$$\begin{array}{llllllll} B7 & B-2 & B4 & B1 & B6 & B-1 & B6 & B-1 \\ -h_{w_{26}} & w_{6_k} & -h_{\zeta_{21}} & \zeta_{u1_k} & -h_{\zeta_{22}} & \zeta_{u2_k} & -h_{\zeta_{23}} & \zeta_{u3_k} \end{array}$$

$$\begin{array}{llllllll} B3 & B2 & B5 & B0 & B3 & B2 & B-1 & B6 \\ -h_{\zeta_{24}} & \zeta_{u4_k} & -h_{\zeta_{25}} & \zeta_{u5_k} & -h_{\zeta_{26}} & \zeta_{u6_k} & -h_{y_{INT2}} & y_{INT} \end{array}$$

$$\begin{array}{llllllll} B3 & B2 & B3 & B2 \\ -h_{\phi_{INT2}} & \phi_{INT} & -h_{\psi_{INT2}} & \psi_{INT} \end{array}$$

$$u_{c2_k}^{B2} = \begin{cases} u_{2min} & \text{for } u_{c2_k} < u_{2min} \\ u_{c2_k} & \text{for } u_{2min} < u_{c2_k} < u_{2max} \\ u_{2max} & \text{for } u_{c2_k} > u_{2max} \end{cases}$$

$$\dot{\delta}_{Rc_k}^{B15} = u_{c2_k}^{B2} \frac{180^{B13}}{\pi} \quad \text{(deg/sec)}$$

$$\delta_{Rc} = \int \dot{\delta}_{Rc_k} + \delta_{R_{trim}} \qquad \text{(deg)}$$

Note: The $\dot{\delta}_{Rc_k}$ signal was integrated at the flight control computer major frame rate (≈20 cps).

IV. PREDICTIONS

A. Longitudinal Predictions

1. State

$$\eta_{L5_k}^{B1} = {}^{1}_{ES11}^{B0}\left(1 + x_{L2_k}^{B-1}\right) - x_{L2_k}^{B-1}\, C\gamma_o^{B0} + x_{L1_k}^{B-2}\, S\gamma_o^{B0}$$

$$+ \left({}^{1}_{ES13}^{B0} - S\gamma_o^{B0}\right) x_{L3_k}^{B-2} + {}^{1}_{ES12}^{B0}\, x_{3_k}^{B0}$$

$$\eta_{L6_k}^{B0} = {}^{1}_{ES31}^{B0}\left(1 + x_{L2_k}^{B-1}\right) + x_{L2_k}^{B-1}\, S\gamma_o^{B0} + x_{L1_k}^{B-2}\, C\gamma_o^{B0}$$

$$+ \left({}^{1}_{ES33}^{B0} - C\gamma_o^{B0}\right) x_{L3_k}^{B-2} + {}^{1}_{ES32}^{B0}\, x_{3_k}^{B0}$$

$$\hat{x}_{L1_{k+1}}^{B-2} = x_{L1_k}^{B-2} + \phi_{L12}\, x_{L2_k}^{B-1} + \phi_{L13}\, x_{L3_k}^{B-1} + \phi_{L14}\, x_{L4_k}^{B0}$$

$$+ \phi_{L17}\, x_{L7_k}^{B-2} + \phi_{L18}\, x_{L8_k}^{B-7} + \phi_{L19}\, x_{L9_k}^{B5}$$

$$+ \gamma_{L11}\, u_{CL1_k}^{B-8} + \gamma_{L12}\, u_{CL2_k}^{B6}$$

$$+ \gamma_{Lw_{11}}^{B0} w_{L1_k}^{B-2} + \gamma_{Lw_{13}}^{B0} w_{L3_k}^{B-2} + \gamma_{Lw_{14}}^{B-1} w_{L4_k}^{B-1}$$

$$+ \gamma_{Lw_{15}}^{B-1} w_{L5_k}^{B-1} + \gamma_{Lw_{16}}^{B0} w_{L6_k}^{B-2} + \psi_{L11}^{B0} \eta_{L1_k}^{B-2} + \psi_{L12}^{B0} \eta_{L2_k}^{B-2}$$

$$+ \psi_{L13}^{B0} \eta_{L3_k}^{B-2}$$

$$\hat{x}_{L2_{k+1}}^{B-1} = \phi_{L21}^{B1} x_{L1_k}^{B-2} + \phi_{L22}^{B0} x_{L2_k}^{B-1} + \phi_{L23}^{B1} x_{L3_k}^{B-2} + \phi_{L24}^{B0} x_{L4_k}^{B-1}$$

$$+ \phi_{L27}^{B-6} x_{L7_k}^{B5} + \phi_{L28}^{B-7} x_{L8_k}^{B8} + \phi_{L29}^{B1} x_{L9_k}^{B-2}$$

$$+ \gamma_{L21}^{B-5} u_{CL1_k}^{B2} + \gamma_{L23}^{B-10} u_{CL3_k}^{B7} + \gamma_{Lw_{21}}^{B1} w_{L1_k}^{B-2}$$

$$+ \gamma_{Lw_{23}}^{B1} w_{L3_k}^{B-2} + \gamma_{Lw_{24}}^{B0} w_{L4_k}^{B-1} + \gamma_{Lw_{25}}^{B0} w_{L5_k}^{B-1}$$

$$+ \gamma_{L2_{26}}^{B1} w_{L6_k}^{B-2} + \psi_{L21}^{B1} \eta_{L1_k}^{B-2} + \psi_{L22}^{B1} \eta_{L2_k}^{B-2}$$

$$+ \psi_{L23}^{B1} \eta_{L3_k}^{B-2}$$

$$\hat{x}^{B-2}_{L3_{k+1}} = \phi^{B0}_{L31}\, x^{B-2}_{L1_k} + \phi^{B-1}_{L32}\, x^{B-1}_{L2_k} + \phi^{B0}_{L33}\, x^{B-2}_{L3_k} + \phi^{B-1}_{L34}\, x^{B-1}_{L4_k}$$

$$+ \phi^{B-7}_{L37}\, x^{B5}_{L7_k} + \phi^{B-8}_{L38}\, x^{B6}_{L8_k} + \phi^{B0}_{L39}\, x^{B-2}_{L9_k}$$

$$+ \gamma^{B-4}_{L31}\, u^{B2}_{CL1_k} + \gamma^{B2}_{L32}\, u^{B-4}_{CL2_k} + \gamma^{B0}_{Lw_{31}}\, w^{B-2}_{L1_k}$$

$$+ \gamma^{B0}_{Lw_{33}}\, w^{B-2}_{L3_k} + \gamma^{B-1}_{Lw_{34}}\, w^{B-1}_{L4_k} + \gamma^{B-1}_{Lw_{35}}\, w^{B-1}_{L5_k}$$

$$+ \gamma^{B0}_{Lw_{36}}\, w^{B-2}_{L6_k} + \psi^{B0}_{L31}\, \eta^{B-2}_{L1_k} + \psi^{B0}_{L32}\, \eta^{B-2}_{L2_k} + \psi^{B1}_{L33}\, \eta^{B-2}_{L3_k}$$

$$\hat{x}^{B-2}_{L4_{k+1}} = \phi^{B0}_{L41}\, x^{B-2}_{L1_k} + \phi^{B-1}_{L42}\, x^{B-1}_{L2_k} + \phi^{B0}_{L43}\, x^{B-2}_{L3_k} + \phi^{B-1}_{L44}\, x^{B-1}_{L4_k}$$

$$+ \phi^{B-6}_{L47}\, x^{B5}_{L7_k} + \phi^{B-7}_{L48}\, x^{B6}_{L8_k} + \phi^{B1}_{L49}\, x^{B-2}_{L9_k}$$

$$+ \gamma^{B-3}_{L41}\, u^{B2}_{CL1_k} + \gamma^{B3}_{L42}\, u^{B-4}_{CL2_k} + \gamma^{B-8}_{L43}\, u^{B-7}_{CL3_k}$$

$$+ \gamma^{B1}_{Lw_{41}}\, w^{B-2}_{L1_k} + \gamma^{B1}_{Lw_{43}}\, w^{B-2}_{L3_k} + \gamma^{B0}_{Lw_{44}}\, w^{B-1}_{L4_k}$$

$$+ \gamma^{B0}_{Lw_{45}}\, w^{B-1}_{L5_k} + \gamma^{B1}_{Lw_{46}}\, w^{B-2}_{L6_k} + \psi^{B1}_{L41}\, \eta^{B-2}_{L1_k}$$

$$+ \psi_{L42}\ {}^{B1}\eta_{L2_k}\ {}^{B-2} + \psi_{L43}\ {}^{B1}\eta_{L3_k}\ {}^{B-2}$$

$$\hat{x}_{L5_{k+1}}^{B10(DP)} = \phi_{L51}\ {}^{B-1}x_{L1_k}\ {}^{B-2} + \phi_{L52}\ {}^{B-2}x_{L2_k}\ {}^{B-1} + \phi_{L53}\ {}^{B-1}x_{L3_k}\ {}^{B-2} + \phi_{L54}\ {}^{B-2}x_{L4_k}\ {}^{B-1}$$

$$+ {}^{B10(DP)}x_{L5_k}\ {}^{B-8} + \phi_{L57}\ {}^{B5}x_{L7_k}\ {}^{B-9} + \phi_{L58}\ {}^{B6}x_{L8_k}\ {}^{B-1} + \phi_{L59}\ {}^{B-2}x_{L9_k}$$

$$+ \gamma_{L51}\ {}^{B-5}u_{CL1_k}\ {}^{B2} + \gamma_{Lw_{51}}\ {}^{B-1}w_{L1_k}\ {}^{B-2} + \gamma_{Lw_{53}}\ {}^{B-1}w_{L3_k}\ {}^{B-2}$$

$$+ \gamma_{Lw_{54}}\ {}^{B-2}w_{L4_k}\ {}^{B-1} + \gamma_{Lw_{55}}\ {}^{B-2}w_{L5_k}\ {}^{B-1} + \gamma_{Lw_{56}}\ {}^{B-1}w_{L6_k}\ {}^{B-2}$$

$$+ \psi_{L51}\ {}^{B-1}\eta_{L1_k}\ {}^{B-2} + \psi_{L52}\ {}^{B-2}\eta_{L2_k}\ {}^{B-1} + \psi_{L53}\ {}^{B-1}\eta_{L3_k}\ {}^{B-2}$$

$$+ \psi_{L55}\ {}^{B-2}\eta_{L5_k}\ {}^{B1}$$

$$\hat{x}_{L6_{k+1}}^{B6(DP)} = \phi_{L61}\ {}^{B-1}x_{L1_k}\ {}^{B-2} + \phi_{L62}\ {}^{B-2}x_{L2_k}\ {}^{B-1} + \phi_{L63}\ {}^{B-1}x_{L3_k}\ {}^{B-2} + \phi_{L64}\ {}^{B-2}x_{L4_k}\ {}^{B-1}$$

$$+ {}^{B6(DP)}x_{L6_k}\ {}^{B-8} + \phi_{L67}\ {}^{B5}x_{L7_k}\ {}^{B-9} + \phi_{L68}\ {}^{B6}x_{L8_k}\ {}^{B-1} + \phi_{L69}\ {}^{B-2}x_{L9_k}$$

$$+ \gamma_{L61}\ {}^{B-5}u_{CL1_k}\ {}^{B2} + \gamma_{Lw_{61}}\ {}^{B-1}w_{L1_k}\ {}^{B-2} + \gamma_{Lw_{63}}\ {}^{B-1}w_{L3_k}\ {}^{B-2}$$

$$+ \gamma_{Lw_{64}}^{B-2} w_{L4_k}^{B-1} + \gamma_{Lw_{65}}^{B-2} w_{L5_k}^{B-1} + \gamma_{Lw_{66}}^{B-1} w_{L6_k}^{B-2}$$

$$+ \psi_{L61}^{B-1} \eta_{L1_k}^{B-2} + \psi_{L62}^{B-1} \eta_{L2_k}^{B-2} + \psi_{L63}^{B-1} \eta_{L3_k}^{B-2}$$

$$+ \psi_{L66}^{B-3} \eta_{L6_k}^{B0}$$

$$\hat{x}_{L7_{k+1}}^{B5} = \phi_{L77}^{B0} x_{L7_k}^{B5} + \phi_{L78}^{B-1} x_{L8_k}^{B6} + \gamma_{L73}^{B-2} u_{CL3_k}^{B7}$$

$$\hat{x}_{L9_{k+1}}^{B-2} = x_{L9_k}^{B-2} + \gamma_{L92}^{B2} u_{CL2_k}^{B-4}$$

2. Winds

$$\hat{w}_{L1_{k+1}}^{B-2} = \phi_{Lw_{11}}^{B0} w_{L1_k}^{B-2} + \phi_{Lw_{12}}^{B0} w_{L2_k}^{B-2}$$

$$\hat{w}_{L2_{k+1}}^{B-2} = \phi_{Lw_{21}}^{B0} w_{L1_k}^{B-2} + \phi_{Lw_{22}}^{B0} w_{L2_k}^{B-2}$$

$$\hat{w}_{L3_{k+1}}^{B-2} = \phi_{Lw_{31}}^{B0} w_{L1_k}^{B-2} + \phi_{Lw_{32}}^{B0} w_{L2_k}^{B-2} + \phi_{Lw_{33}}^{B0} w_{L3_k}^{B-2}$$

$$\hat{w}_{L4_{k+1}}^{B-1} = \phi_{Lw_{44}}^{B0} w_{L4_k}^{B-1}$$

$$\hat{w}^{B-1}_{L5_{k+1}} = w^{B-1}_{L5_k} + \phi^{B1}_{Lw_{57}} w^{B-2}_{L7_k}$$

$$\hat{w}^{B-2}_{L6_{k+1}} = w^{B-2}_{L6_k}$$

$$\hat{w}^{B-2}_{L7_{k+1}} = w^{B-2}_{L7_k}$$

3. Biases

$$\hat{b}^{B-2(DP)}_{L1_{k+1}} = \hat{b}^{B-2(DP)}_{L1_k} + f^{B0}_{Lb_{11}} \nu^{B-2}_{L1_k} + f^{B-6}_{Lb_{13}} \nu^{B4}_{L3_k} + f^{B-6}_{Lb_{14}} \nu^{B4}_{L4_k}$$

$$+ f^{B-6}_{Lb_{15}} \nu^{B4}_{L5_k} + f^{B0}_{Lb_{16}} \nu^{B-2}_{L6_k} + f^{B0}_{Lb_{17}} \nu^{B-2}_{L7_k}$$

$$+ f^{B-1}_{Lb_{18}} \nu^{B-1}_{L8_k} + f^{B0}_{Lb_{19}} \nu^{B-2}_{L9_k}$$

$$\hat{b}^{B4(DP)}_{L5_{k+1}} = \hat{b}^{B4(DP)}_{L5_k} + f^{B4}_{Lb_{51}} \nu^{B-2}_{L1_k} + f^{B-2}_{Lb_{53}} \nu^{B4}_{L3_k} + f^{B-2}_{Lb_{54}} \nu^{B4}_{L4_k}$$

$$+ f^{B-2}_{Lb_{55}} \nu^{B4}_{L5_k} + f^{B4}_{Lb_{56}} \nu^{B-2}_{L6_k} + f^{B4}_{Lb_{57}} \nu^{B-2}_{L7_k}$$

$$+ f^{B3}_{Lb_{58}} \nu^{B-1}_{L8_k} + f^{B4}_{Lb_{59}} \nu^{B-2}_{L9_k}$$

$$\hat{b}^{B-2(DP)}_{L6_{k+1}} = \hat{b}^{B-2(DP)}_{L6_k} + f^{B0\ B-2}_{Lb_{61}} \nu_{L1_k} + f^{B-6\ B4}_{Lb_{63}} \nu_{L3_k} + f^{B-6\ B4}_{Lb_{64}} \nu_{L4_k}$$

$$+ f^{B-6\ B4}_{Lb_{65}} \nu_{L5_k} + f^{B0\ B-2}_{Lb_{66}} \nu_{L6_k} + f^{B0\ B-2}_{Lb_{67}} \nu_{L7_k}$$

$$+ f^{B-1\ B-1}_{Lb_{68}} \nu_{L8_k} + f^{B0\ B-2}_{Lb_{69}} \nu_{L9_k}$$

$$\hat{b}^{B-2(DP)}_{L7_{k+1}} = \hat{b}^{B-2(DP)}_{L7_k} + f^{B-4\ B-2}_{Lb_{71}} \nu_{L1_k} + f^{B-10\ B4}_{Lb_{73}} \nu_{L3_k} + f^{B-10\ B4}_{Lb_{74}} \nu_{L4_k} + f^{B-10\ B4}_{Lb_{75}} \nu_{L5_k}$$

$$+ f^{B-4\ B-2}_{Lb_{76}} \nu_{L6_k} + f^{B-4\ B-2}_{Lb_{77}} \nu_{L7_k} + f^{B-5\ B-1}_{Lb_{78}} \nu_{L8_k}$$

$$+ f^{B-4\ B-2}_{Lb_{79}} \nu_{L9_k}$$

$$\hat{b}^{B-2(DP)}_{L9_{k+1}} = \hat{b}^{B-2(DP)}_{L9_k} + f^{B-4\ B-2}_{Lb_{91}} \nu_{L1_k} + f^{B-10\ B4}_{Lb_{93}} \nu_{L3_k} + f^{B-10\ B4}_{Lb_{94}} \nu_{L4_k}$$

$$+ f^{B-10\ B4}_{Lb_{95}} \nu_{L5_k} + f^{B-4\ B-2}_{Lb_{96}} \nu_{L6_k} + f^{B-4\ B-2}_{Lb_{97}} \nu_{L7_k}$$

$$+ f^{B-5\ B-1}_{Lb_{98}} \nu_{L8_k} + f^{B-4\ B-2}_{Lb_{99}} \nu_{L9_k}$$

4. Measurement Vector

$$\hat{y}^{B-2(DP)}_{L6_{k+1}} = c^{B0}_{Lx_{61}} \hat{x}^{B-2}_{L1_{k+1}} + c^{B-1}_{Lx_{62}} \hat{x}^{B-1}_{L2_{k+1}} + c^{B0}_{Lx_{63}} \hat{x}^{B-2}_{L3_{k+1}} + \hat{b}^{B-2(DP)}_{L6_{k+1}}$$

$$\hat{y}^{B-2(DP)}_{L7_{k+1}} = c^{B0}_{Lx_{71}} \hat{x}^{B-2}_{L1_{k+1}} + c^{B-1}_{Lx_{72}} \hat{x}^{B-1}_{L2_{k+1}} + c^{B0}_{Lx_{73}} \hat{x}^{B-2}_{L3_{k+1}}$$

$$+ c^{B-1}_{Lx_{74}} \hat{x}^{B-1}_{L4_{k+1}} + c^{B-7}_{Lx_{77}} \hat{x}^{B5}_{L7_{k+1}} + c^{B0}_{Lx_{79}} \hat{x}^{B-2}_{L9_{k+1}}$$

$$+ c^{B0}_{Lw_{71}} \hat{w}^{B-2}_{L1_{k+1}} + c^{B0}_{Lw_{73}} \hat{w}^{B-2}_{L3_{k+1}} + c^{B-1}_{Lw_{74}} \hat{w}^{B-1}_{L4_{k+1}}$$

$$+ c^{B-1}_{Lw_{75}} \hat{w}^{B-1}_{L5_{k+1}} + c^{B0}_{Lw_{76}} \hat{w}^{B-2}_{L6_{k+1}} + \hat{b}^{B-2(DP)}_{L7_{k+1}}$$

$$\hat{y}^{B-1(DP)}_{L8_{k+1}} = \hat{x}^{B-1(DP)}_{L2_{k+1}} + c^{B1}_{Lw_{81}} \hat{w}^{B-2}_{L1_{k+1}} + c^{B0}_{Lw_{84}} \hat{w}^{B-1}_{L4_{k+1}}$$

$$+ c^{B0}_{Lw_{85}} \hat{w}^{B-1}_{L5_{k+1}} + c^{B1}_{Lw_{86}} \hat{w}^{B-2}_{L6_{k+1}}$$

$$\hat{y}^{B-2(DP)}_{L9_{k+1}} = c^{B0}_{Lx_{91}} \hat{x}^{B-2}_{L1_{k+1}} + c^{B-1}_{Lx_{92}} \hat{x}^{B-1}_{L2_{k+1}} + c^{B0}_{Lx_{93}} \hat{x}^{B-2}_{L3_{k+1}}$$

$$+ c^{B0}_{Lw_{85}} \hat{w}^{B-1}_{L5_{k+1}} + c^{B1}_{Lw_{86}} \hat{w}^{B-2}_{L6_{k+1}}$$

$$\hat{y}^{B-2(DP)}_{L9_{k+1}} = c_{Lx_{91}} \hat{x}^{B0}_{L1_{k+1}}{}^{B-2} + c_{Lx_{92}} \hat{x}^{B-1}_{L2_{k+1}}{}^{B-1} + c_{Lx_{93}} \hat{x}^{B0}_{L3_{k+1}}{}^{B-2}$$

$$+ c_{Lx_{94}} \hat{x}^{B-1}_{L4_{k+1}}{}^{B-1} + c_{Lx_{97}} \hat{x}^{B-7}_{L7_{k+1}}{}^{B5} + c_{Lx_{99}} \hat{x}^{B0}_{L9_{k+1}}{}^{B-2}$$

$$+ c_{Lw_{91}} \hat{w}^{B0}_{L1_{k+1}}{}^{B-2} + c_{Lw_{94}} \hat{w}^{B-1}_{L4_{k+1}}{}^{B-1} + c_{Lw_{95}} \hat{w}^{B-1}_{L5_{k+1}}{}^{B-1}$$

$$+ c_{Lw_{96}} \hat{w}^{B0}_{L6_{k+1}}{}^{B-2} + \hat{b}^{B-2(DP)}_{L9_{k+1}}$$

B. Lateral Predictions

1. State

$$\hat{x}^{B0}_{1_{k+1}} = \phi_{11}\, x^{B0}_{1_k}{}^{B0} + \phi_{14}\, x^{B1}_{4_k}{}^{B-1} + \phi_{15}\, x^{B1}_{5_k}{}^{B-1} - \psi_{11}\, \zeta^{B-1}_{1_k}{}^{B1}$$

$$- \psi_{13}\, \zeta^{B1}_{3_k}{}^{B-1} - \psi_{14}\, \zeta^{B-2}_{4_k}{}^{B2} - \psi_{15}\, \zeta^{B0}_{5_k}{}^{B0}$$

$$\hat{x}^{B2}_{2_{k+1}} = \phi_{21}\, x^{B2}_{1_k}{}^{B0} + x^{B2}_{2_k}{}^{B0} + \phi_{24}\, x^{B3}_{4_k}{}^{B-1} + \phi_{25}\, x^{B3}_{5_k}{}^{B-1}$$

$$- \psi_{21}\, \zeta^{B1}_{1_k}{}^{B1} - \psi_{22}\, \zeta^{B3}_{2_k}{}^{B-1} - \psi_{23}\, \zeta^{B3}_{3_k}{}^{B-1} - \psi_{24}\, \zeta^{B0}_{4_k}{}^{B2} - \psi_{25_k}\, \zeta^{B2}_{5}{}^{B0}$$

$$\hat{x}_{3_{k+1}}^{B0} = \phi_{31}^{B0\,B0}\, x_{1_k} + \phi_{33}^{B0\,B0}\, x_{3_k} \phi_{34}^{B1\,B-1}\, x_{4_k} + \phi_{35}^{B1\,B-1}\, x_{5_k} + \phi_{37}^{B1\,B-1}\, x_{7_k}$$

$$+ \gamma_{31}^{B-2\,B2}\, u_{C1_k} + \gamma_{32}^{B-2\,B2}\, u_{C2_k} + \gamma_{w_{31}}^{B1\,B-1}\, w_{1_k} + \gamma_{w_{33}}^{B2\,B-2}\, w_{3_k}$$

$$+ \gamma_{w_{34}}^{B2\,B-2}\, w_{4_k} + \gamma_{w_{35}}^{B1\,B-1}\, w_{5_k} - \psi_{31}^{B-1\,B1}\, \zeta_{1_k} - \psi_{33}^{B1\,B-1}\, \zeta_{3_k}$$

$$- \psi_{34}^{B-2\,B2}\, \zeta_{4_k} - \psi_{35}^{B0\,B0}\, \zeta_{5_k}$$

$$\hat{x}_{4_{k+1}}^{B-1} = \phi_{41}^{B-1\,B0}\, x_{1_k} + \phi_{43}^{B-1\,B0}\, x_{3_k} + \phi_{44}^{B0\,B-1}\, x_{4_k} + \phi_{45}^{B0\,B-1}\, x_{5_k} + \phi_{47}^{B0\,B-1}\, x_{7_k}$$

$$+ \gamma_{41}^{B-1\,B2}\, u_{C1_k} + \gamma_{42}^{B-3\,B2}\, u_{C2_k} + \gamma_{w_{41}}^{B0\,B-1}\, w_{1_k} + \gamma_{w_{43}}^{B1\,B-2}\, w_{3_k}$$

$$+ \gamma_{w_{44}}^{B1\,B-2}\, w_{4_k} + \gamma_{w_{45}}^{B0\,B-1}\, w_{5_k} - \psi_{41}^{B-2\,B1}\, \zeta_{1_k} - \psi_{43}^{B0\,B-1}\, \zeta_{3_k}$$

$$- \psi_{44}^{B-3\,B2}\, \zeta_{4_k} - \psi_{45}^{B-1\,B0}\, \zeta_{5_k}$$

$$\hat{x}_{5_{k+1}}^{B-1} = \phi_{51}^{B-1\,B0}\, x_{1_k} + \phi_{53}^{B-1\,B0}\, x_{3_k} + \phi_{54}^{B0\,B-1}\, x_{4_k} + \phi_{55}^{B0\,B-1}\, x_{5_k} + \phi_{57}^{B0\,B-1}\, x_{7_k}$$

$$+ \gamma_{51}^{B-3\,B2}\, u_{C1_k} + \gamma_{52}^{B-3\,B2}\, u_{C2_k} + \gamma_{w_{51}}^{B0\,B-1}\, w_{1_k} + \gamma_{w_{53}}^{B0\,B-1}\, w_{3_k}$$

$$+ \gamma_{w_{54}}{}^{B1}\, w_{4_k}{}^{B-2} + \gamma_{w_{55}}{}^{B0}\, w_{5_k}{}^{B-1} - \psi_{51}{}^{B-2}\, \zeta_{1_k}{}^{B1} - \psi_{53}{}^{B0}\, \zeta_{3_k}{}^{B-1}$$

$$- \psi_{54}{}^{B-3}\, \zeta_{4_k}{}^{B2} - \psi_{55}{}^{B-1}\, \zeta_{5_k}{}^{B0}$$

$$\hat{x}_{6_{k+1}}{}^{B6(DP)} = \phi_{61}{}^{B0}\, x_{1_k}{}^{B0} + \phi_{62}{}^{B-2}\, x_{2_k}{}^{B2} + \phi_{63}{}^{B0}\, x_{3_k}{}^{B0} + \phi_{64}{}^{B1}\, x_{4_k}{}^{B-1} + \phi_{65}{}^{B1}\, x_{5_k}{}^{B-1}$$

$$+ x_{6_k}{}^{B6(DP)} + \phi_{67}{}^{B1}\, x_{7_k}{}^{B-1} + \gamma_{61}{}^{B-2}\, u_{c1_k}{}^{B2} + \gamma_{62}{}^{B-2}\, u_{c2_k}{}^{B2}$$

$$+ \gamma_{w_{61}}{}^{B1}\, w_{1_k}{}^{B-1} + \gamma_{w_{63}}{}^{B2}\, w_{3_k}{}^{B-2} + \gamma_{w_{64}}{}^{B2}\, w_{4_k}{}^{B-2} + \gamma_{w_{65}}{}^{B1}\, w_{5_k}{}^{B-1}$$

$$- \psi_{61}{}^{B-1}\, \zeta_{1_k}{}^{B1} - \psi_{62}{}^{B1}\, \zeta_{2_k}{}^{B-1} - \psi_{63}{}^{B1}\, \zeta_{3_k}{}^{B-1} - \psi_{64}{}^{B-1}\, \zeta_{4_k}{}^{B2}$$

$$- \psi_{65}{}^{B0}\, \zeta_{5_k}{}^{B0} - \psi_{66}{}^{B-2}\, \zeta_{6_k}{}^{B2}$$

$$\hat{x}_{7_{k+1}}{}^{B-1} = x_{7_k}{}^{B-1} + \gamma_{72}{}^{B-3}\, u_{c2_k}{}^{B2}$$

2. Winds

$$\hat{w}_{1_{k+1}}{}^{B-1} = \phi_{w_{11}}{}^{B0}\, w_{1_k}{}^{B-1} + \phi_{w_{12}}{}^{B1}\, w_{2_k}{}^{B-2}$$

$$\hat{w}_{2_{k+1}}{}^{B-2} = \phi_{w_{21}}{}^{B-1}\, w_{1_k}{}^{B-1} + \phi_{w_{22}}{}^{B0}\, w_{2_k}{}^{B-2}$$

$$\hat{w}_{3_{k+1}}^{B-2} = \phi_{w_{31}}^{B-1} w_{1_k}^{B-1} + \phi_{w_{32}}^{B0} w_{2_k}^{B-2} + \phi_{w_{33}}^{B0} w_{3_k}^{B-2}$$

$$\hat{w}_{4_{k+1}}^{B-2} = \phi_{w_{44}}^{B0} w_{4_k}^{B-2}$$

$$\hat{w}_{5_{k+1}}^{B-1} = w_{5_k}^{B-1} + \phi_{w_{56}}^{B1} w_{6_k}^{B-2}$$

$$\hat{w}_{6_{k+1}}^{B-2} = \phi_{w_{66}}^{B0} w_{6_k}^{B-2}$$

3. Biases

$$\hat{b}_{\phi_{k+1}}^{B0(DP)} = \hat{b}_{\phi_k}^{B0(DP)B0} + g_\phi \nu_{1_k}^{B0}$$

$$\hat{b}_{\psi_{k+1}}^{B2(DP)} = \hat{b}_{\psi_k}^{B2(DP)B0} + g_\psi \nu_{2_k}^{B2}$$

$$\hat{b}_{f_{y\ k+1}}^{B-2(DP)} = \hat{b}_{f_{y_k}}^{B-2(DP)} + g_{f_y} \nu_{6_k}^{B1}$$

4. Measurement Vector

$$\hat{y}_{6_{k+1}}^{B-3(DP)} = c_{x_{63}}^{B-2} \hat{x}_{3_{k+1}}^{B0} + c_{x_{64}}^{B-1} \hat{x}_{4_{k+1}}^{B-1} + c_{x_{65}}^{B-1} \hat{x}_{5_{k+1}}^{B-1}$$

$$+ c_{x_{67}}^{B-1} \hat{x}_{7_{k+1}}^{B-1} + c_{w_{61}}^{B-1} \hat{w}_{1_{k+1}}^{B-1} + c_{w_{63}}^{B0} \hat{w}_{3_{k+1}}^{B-2}$$

$$+ \overset{B0}{c_{w_{64}}} \overset{B-2}{\hat{w}_{4_{k+1}}} + \overset{B-1}{c_{w_{65}}} \overset{B-1}{\hat{w}_{5_{k+1}}} + \overset{B-2(DP)}{\hat{b}_{fy_{k+1}}}$$

C. Euler Prediction Matrices

$$\begin{matrix}\sin \\ \cos\end{matrix} \hat{\theta} = \begin{matrix}\sin \\ \cos\end{matrix} \begin{bmatrix} \overset{B2}{\theta_o} + \overset{B-2}{\hat{x}_{L1_{k+1}}} & \overset{B-1}{\frac{1}{\pi}} \end{bmatrix}$$

$$\begin{matrix}\sin \\ \cos\end{matrix} \hat{\phi} = \begin{matrix}\sin \\ \cos\end{matrix} \left(\overset{B0}{\hat{x}_{1_{k+1}}} \quad \overset{B1}{\frac{1}{\pi}} \right)$$

$$\begin{matrix}\sin \\ \cos\end{matrix} \hat{\psi} = \begin{matrix}\sin \\ \cos\end{matrix} \left(\overset{B2}{\hat{x}_{2_{k+1}}} \quad \overset{B1}{\frac{1}{\pi}} \right)$$

$$\hat{1}_{ES22} = \sin \hat{\phi} \sin \hat{\theta} \sin \hat{\psi} + \cos \hat{\phi} \cos \hat{\psi}$$

$$\hat{1}_{EB31} = -\sin \hat{\theta}$$

$$\hat{1}_{EB32} = \sin \hat{\phi} \cos \hat{\theta}$$

$$\hat{1}_{EB33} = \cos \hat{\phi} \cos \hat{\theta}$$

$$\hat{1}_{ES31} = \hat{1}_{EB31} C_{\alpha_o} + \hat{1}_{EB33} S_{\alpha_o}$$

$$\hat{1}_{ES33} = \hat{1}_{EB31} (-S_{\alpha_o}) + \hat{1}_{EB33} C_{\alpha_o}$$

D. Altitude and Path Parameter Prediction

1. Altitude Prediction

If not GSENG, Go to 2.

$$\hat{\eta}^{B0}_{L6_{k+1}} = (\hat{1}^{B0}_{ES31} + S\alpha_o)\,\hat{x}^{B-1}_{L2_{k+1}} + \hat{1}^{B0}_{ES31}$$

$$+ \hat{x}^{B-2}_{L1_{k+1}}\, C\gamma_o^{B0} + (\hat{1}^{B0}_{ES33} - C\gamma_o)\,\hat{x}^{B-2}_{L3_{k+1}} + \hat{1}^{B0}_{ES32}\,\hat{x}^{B0}_{3_{k+1}}$$

B13 B6(DP) B8

$$\bar{H} = -x_{L6_k}\, U_o$$

2. Sideslip Parameters

If not LOCE, skip over $\hat{\beta}_k$ and $\hat{\xi}_k$ computations

$$\hat{\beta}^{B-1}_{k+1} = \frac{\hat{w}^{B-1}_{5_{k+1}}}{\hat{1}^{B0}_{ES22}}$$

$$\hat{\xi}^{B-1}_{k+1} = \hat{\beta}^{B-1}_{k+1} - \hat{w}^{B-1}_{1_{k+1}} - \hat{w}^{B-1}_{5_{k+1}}$$

V. INITIALIZATION

A. Computation of α_o, θ_o

U_{ok} = calibrated airspeed selected by pilot (knots)
WEITO = empty fuel weight (LBS/10)

B7

$$\frac{WEIGHT}{1000} = WEITO/100 + TFQ/1000$$

If $(U_{ok} \leq 127)$, then

B-6 B-14 B8 B-6(DP)

$$a_1 = 0.000056791\ (U_{ok}) - 0.007992711$$

B1 B-7 B8 B1(DP)

$$a_2 = -0.003278089\ (U_{ok}) + 0.465299649$$

B1 B-7 B8 B1(DP)

$$b_1 = -0.003272937\ (U_{ok}) + 0.559452617$$

B8 B0 B8 B8(DP)

$$b_2 = 0.061661686\ (U_{ok}) - 18.39413409$$

Otherwise

B-6 B-14 B8 B-6(DP)

$$a_1 = .000029097\ (U_{ok}) + -0.004475519$$

B1 B-7 B8 B1(DP)

$$a_2 = -0.001527618\ (U_{ok}) + 0.242989939$$

B1 B-7 B8 B1(DP)

$$b_1 = -0.004484078\ (U_{ok}) + 0.713267456$$

B8 B0 B8 B8(DP)

$$b_2 = 0.195679600\ (U_{ok}) - 35.41440925$$

B1 B-6 B7 B1

$$a_3 = a_1\ (\frac{\text{WEIGHT}}{1000}) + a_2$$

B8 B1 B7 B8

$$b_3 = b_1\ (\frac{\text{WEIGHT}}{1000}) + b_2$$

γ_o = GAMO where GAMO is entered value

$$\alpha_o = (a_3\gamma_o + b_3)$$

$$\theta_o = \alpha_o + \gamma_o$$

B0

$$S_{\alpha_o} = \sin \alpha$$

B0

$$C_{\alpha_o} = \cos \alpha_o$$

B0

$$S\gamma_o = \sin \gamma_o$$

B0

$$C\gamma_o = \cos \gamma_o$$

B0 B0

$$c_{Lx}\ (6,1) = -\cos \gamma_o$$

B-1 B0

$$c_{Lx}\ (6,2) = -\sin \gamma_o$$

B0 B0

$$c_{Lx}(6,3) = \cos \gamma_o$$

B1

$$SC\gamma_o = 1/C\gamma_o$$

B1

$$T_{\gamma_o} = \tan \gamma_o$$

B0

$$S_{\theta_o} = \sin \theta_o$$

B0

$$C_{\theta_o} = \cos \theta_o$$

B8 B7

$$U_o = U_o \quad (1.6878)$$

B-7 B1 B8

$$UOI = 1./U_o$$

B. Computation of T_o, Th_o (Routine: INIAT)

B-7 B-14 B7 B-7

$$a_1 = 0.000034840605 \left(\frac{WEIGHT}{1000}\right) - .00201123645$$

B1 B-6 B7 B1

$$a_2 = .01299031000 \left(\frac{WEIGHT}{1000}\right) + .29543500$$

B-1 B-8 B7 B-1

$$b_1 = -.00245252350 \left(\frac{WEIGHT}{1000}\right) + .279123915$$

B7 B0 B7 B7

$$b_2 = .405932250 \left(\frac{WEIGHT}{1000}\right) - 29.95779350$$

B1 B-7 B8 B1

$$a_3 = a_1 \; U_{ok} + a_2$$

B7 B-1 B8 B7

$$b_3 = b_1 \; U_{ok} + b_2$$

B5 B1 B6 B7

$$T_o = a_3 \gamma_o + b_3$$

1000 lbs

where γ_o is in deg

B6 B1 B6

$$Th_o = 1.51994 \; T_o + 5.257256565$$

C. Glideslope Parameters

$$z_{INT} = 0$$

$$J_{GSC} = 0$$

$$K_{FL} = 0$$

$$e_{LX6_k} = 0.125$$

$$\hat{b}_{L1_k} = 0$$

$$\hat{b}_{\phi} = 0$$

D. Flare Parameters

$EZ5 = 0$

$EZ7 = 0$

$J_{Flare} = 0$

$\Delta V_{FK} = 0$

$K_{FL} = 0$

$T_{\gamma D} = T_{\gamma_o}$

B-1 B6 B-7

$\Delta V_{FL} = -25$ UOI

B-2 B5 B-7

$\Delta V_{FR} = 1.25$ UOI

B-1(DP) B-3 B-7

$\Delta V_{FD} = (1.25\Delta T)$ UOI

B6 B13 B-7

$h_{FLR} = HFLR_F$ UOI

B6 B13 B-7

$x_{FLR} = XFLR_F$ UOI

$$h^{B6}_{1/2\,p} = \frac{h^{B6}_{FLR} - T^{B0}_{\gamma_o}\, x^{B6}_{FLR}}{T^{B0}_{\gamma TD} - T^{B0}_{\gamma_o}}$$

B6 B6 B6

$$\Delta x_f = h_{1/2\,p} - x_{FLR}$$

B6(DP) B0 B6 B6

$$h_f = T_{\gamma_o} (x_{FLR} - 2h_{1/2\,p})$$

B10(DP) B6

$$x_{FLR} = x_{FLR}$$

$$h'' = h''' = 0$$

$$z_{L6} = 0$$

$$\left.\begin{aligned} h_{Lx3}(i) &= h_{Lx0i3} \\ h_{Lx4}(i) &= h_{Lx0i4} \\ h_{Lx6}(i) &= h_{Lxi6} \end{aligned}\right\} \quad \text{for } i = 1, 2, 3$$

E. Wind Parameters

B-1 B8 B-9

$$DT(4) = U_o * .00099758$$

$$\phi_{L5i} = -\sin \gamma_o \quad \psi_{L1i} + \cos \gamma_o \quad \psi_{L2i} + \sin \gamma_o \quad \psi_{L3i}$$

$$\phi_{L6i} = -\cos \gamma_o \quad \psi_{L1i} - \sin \gamma_o \quad \psi_{L2i} + \cos \gamma_o \quad \psi_{L3i}$$

for i = 1, 4 and i = 7,9

VI. PATH CAPTURE CRITERIA AND LOGIC

A. Pre-Capture Equations

$$\bar{\theta}^{B-2}_{B0} = \text{Asin}(\sin\theta)^{B0}_{B0}$$

$$\bar{\phi}^{B0}_{B0} = \text{Asin}(\sin\phi)^{B0}_{B0}$$

$$\bar{\psi}^{B2}_{B2} = \psi^{B2}_{T} - \psi^{B2}_{R/W}$$

Calculate Transformation Matrices L_{EB} and L_{ES} according to equations in Section II. G. and H.

$$\dot{X}'^{B1}_{k} = -\dot{X}^{B9}_{B-7}{}_{UOI}$$

$$\dot{Y}'^{B1}_{k} = \dot{Y}^{B9}_{B-7}{}_{UOI}$$

$$\dot{Z}'^{B1}_{k} = -\dot{Z}^{B9}_{B-7}{}_{UOI}$$

where $\hat{\dot{X}}$, $\hat{\dot{Y}}$, and $\hat{\dot{Z}}$ are the velocity estimates in the MLS coordinate frame, from the third order complementary filters in the flight control computer.

$$u'^{B-1}_{k}{}_{B0} = {}^{1}_{ES11}\dot{X}'^{B1}_{k}{}_{B0} + {}^{1}_{ES21}\dot{Y}'^{B1}_{k}{}_{B0} + {}^{1}_{ES31}\dot{Z}'^{B1}_{k}{}_{B1} - 1.0$$

$$\beta^{B-1}_{I_k}{}_{B0} = {}^{1}_{ES12}\dot{X}'^{B1}_{k}{}_{B0} + {}^{1}_{ES22}\dot{Y}'^{B1}_{k}{}_{B0} + {}^{1}_{ES32}\dot{Z}'^{B1}_{k}$$

$$\alpha_k^{B-2} = {}^{1}_{ES13}{}^{B0}\hat{X}'^{B1}_k + {}^{1}_{ES23}{}^{B0}\hat{Y}'^{B1}_k + {}^{1}_{ES33}{}^{B0}\hat{Z}'^{B1}_k$$

If (GSENG = 1) Go to VI. C.

B. Glideslope Capture Criteria

$$z_{L3_k}^{B-2} = \frac{-\left[{}^{1}_{ES31}{}^{B0} + T_{\gamma_o}\,{}^{1}_{ES11}{}^{B0}\,(1 + u_k'^{B-1}) + ({}^{1}_{ES32}{}^{B0} + T_{\gamma_o}\,{}^{1}_{ES12}{}^{B0})\,\beta_{I_k}^{B-1}\right]}{({}^{1}_{ES33}{}^{B0} + T_{\gamma_o}\,{}^{1}_{ES13}{}^{B0})\text{ at B1}}$$

$$\hat{x}_{L1_k}^{B-2} = x_{L1_k}^{B-2} = \bar{\theta}^{B-2} - \theta_o$$

$$\hat{x}_{L2_k}^{B-1} = x_{L2_k}^{B-1} = u_k'^{B-1}$$

$$\hat{x}_{L3_k}^{B-2} = x_{L3_k}^{B-2} = \alpha_k^{B-2}$$

$$e_{Lx1_k}^{B-2} = \hat{x}_{L1_k}^{B-2}$$

$$e_{Lx2_k}^{B-2} = V_a^{B9}\ {}^{B-7}UOI^{B2} - 1$$

$$e_{Lx3_k}^{B-2} = \alpha_k^{B-2} - z_{L3_k}^{B-2}$$

$$e_{Lx7_k}^{B5} = T^{B5} - T_o$$

$$e_{Lx8_k}^{B6} = \frac{TH_{LF} + TH_{RF}}{2}^{B6} - Th_o$$

$$e_{Lx9_k}^{B-2} = s - s_o$$

$$(\zeta_{L6_k} - \eta_{L6_k})^{B-2} = SC\gamma_o^{B1}\, e_{Lx3_k}^{B-2} - e_{Lx1_k}^{B-2} - \hat{\dot{Z}}'^{B1} - T_{\gamma_o}^{B0}\, \hat{\dot{X}}'^{B1}$$

$$h'^{B6(DP)}_{GSC} = T_{\gamma_o}^{B0}\, (x_{GPIP}^{B25(DP)} - \hat{X}^{B8}) / U_o + a_{GSC1}^{B2}\, e_{Lx1_k}^{B-2} + a_{GSC2}^{B2}\, e_{Lx2_k}^{B-2}$$

$$+ a_{GSC3}^{B2}\, e_{Lx3_k}^{B-2} + a_{GSC7}^{B5}\, e_{Lx7_k}^{B-5} + a_{GSC8}^{B6}\, e_{Lx8_k}^{B-6}$$

$$+ a_{GSC9}^{B2}\, e_{Lx9}^{B-2} + a_{GSC\zeta}^{B2}\, (\zeta_{L6_k} - \eta_{L6_k})^{B-2} + a_{GSCZ}^{B2}\, z_{L3}^{B-2}$$

Where $\hat{X}$ is the MLS frame x-coordinate estimate from the third order complementary filter.

C. State Initialization

$$\hat{x}_{L5}^{B10(DP)} = (x_{GPIP}^{B25(DP)} - \hat{X}^{B8}) / U_o$$

$$\hat{x}_{L6}^{B6(DP)} = x_{L6}^{B6(DP)} = -(\hat{Z}^{B25} + HTDC)\, UOI$$

(where $\hat{Z}$ is the z-coordinate from the third order complementary filter)

If $\hat{x}_{L6}^{B6(DP)} < h'^{B6(DP)}_{GSC}$ Go to end of section.

GSENG = 1

$u_{CL1} = 0$

B-1 27.4mu/dps B6

y_{L2} = q (41.7452) (rad/sec)

KFLC = 305

$\hat{w}_{L1} = \hat{w}_{L2} = \hat{w}_{L3} = \hat{w}_{L6} = \hat{w}_{L7} = 0$

B-1 B9 B-7 B-1 B0

$\hat{w}_{L4} = (V_a \ UOI - \hat{x}_{L2}) \ Pw_4$

B-1 B9 B-7 B2 B-1

$\hat{w}_{L5} = (V_a \ UOI - 1 - \hat{x}_{L2}) * (1-Pw_4)$

B-2(DP) B0 B-2 B-1 B-1 B0 V-2

$\hat{y}_{L6} = c_{Lx_{61}} \hat{x}_{L1} + c_{Lx_{62}} \hat{x}_{L2} + c_{Lx_{63}} \hat{x}_{L3}$

B-2(DP) B0 B-2 B-1 B-1 B0 B-2 B-1 B-1 B-1 B-1

$\hat{y}_{L7} = c_{Lx_{71}} \hat{x}_{L1} + c_{Lx_{72}} \hat{x}_{L2} + c_{Lx_{73}} \hat{x}_{L3} + c_{Lw_{74}} \hat{w}_{L4} + c_{Lw_{75}} \hat{w}_{L5}$

B-1(DP) B-1 B0 B-1 B0 B-1

$\hat{y}_{L8} = \hat{x}_{L2} + c_{Lw_{84}} \hat{w}_{L4} + c_{Lw_{85}} \hat{w}_{L5}$

B-2(DP) B0 B-2 B-1 B-1 B0 B-2 B-1 B-1 B-1 B-1

$\hat{y}_{L9} = c_{Lx_{91}} \hat{x}_{L1} + c_{Lx_{92}} \hat{x}_{L2} + c_{Lx_{93}} \hat{x}_{L3} + c_{Lw_{94}} \hat{w}_{L4} + c_{Lw_{95}} \hat{w}_{L5}$

$$z_{L1} = z_{L4} = z_{L6} = 0$$

$$\hat{b}_{L1} = \hat{b}_{L6} = \hat{b}_{L7} = \hat{b}_{L9} = 0 \text{ (DP)}$$

$$\hat{b}_{L5}^{B4(DP)B25(DP)B16(DP)B27(DP)B8\ B6(DP)} = (HBC - h_B - H_{TDC})/U_o - \hat{x}_{L6}$$

$$\hat{\eta}_{L6}^{B0} = (l_{ES31}^{B0} + \sin \gamma_o^{B0})\ \hat{x}_{L2}^{B-1} + l_{ES31}^{B0} + \hat{x}_{L1}^{B-2}\ \cos \gamma_o^{B0}$$

$$+ (l_{ES33}^{B0} - \cos \gamma_o^{B0})\ \hat{x}_{L3}^{B-2} + L_{ES32}^{B0}\ \beta_{I_k}^{B-1}$$

D. Localizer Capture Criteria

$$x_{1_k}^{B0} = \hat{x}_{1_k}^{B0} = \bar{\phi}^{B0}$$

$$x_{2_k}^{B2} = \hat{x}_{2_k}^{B2} = \bar{\psi}^{B2}$$

$$x_{3_k}^{B0} = \hat{x}_{3_k}^{B-1} = \beta_{I_k}^{B-1}$$

$$x_{4_k}^{B-1} = \hat{x}_{4_k}^{B-1} = p_k^{B-1} = p^{B-1}$$

$$x_{5_k}^{B-1} = \hat{x}_{5_k}^{B-1} = r_k^{B-1} = r^{B-1}$$

$$\hat{\beta}_k^{B-1} = \frac{1_{ES21}^{B0}}{1_{ES22}^{B9}} [\ (V_a^{B8} - U_o^{B-7})\ UOI^{B-1} - u_k'^{B-1}] - \beta_{I_k}^{B-1}$$

$$z_{3_k}^{B0} = -\hat{\beta}_k^{B-1}$$

$$\hat{w}_{5_k}^{B-1} = \hat{\beta}_k^{B-1} \; {}^{1}ES22^{B0}$$

$$\hat{\zeta}_k^{B-1} = \hat{\beta}_k^{B-1} - \hat{w}_{5_k}^{B-1}$$

$$Y_{Loc} = \left| \frac{h_{x12}}{h_{x16}}^{B4} \bar{\Psi}^{B2} + \frac{h_{x13}}{h_{x16}}^{B7} \beta_{I_k}^{B-1} + \frac{HSUM}{h_{x16}}^{B7} \hat{w}_5^{B-1} \right|$$

If $(|\hat{Y}|$ UOI $> Y_{Loc})$ skip to end.

where $\hat{Y}$ is the MLS frame y-coordinate from the third order complimentary filter. And

$$HSUM = h_{w_{15}} + h_{\zeta_{13}} a_{x33} + h_{\zeta 14} a_{x43} + h_{\zeta 15} a_{x53} + h_{\zeta 16} a_{x63}$$

$$LOCE = 1$$

$$\hat{b}_\phi = \hat{b}_\psi = \hat{b}_{f_y} = 0$$

$$\hat{w}_1 = \hat{w}_2 = \hat{w}_3 = \hat{w}_4 = \hat{w}_6 = 0$$

$$z_1 = z_2 = z_4 = z_5 = z_6 = 0,$$

$$\dot{z}_1 = \dot{z}_2 = 0, \quad J_{LGN} = 0, \quad JPHINT = 0, \quad u_{c1} = 0,$$

$$y_{INT} = \psi_{INT} = \phi_{INT} = 0, \quad C_{LGN} = 305$$

$$\hat{x}_{6_k} = \hat{Y} / U_o \quad \text{B6(DP)B25(DP)B8}$$

$$\hat{y}_6 = cx_{63}\,\hat{x}_{3_k} + cx_{64}\,\hat{x}_{4_k} + cx_{65}\,\hat{x}_{5_k} + cw_{65}\,\hat{w}_5 \quad \text{B-3(DP) B-2B0 B-1 B-1 B-1 B-1 B-1 B-1}$$

2. System Flowchart

The order of execution and logic controlling the execution of the previously presented software equations is shown by the following flowchart:

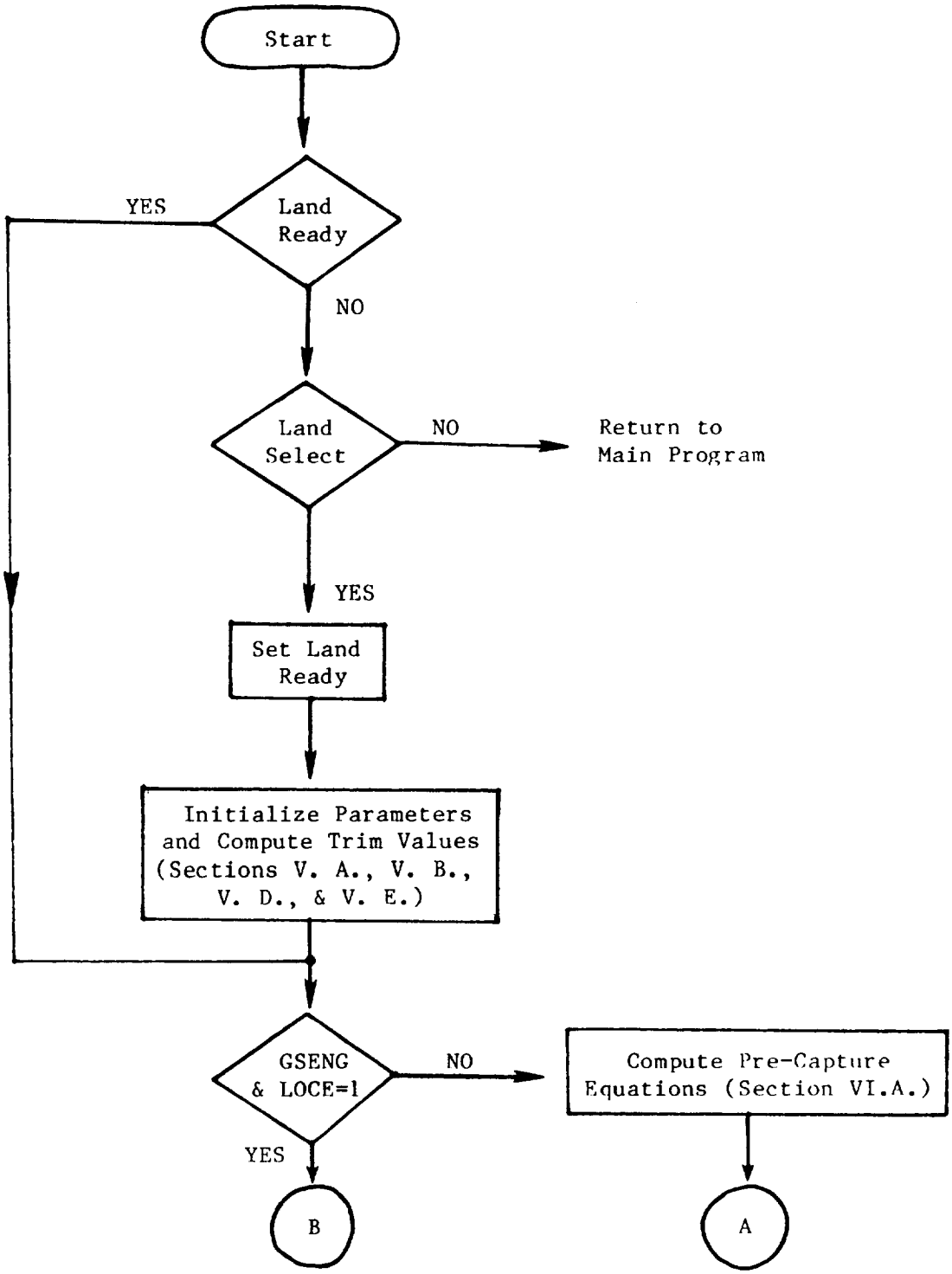

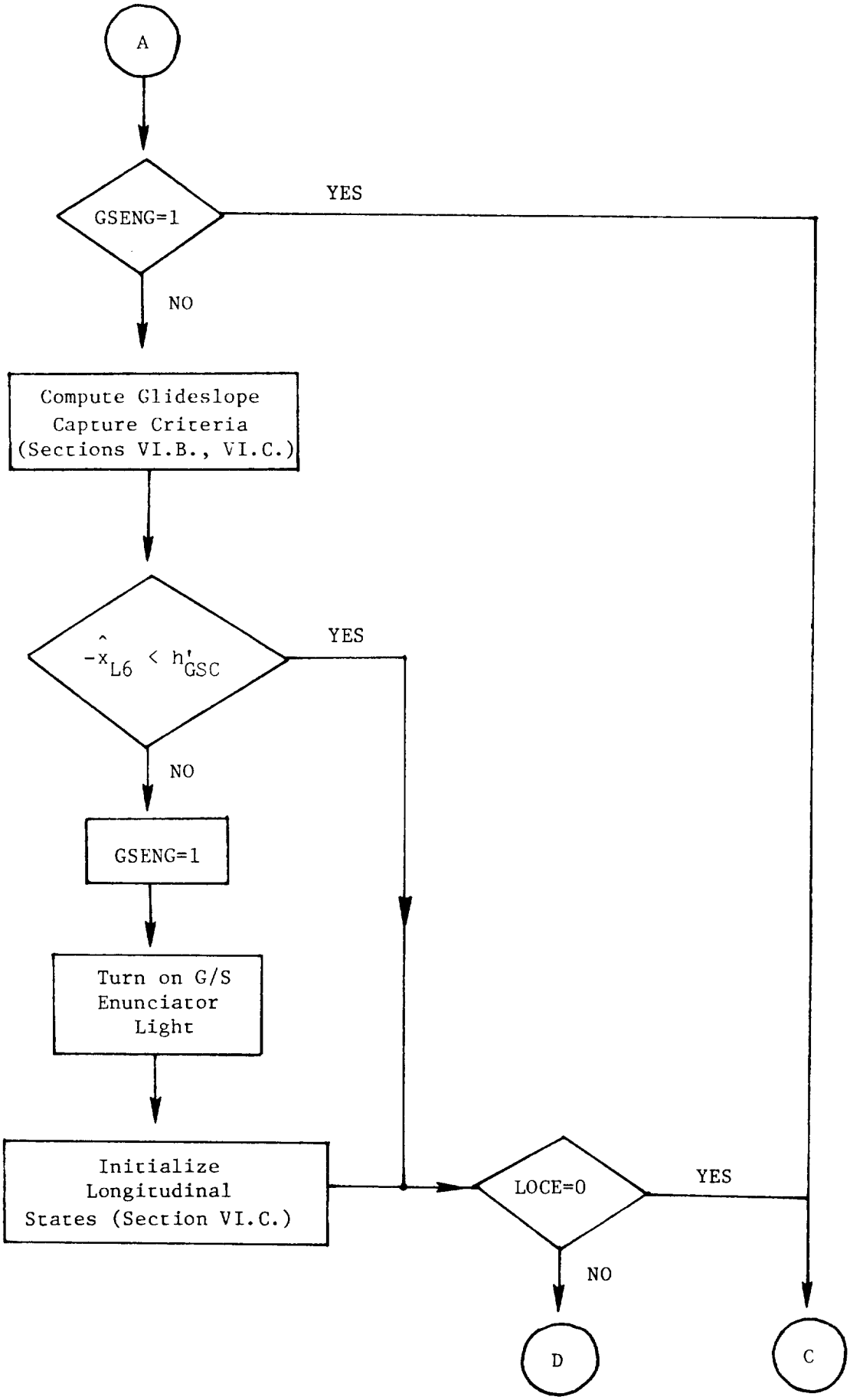
A
GSENG=1
YES
NO
Compute Glideslope Capture Criteria (Sections VI.B., VI.C.)
$-\hat{x}_{L6} < h'_{GSC}$
YES
NO
GSENG=1
Turn on G/S Enunciator Light
Initialize Longitudinal States (Section VI.C.)
LOCE=0
YES
NO
D
C

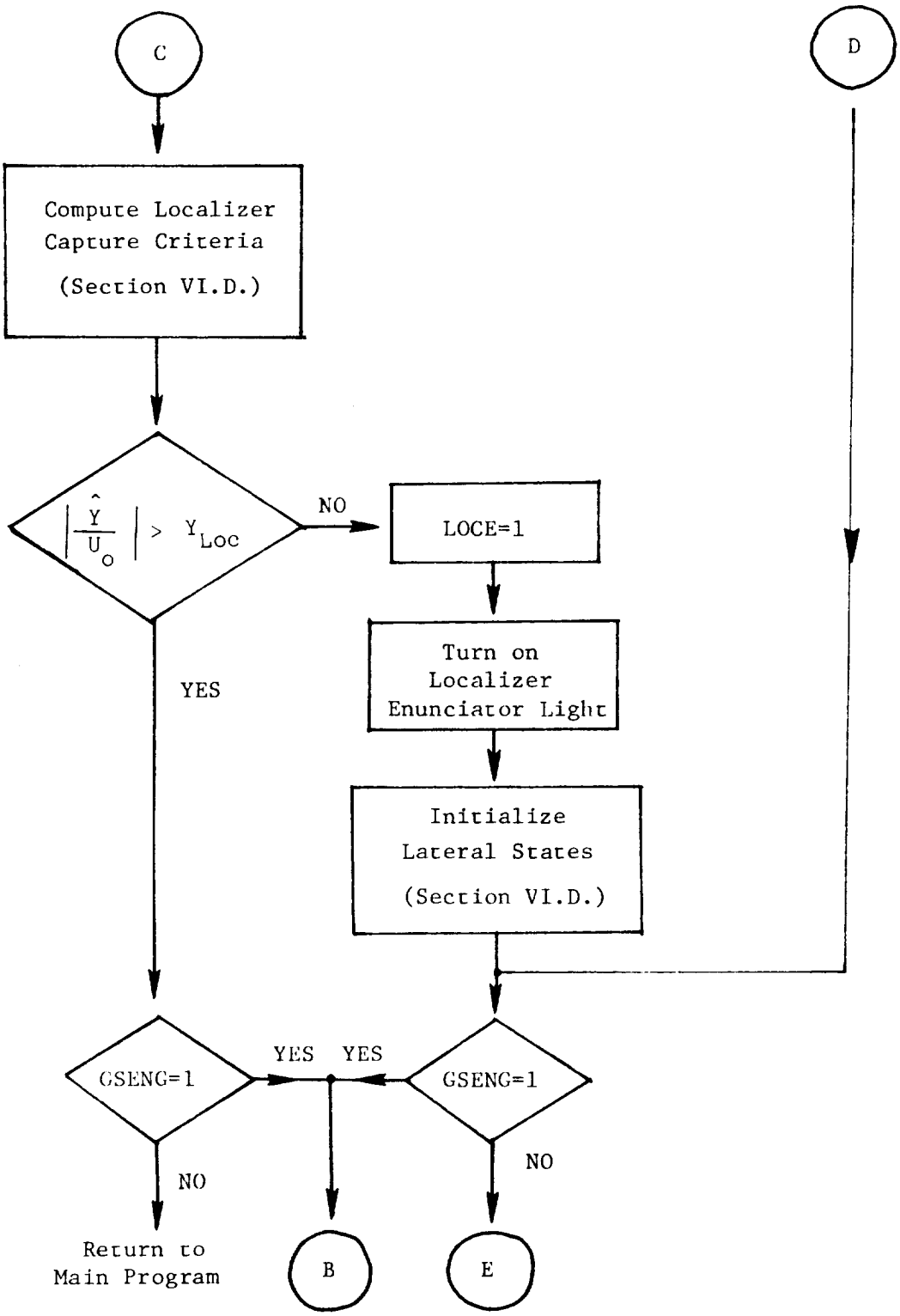
C
D
Compute Localizer Capture Criteria
(Section VI.D.)
$\left|\frac{\hat{Y}}{U_o}\right| > Y_{Loc}$
NO
LOCE=1
YES
Turn on Localizer Enunciator Light
Initialize Lateral States
(Section VI.D.)
GSENG=1
YES
YES
GSENG=1
NO
NO
Return to Main Program
B
E

3. System Gains and Constants

MLS Coordinate Constants

H_{TDC} = -2.79 ft., KZO = 36.2 ft., 2KN2 = 2.3914E-8 ft^{-1}

x_{GPIP} = 9500 ft. (531.3 ft. past runway threshold)

Filter Gains

$f_{x_{ij}}$

i \ j	1	2	5	6
1	.25			
2		.25		
3	1.4527E-3	-.012031	.095648	-3.4226
4	8.4845E-5	1.2069E-3	.2	-4.3845E-3

$f_{w_{ij}}$

i \ j	1	2	5	6
1	2.5885E-5	1.7791E-3	-.05	-.6
2	-1.7972E-5	-3.3051E-4	2.3510E-3	.045303
3	-2.49E-4	4.3609E-4	-1.7487E-3	-.79396
4	-8.7187E-5	-1.9265E-5	1.2606E-4	.012412
5	-5.6022E-4	9.9608E-3	-.04	-.6
6	-3.131E-5	5.4918E-4	-.006	-.05

$f_{Lx_{ij}}$

i \ j	1	3	4	5
1	.25	5.6467E-4	-4.0931E-4	-3.4639E-6
2	-5.6338E-4	.023912	8.3565E-5	7.0719E-6
3	.052637	-2.3153E-3	.004	8.1997E-5
4				
5	2.1364E-3	.11542	-9.1584E-6	7.75E-7
6	-9.483E-3	-6.6035E-4	.025	1.3681E-3

b_{L31} = -.03969, b_{31} = -.049268*, d_{31} = -.15584

* This value was four times larger than intended due to a coding error.

$f_{Lx_{ij}}$

i \ j	6	7	8	9
1	-8.6117E-3	-.016195	-5.2891E-4	-.054016
2	2.0860E-3	6.7456E-3	.01	.080079
3	.075	.057774	-1.0994E-3	2.0007E-3
4				
5	9.6907E-4	-1.5573E-4	2.0361E-4	.029937
6	.061126	.0	-9.9527E-4	.013384

$f_{Lw_{ij}}$

i \ j	1	3	4	5
1	-.01996	7.1874E-4	-4.8671E-4	-4.1189E-5
2	6.115E-3	-2.5455E-4	1.566E-4	1.3253E-5
3	-.019298	1.7375E-3	-5.1174E-4	4.3308E-5
4	-.024322	-6.3055E-3	-7.6684E-5	-6.4896E-6
5	-.02155	-.012199	-4.6105E-4	-3.9018E-5
6	-2.442E-3	-1.8726E-3	1.7703E-4	1.4982E-5
7	-1.218E-3	-5.5562E-4	-1.9102E-5	-1.6166E-6

$f_{Lw_{ij}}$

i \ j	6	7	8	9
1	-.017505	-.5	-8.3561E-3	.31912
2	5.2377E-3	.10634	2.5579E-3	-.088826
3	-.016011	.01523	-6.3083E-3	-.084913
4	-4.7758E-3	-.49933	.05	-.45852
5	-9.7476E-3	-.35123	.05	-.23454
6	1.6052E-3	.06	2.2799E-3	-.044586
7	-4.9444E-4	-.02054	.0015	-.014538

Lateral Guidance

$\phi_{z_{ij}}$

i \ j	1	2	3	4	5
1	.99989		-.0208654	.090789	-7.043E-5
2	2.021E-5		4.046E-3	4.228E-4	.099275
4	-3.1003E-3		-.39773	.82313	.11301
5	6.0534E-4		.080836	-8.2343E-3	.97851
6	-6.2007E-3	.099452	.099267	-2.6571E-4	4.4398E-5

ψ_{ij}

i \ j	1	2	3	4	5
1	.099997		-7.0873E-4	4.6862E-3	-9.1594E-5
2	5.05E-7	.1	1.3475E-4	-1.4251E-5	4.9817E-3
3	7.455E-4		.099084	7.401E-5	-4.9163E-3
4	-1.0533E-4		-.020671	.090885	5.4882E-3
5	2.0160E-5		4.0361E-3	-4.2768E-3	.090996
6	-3.2244E-4	4.9726E-3	4.9752E-3	-9.1995E-6	1.3668E-6

$a_{x_{ij}}$

i \ j	1	2	3	4	5
1				.99869	-.054654
2				6.688E-5	1.0028
3	.14998		-.15584	7.694E-3	-.99495
4			-4.4602	-1.9377	1.0274
5			.80364	-.092066	-.17208
6	-.069469	.99452	1.0		

d_{31} = -.15584, d_{41} = -4.4602, d_{51} = .80364

h_{F6} = 4.0(cross-track error gain factor limit), y_{LIM} = 30., C_{CGN} = 305

Flare

$\Delta\mu_k = (.0125)\pi$

$\Delta V_{FR} = 1.65/U_o$

$x_{FLR} = 1300.$

$T_{\gamma TD} = \tan(-.6^o) = -.0104723$

$h_{Lxf_3} = 1.25$

$h_{Lxf_4} = 1.0$

$h_{Lxf_6} = 1.25$

Glideslope

$Z_{Lim} = 0.,$ $\Delta EZ7 = .025$ (4 second glideslope $\dot{h}$ command)

KFLC = 305, $\Delta EZ4 = .05$ (2 second easy-on for glideslope gains)

$CWB_{11} = -.06947,$ $CWB_{14} = .99758,$ $CWB_{15} = .99452,$ $CWB_{16} = .10453$

$DT(2) = -.06947,$ $DT(4) = \frac{-(CWB_{14})U_o}{Lu},$ $G_{\zeta_4} = 0$

$a_{GSC1} = -3.1003,$ $a_{GSC2} = .81128,$ $a_{GSC3} = 1.7019$

$a_{GSC7} = 4.576E\text{-}4,$ $a_{GSC8} = 4.0187E\text{-}3,$ $a_{GSC9} = 1.0369$

$a_{GSC\zeta} = -.41860,$ $a_{GSCZ} = 0.$

Decrab

$\phi_{Lim} = 4.8/57.3,$ $\Delta EZ1 = .003$

$h_{DC} = 250$ ft., $A_{EZ} = .997$

$A_\phi = 0,$ $A_\psi = 0$

Longitudinal Feedback Gains

$h_{Lx_{ij}}$

i \ j	1	2	3	4
1	-4.5	1.1968	2.5107	-2.2
2	-.2765	.03	.1864	-.25
3	-5.253	51.2	-5.509	.26

$h_{Lx_{ij}}$

i \ j	6	7	8	9
1	1.4752	6.75E-4	6.0213E-3	1.5297
2	.04361	.001	.00018	.6357
3	-6.928	.1661	.3116	.001476

$h_{Lw_{ij}}$

i \ j	1	2	3	4	5	6	7
1	-.21480	.56187	-.34370	-1.2630	-1.5543	.53799	-1.7737
2	.020956	8.2279E-3	.0538	-.11131	-.16507	.025812	-.3678
3	46.01	87.964	-.1112	.9008	4.3022	-61.038	14.831

$h_{Lz_{ij}}$

i \ j	1	2	3	4	6
1	-1.3942	-1.5164	-.61752	3.0523	-1.2555E-5
2	.047738	-.16507	-.042866	.47211	1.15E-5
3	-61.085	-2.0562	61.159	-294.24	1.9759E-3

$h_{L\zeta_{ij}}$

i \ j	1	2	3	4	6
1	3.3246	-10.306	-5.3047	22.791	-2.8184
2	.6271	-.7106	-.645	2.053	-.2406
3	-296.4	-394.9	291.7	-382.2	60.39

$h_{zP1} = 1.3$, $h_{zP2} = .2$, $h_{zP3} = 0$

$h_{zT1} = .39$, $h_{zT2} = .03$, $h_{zT3} = -3.5$

$f_c = 1.0$, $\alpha_e = .24758$, GSTAB = .2

Lateral Feedback Gains

$h_{x_{ij}}$

i \ j	1	2	3	4	5	6	7
1	1.2	1.4988	.2	.8	.38965	.12095	.30967
2	-2.8358	-1.3958	-2.7222	.04	-.76635	-.11293	1.7497

$h_{w_{ij}}$

i \ j	1	2	3	4	5	6
1	-1.5518	-.55723	.15783	-.34191	-1.5757	-.73164
2	-1.8656	-.29878	.13922	.059698	-1.7612	.22975

$h_{\zeta_{ij}}$

i \ j	1	2	3	4	5	6
1	-.57446	-5.6988	-5.7242	-.11086	-.27049	-1.3860
2	-.19253	6.8307	5.4837	-.069738	2.4134	1.3

$h_{y_{INT1}} = .0119$, $h_{\phi_{INT1}} = .1$, $h_{\psi_{INT1}} = -.17$

$h_{y_{INT2}} = -.018$, $h_{\phi_{INT2}} = .03$, $h_{\psi_{INT2}} = -.2$

Longitudinal Prediction Gains

$\Phi_{L_{ij}}$

i \ j	1	2	3	4	7	8	9
1		-1.1024E-4	-3.281E-3	.097642	2.7694E-5	2.773E-7	-.010182
2	-.015639	.99530	8.2595E-3	-3.5892E-4	1.6998E-4	2.5566E-6	-9.6881E-6
3	1.8684E-3	-.030868	.93775	.095028	1.2813E-5	6.90E-8	-.018012
4	-1.0865E-4	-1.8386E-3	-.064433	.95213	5.4485E-4	8.2527E-6	2.20189
5	9.6659E-3	.099383	-9.7267E-3	3.1038E-6	8.6052E-6	8.58E-8	4.1289E-5
6	0.099444	8.8823E-3	.096535	-8.4780E-5	2.016E-7	2.3E-9	-3.9796E-4
7					.95123	.029067	

$\Phi_{Lw_{ij}}$

i \ j	1	2	3	4	5	7
1	.99980	.097995				
2	-4.0198E-3	.96010				
3	.15721	7.9749E-3	.84278			
4				.97995		
5						.1

$\Upsilon_{Lw_{ij}}$

i \ j	1	3	4	5	6
1	-6.5006E-3	3.235E-3	-3.3792E-4	-4.5252E-4	3.2577E-3
2	8.5510E-3	1.5354E-5	-4.1188E-3	-3.8148E-3	-8.7060E-3
3	-.068531	8.5789E-3	-.035110	-.037206	.058680
4	-.12826	.064114	-6.3103E-3	-8.5636E-3	.063888
5	7.5708E-4	2.7788E-5	-1.8787E-5	6.8865E-6	-7.2950E-4
6	-3.0713E-3	2.6995E-4	-1.7695E-3	-1.8570E-3	2.7373E-3

$\gamma_{L_{ij}}$

i \ j	1	2	3
1	-4.9041E-3	-3.4083E-3	7.0E-9
2	-4.6466E-6	-5.36E-7	8.56E-8
3	-8.6713E-3	-7.4093E-4	2.0E-10
4	-.097244	-.010182	2.773E-7
5	1.9865E-5	1.3909E-6	.2.20E-9
6	-1.9146E-4	-1.3392E-5	1.0E-10
7			1.4655E-3
9		.1	

$f_{Lb_{ij}}$

i \ j	1	3	4	5
1	.01	-5.6467E-5	4.0931E-6	3.464E-7
5	9.4839E-4	6.6035E-5	-.007	.007
6	2.8373E-3	3.6467E-5	-.005	-8.5732E-6
7	2.75E-4	8.4248E-5	-1.50E-5	0.0
9	7.9932E-4	-5.0E-5	-4.6405E-6	-3.927E-7

$f_{Lb_{ij}}$

i \ j	6	7	8	9
1	8.6117E-4	1.6195E-3	-1.0E-5	-.001
5	-6.1126E-3	.0	9.9527E-5	-1.3384E-3
6	.008	-7.2859E-3	5.6910E-5	-6.010E-3
7	-1.5E-4	.005	9.276E-5	1.025E-5
9	-2.5528E-4	-5.1751E-4	-.002	.005

(-2

$\psi_{L_{ij}}$

i \ j	1	2	3	5	6
1	.1	-3.9831E-6	-1.1037E-4		
2	-7.8267E-4	.099767	4.1728E-4		
3	9.0313E-5	-1.5581E-3	.09612		
4	-4.7998E-6	-1.1024E-4	-3.2912E-3		
5	4.9638E-4	4.9704E-3	-4.9831E-4	1.0	
6	-4.9724E-3	4.7001E-4	4.8749E-4		.1

$c_{Lx_{ij}}$

i \ j	1	2	3	4	7	9
6	-.99452	.10453	.99452			
7	.016793	-.31778	-.60698	.00242	-.2401E-4	.082499
9	-.15682	-/045824	.085245	0.0	1.7480E-3	0.0

$c_{Lw_{ij}}$

i \ j	1	3	4	5	6
7	-.63909	.055650	-.35918	-.37948	.57044
8	-.069469		.99758	.99452	.10453
9	.088223		-.039791	-.036662	-.089568

Lateral Prediction Gains

ϕ_{ij}

i \ j	1	3	4	5	7
1	.99989		.090789	-7.043E-5	
2	2.021E-5		-4.2280E-4	.099274	
3	.014861	.98028	1.8161E-3	-.097702	7.3540E-3
4	-3.1003E-3	-.39773	.82313	.11301	.055371
5	6.0534E-4	.080836	-8.2343E-3	.97851	-.068410
6	-6.2007E-3	.099267	-2.6571E-4	4.4398E-5	1.8951E-4

ψ_{ij}

i \ j	1	2	3	4	5	6
1	.099997		-7.0873E-4	4.6862E-3	-9.1594E-5	
2		.1		-1.4251E-5	4.9817E-3	
3	7.455E-4		1.3475E-4	7.401E-5	-4.9163E-3	
4	-1,0533E-4		.099084	.090885	5.4882E-3	
5	2.0160E-5		4.0361E-3	-4.2768E-4	.098996	
6	-3.2244E-4		4.9752E-4	9.1995E-6	1.3668E-6	.1

γ_{ij}

i \ j	1	2
3	-2.3897E-3	3.1118E-4
4	.33692	2.9439E-3
5	.027412	-3.4310E-3
6	-9.4793E-5	6.3812E-6
7		.1

$\phi_{w_{ij}}$

i \ j	1	2	3	4	5	6
1	.99978	.097897				
2	-4.4207E-3	.95817				
3	-4.9246E-4	.20815	.78720			
4				.83572		
5					1.0	.099750
6						.99501

$\gamma_{w_{ij}}$

i \ j	1	3	4	5
3	-.019723	1.4934E-3	9.702E-4	-.019723
4	-.39773	.079826	-.18276	-.39773
5	.080836	-.017985	-7.022E-3	.080836
6	-7.3323E-4	1.9287E-5	%.4773E-5	-7.3323E-4

$g_{\phi} = .001, \quad g_{\psi} = .001, \quad g_{f_y} = .035$

$c_{x_{63}} = -.15584, \quad c_{x_{64}} = 7.6943E-5$

$c_{x_{65}} = 5.0496E-3, \quad c_{x_{67}} = .039501$

$c_{w_{61}} = -.15584, \quad c_{w_{63}} = 5.5719E-3$

$c_{w_{65}} = 7.3249E-3, \quad c_{w_{65}} = -.15584$

APPENDIX B

MLS SIGNAL PROCESSING

The Microwave Landing System (MLS) used in the flight tests provided three signals from which the aircraft's position, relative to the MLS installation, could be determined. Two signals were from the MLS angle receiver--azimuth angle relative to runway centerline (±60 degrees coverage) updated at 13.3 Hz and elevation angle relative to the local level at the elevation antenna site (1 to 20 degrees coverage) updated at 40 Hz. The third signal was from the MLS DME receiver representing the distance or range to the DME antenna site and was updated at approximately 20 Hz. The location of these MLS ground antenna sites is shown in figure B1. Using these signals, the aircraft position in x-, y-, and z-coordinates relative to an origin at the MLS azimuth antenna phase center was computed as follows (see fig. B1):
The range, R, to the origin was computed using the equation

$$R = R_m - y_{DME} \sin AZ + R_o$$

where R_m was the MLS DME receiver measurement, y_{DME} the DME ground antenna y-coordinate, AZ the MLS azimuth measurement, and R_o a constant accounting for the x-coordinate of the DME ground antenna, x_{DME}, and cable length bias, R_c between the aircraft's antenna and the MLS DME receiver. R_o is given as

$$R_o = x_{DME} - R_c$$

The equations for the x-, y-, and z-coordinates are

$$x = g\,(g^2 - h)^{1/2}$$

$$y = -R \sin AZ$$

$$z_E = z_{E\ell} + \tan E\ell \sqrt{(x - x_{E\ell})^2 + (y - y_{E\ell})^2}$$

where $x_{E\ell}$, $y_{E\ell}$, and $z_{E\ell}$ are the coordinates of the MLS ground elevation antenna's phase center and g and h are defined as

$$g = x_{E\ell} \sin^2 E\ell$$

$$h = (x_{E\ell}^2 + y_{E\ell}^2) \sin^2 E\ell + y^2 - R^2 \cos^2 E\ell - 2y\, y_{E\ell} \sin^2 E\ell$$

where $E\ell$ is the elevation angle measurement.

When the aircraft approaches the touchdown point on the runway, the elevation signal from the MLS becomes invalid due to the aircraft flying out of the elevation coverage (the antenna siting is usually 250 to 400 feet from the runway centerline and 800 to 1000 feet from the threshold; a nominal touchdown point is on the order of 1500 feet). Thus, the altitude information provided by the elevation signal was replaced by an alternate measurement, radar altitude (h_R). The x-, y-, and z-coordinates were computed when using h_R as

$$z_{h_R} = h_R + h_{R1} - 0.38\theta - 0.0023\ (\hat{X} - x_o)$$

(Pitch Correction; Runway Slope Correction)

$$x = \sqrt{R\ (1 - \sin^2 AZ) - z^2}$$

$$y = -R \sin AZ$$

where h_{R1} is a constant to transform the radar altitude measurement to the roof antenna, θ is the pitch attitude in degrees, $\hat{X}$ is an estimate of the x-coordinate from the third-order complementary filter to be described later and x_o is a constant. The values used for h_{R1} and x_o were, respectively, 8.86 and 8049.5 feet. If x was less than x_o the runway correction was not used.

The switch from $E1$ to h_R occurred when the aircraft crossed over the runway threshold according to

$$\text{if } \hat{X} < 9630 \text{ feet (approx. 400 feet from threshold) use } h_R.$$

When the above logic became true, the z-coordinate computed from h_R was entered into the calculations through an easy-on with a 2 second turn-on time. The equation for the z-coordinate transition is

$$z = \alpha\ z_{hR} + (1 - \alpha)\ z_E$$

where α goes from 0 to 1 during the transition, z_{hR} is the z-coordinate computed from h_R, and z_E is the z-coordinate computed from $E\ell$.

The above equations will give the x-, y-, and z-coordinates values of the aircraft's receiving antenna in the MLS coordinate frame. In general, control of the aircraft's center-of-gravity or c.g. position relative to some desired flight is desired. Thus, given the position of the aircraft's antenna the coordinates of the aircraft's c.g. position were determined as

$$\begin{bmatrix} x_{cg} \\ y_{cg} \\ z_{cg} \end{bmatrix} = \begin{bmatrix} x \\ y \\ z \end{bmatrix} + T_{MB} \begin{bmatrix} x_a \\ y_a \\ z_a \end{bmatrix}$$

where T_{MB} is an Euler transformation matrix which transforms a vector in the aircraft's body coordinates to the MLS coordinates and x_a, y_a, and z_a are the body axis coordinates of the aircraft's MLS receiving antenna. The aircraft's MLS antenna was mounted above the cockpit on the roof of the aircraft resulting in coordinates defined as $x_a = -35.05$, $y_a = 0.83$, $z_a = 6.07$ (the positive direction of the antenna vector was from the aircraft antenna to the c.g.). T_{MB} is computed using the attitude measurements--pitch, roll, and true heading (yaw). The coordinates, x_{cg}, y_{cg}, and z_{cg}, were input directly to the DIALS innovation equations.

The x_{cg}, y_{cg}, and z_{cg} coordinates were also input to three third-order complementary filters--all identical and one for each coordinate axis. The form of these filters is shown in figure B2. The filters were developed for MLS processing (ref. 9) and were a part of the baseline software of the test vehicle. The filters provided estimates of the aircraft's position and velocity in the MLS coordinate frame. The position coordinate estimates are X, Y, and Z. The velocity estimate of the MLS z-coordinate axis was designated as $\dot{h}_{MLS}$ which replaced the barometric altitude rate in DIALS during the flight tests.

Item	Lat	Lon	h_{MSL}
Az	37.92396178°	-75.47307466°	41.1 ft.
DME	37.92406643°	-75.47384547°	49.7 ft.
EL	37.94479934°	-75.45547285°	34.7 ft.
T.P.6	37.92694443°	-75.47130358°	34.19 ft.
T.P.12	37.92926846°	-75.46945693°	34.75 ft.
T.P.74	37.94693043°	-75.45541772°	32.6 ft.
T.P.75	37.94727391°	-75.45514466°	32.18 ft.

True Heading Runway 22 = 212.193°

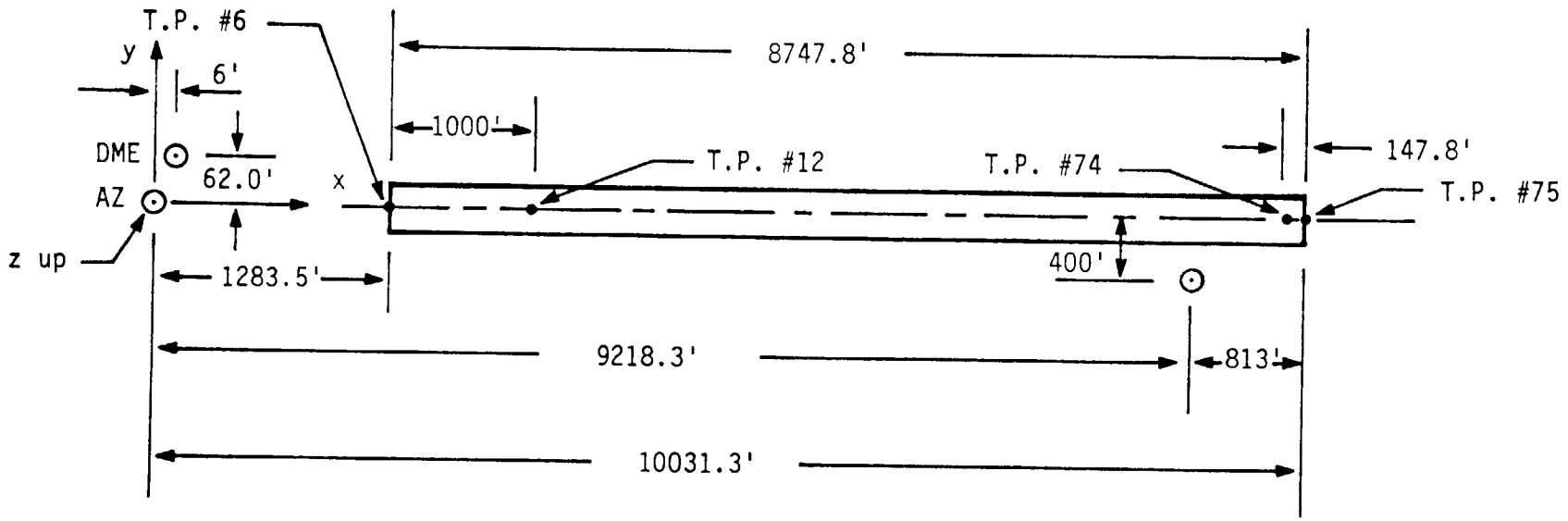

Figure B1. - WFC MLS Antenna Locations on Runway 22.

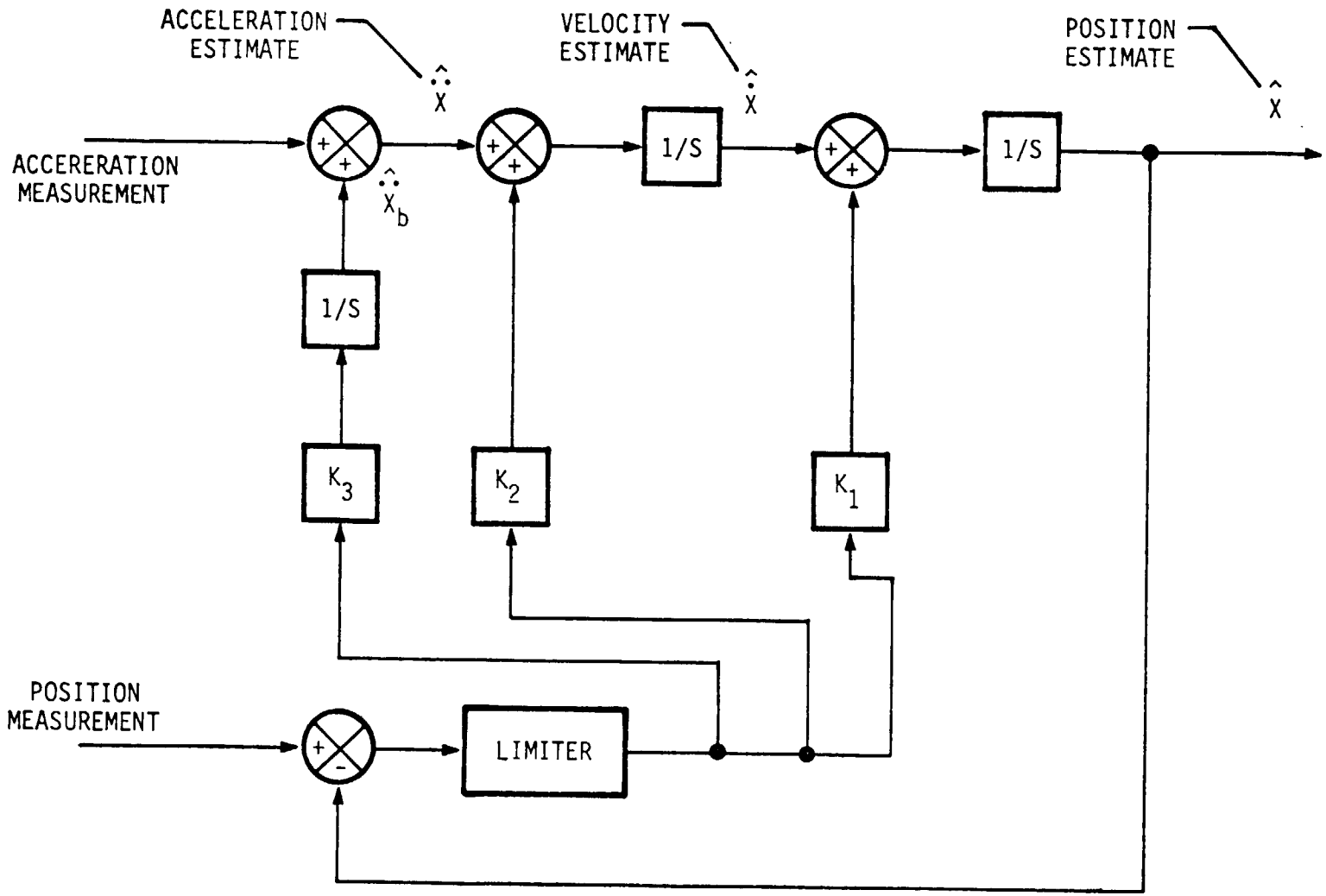

Figure B2. - Third Order Complementary Filter.

APPENDIX C

ALPHA BETA FILTERS

Software filters were used in the flight control computers to provide filtering for the three body-mounted accelerometer measurements, in addition to that provided by the standard hardware input filters. These filters, activated on one run of the flight test data presented, were executed each minor frame or data input cycle of the flight control computer, that is, every 6.144 msec. The same filter was used for each of the three accelerometer measurements and thus the equations for each filter are the same. The equations for this filter are given as

$$\hat{x}_n = (1 - \alpha_f)\ x_{Pn} + \gamma\ x_n$$

$$\hat{\dot{x}}_n = \hat{\dot{x}}_{n-1} + \beta_f/_T\ (x_n - x_{Pn})$$

$$x_{Pn+1} = \hat{x}_n + T\ \hat{\dot{x}}_n$$

where x_n is the measurement, $\hat{x}_n$ is the estimate or filtered value, and $\hat{\dot{x}}_n$ is an estimate of the rate of change of the measured value. The filter is initialized by setting x_{Pn} equal to x_n and $\hat{\dot{x}}_{n-1}$ equal to zero. The values of the filter constants were

$$\alpha_f = 0.13$$

$$\beta_f = 0.009037$$

$$T = 0.006144 \text{ sec}$$

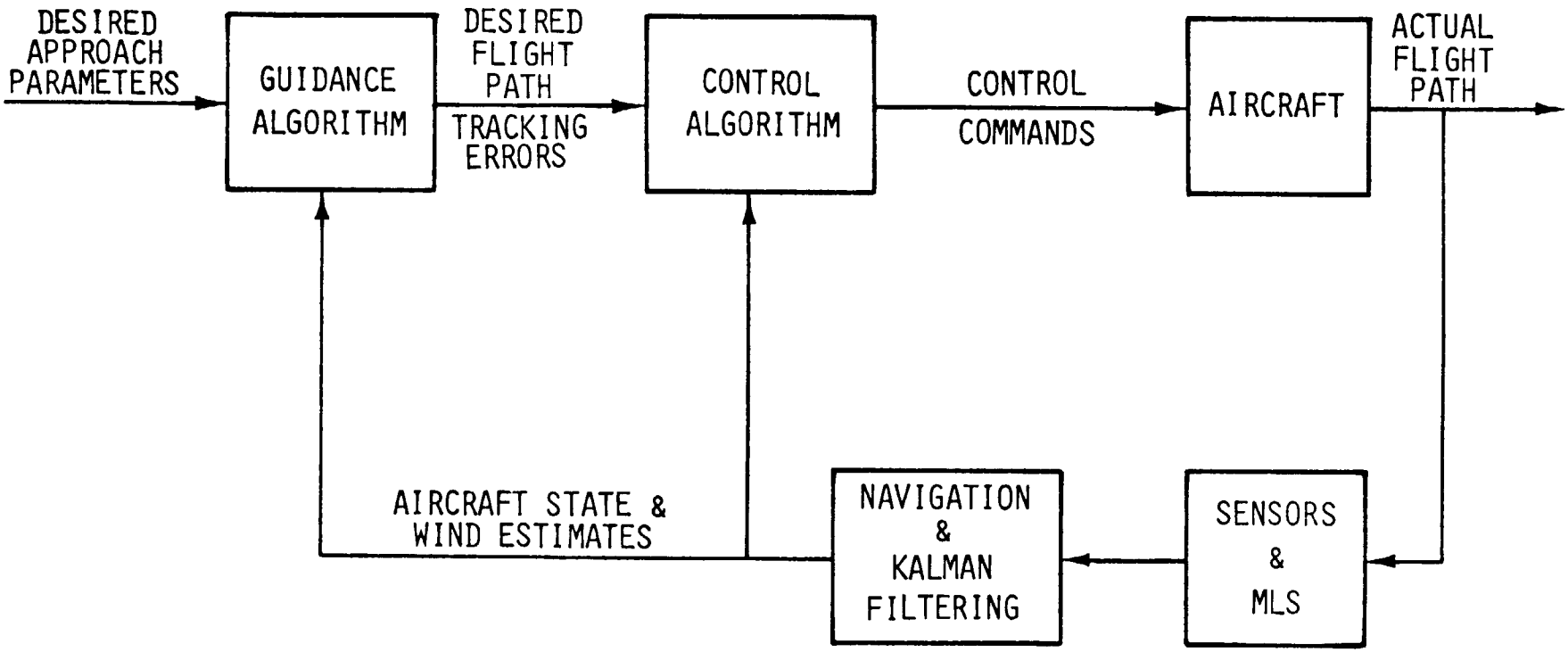

Figure 1. - The DIALS Block Diagram.

Figure 2. - Small Twin-jet Test Aircraft.

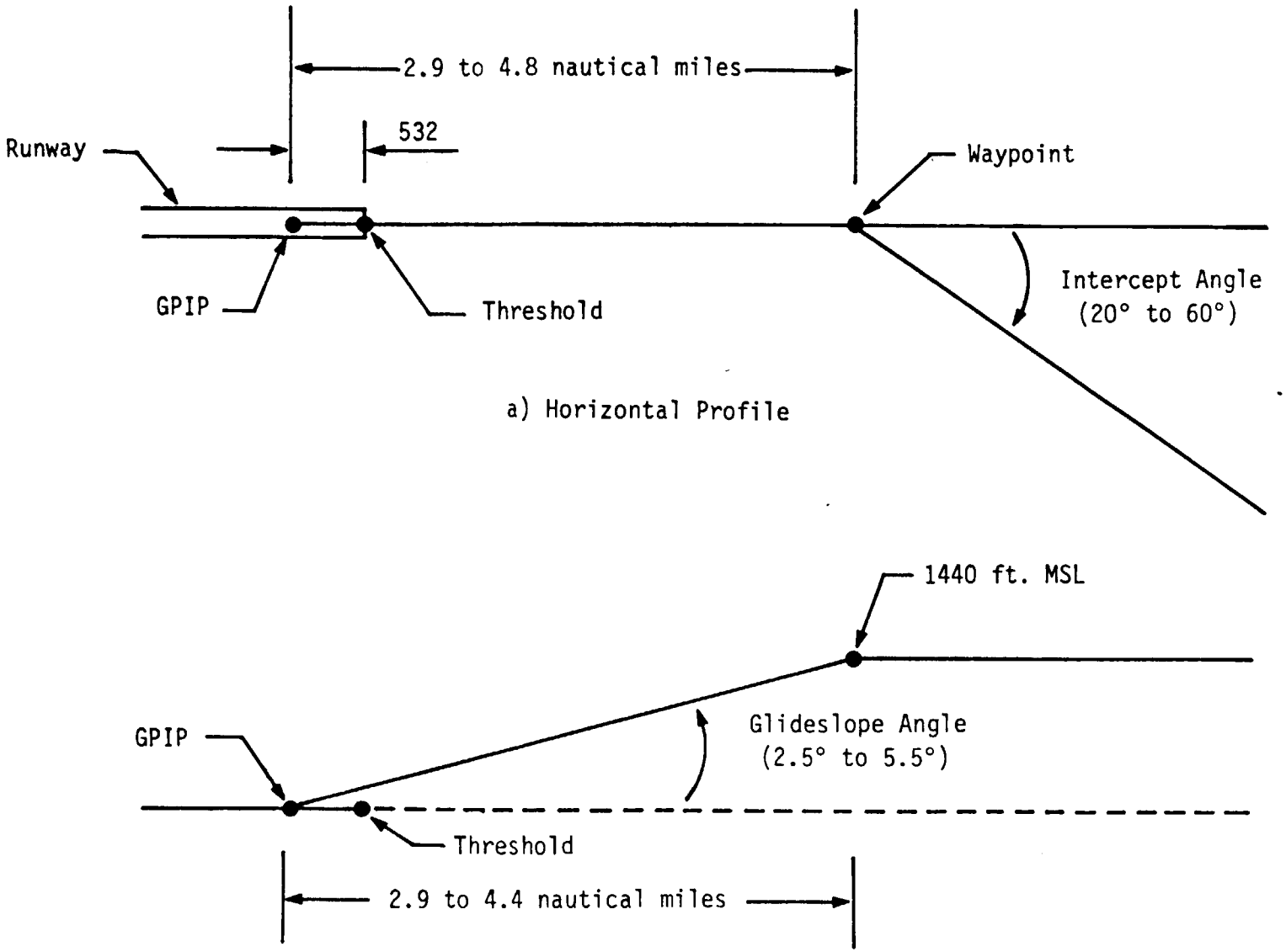

Figure 3. - DIALS Horizontal and Vertical Profiles.

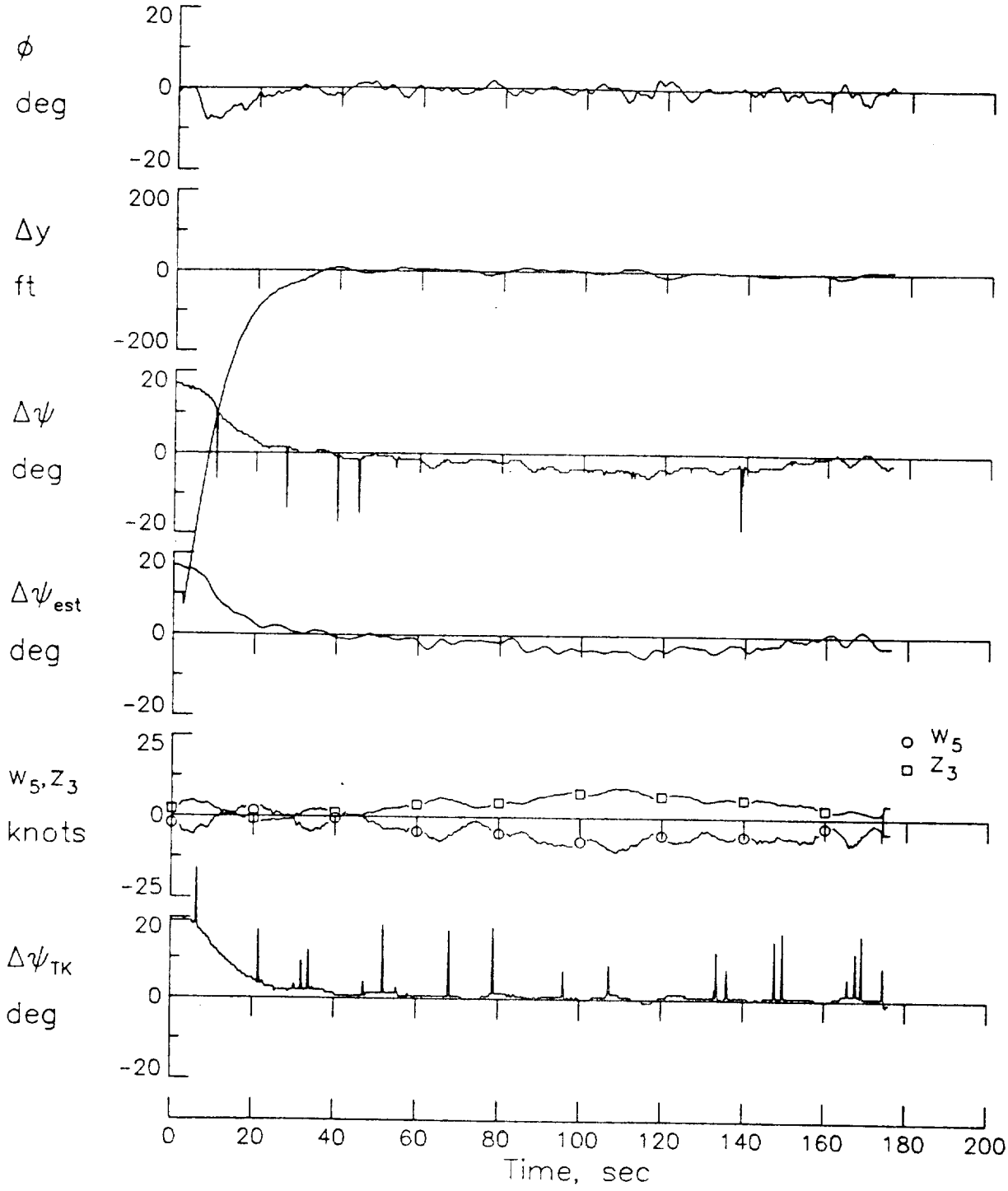

(a) 20° Intecept Capture

Figure 4. Localizer Capture & Track

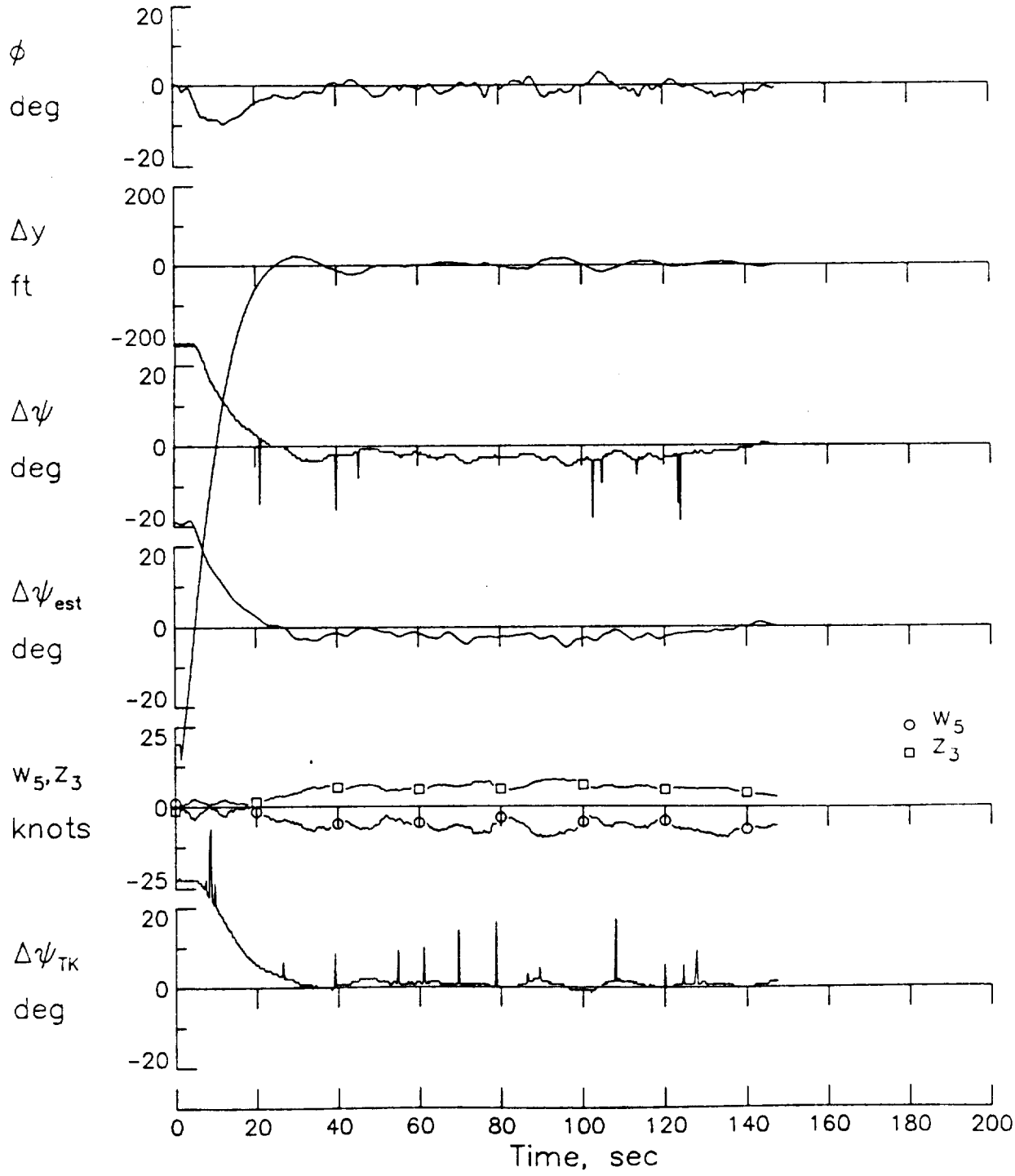

(b) 30° Intercept Capture

Figure 4. Continued

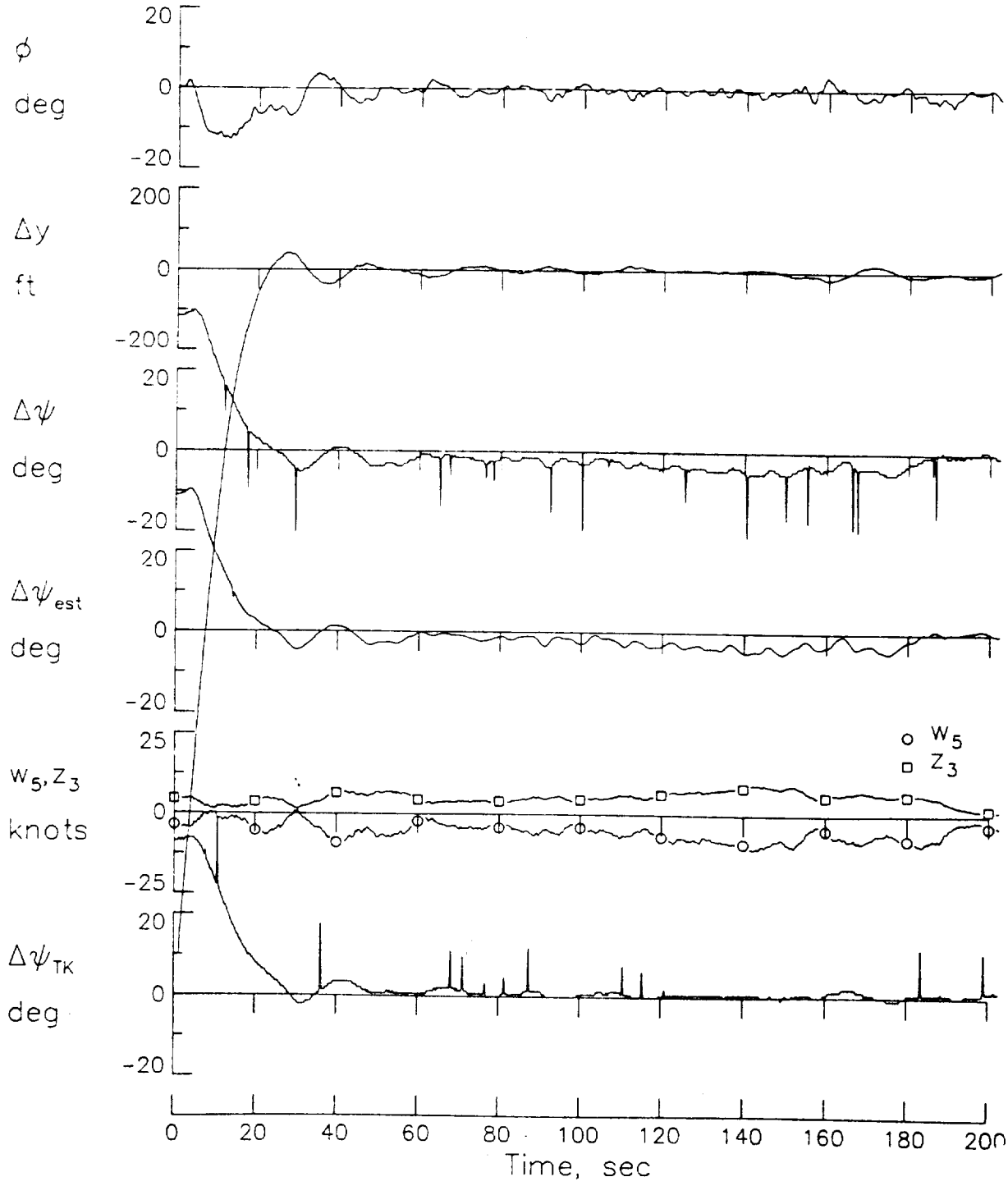

(c) 40^{o} Intercept Capture

Figure 4. Continued

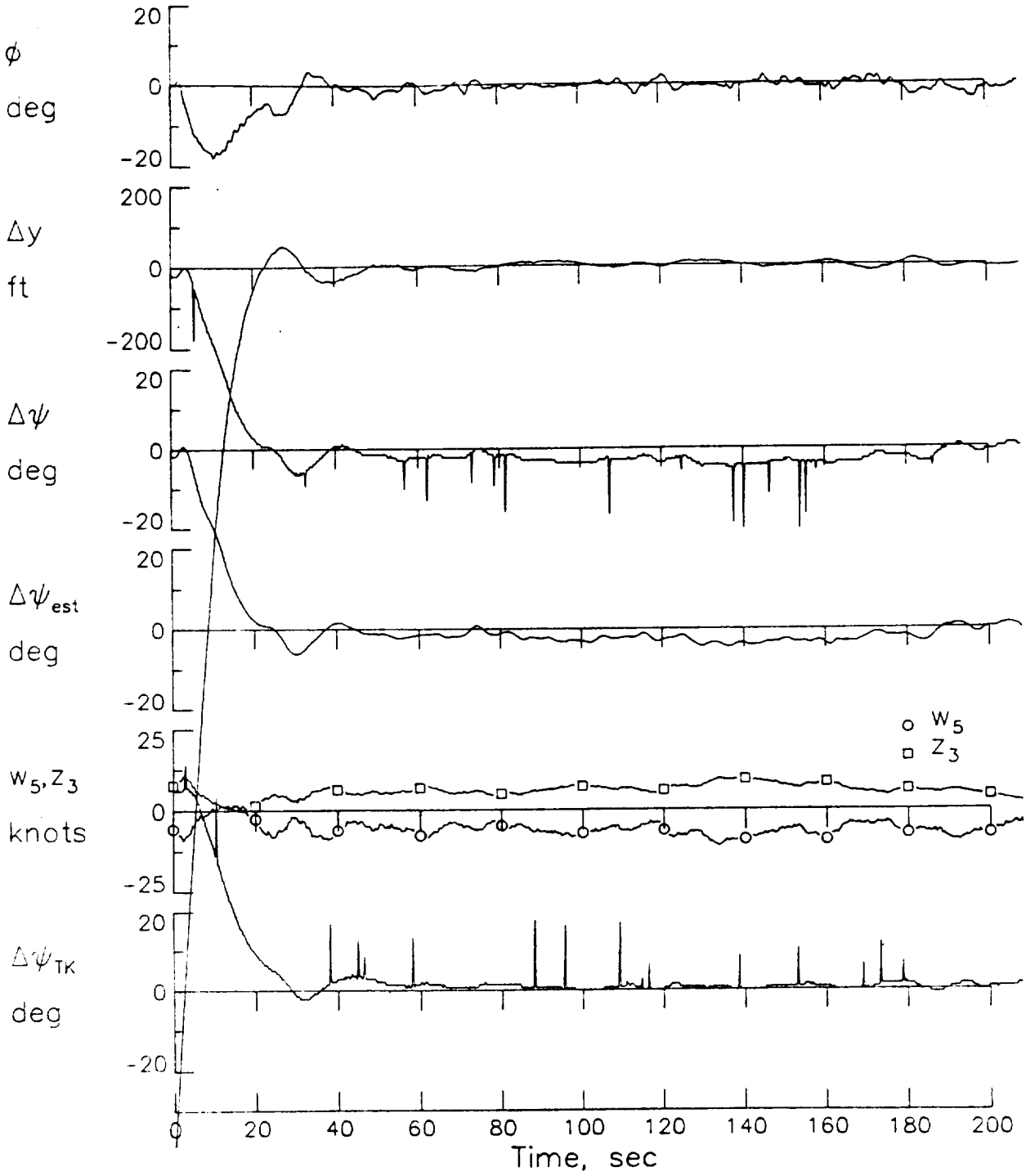

(d) 50^{o} Intercept Capture

Figure 4. Concluded

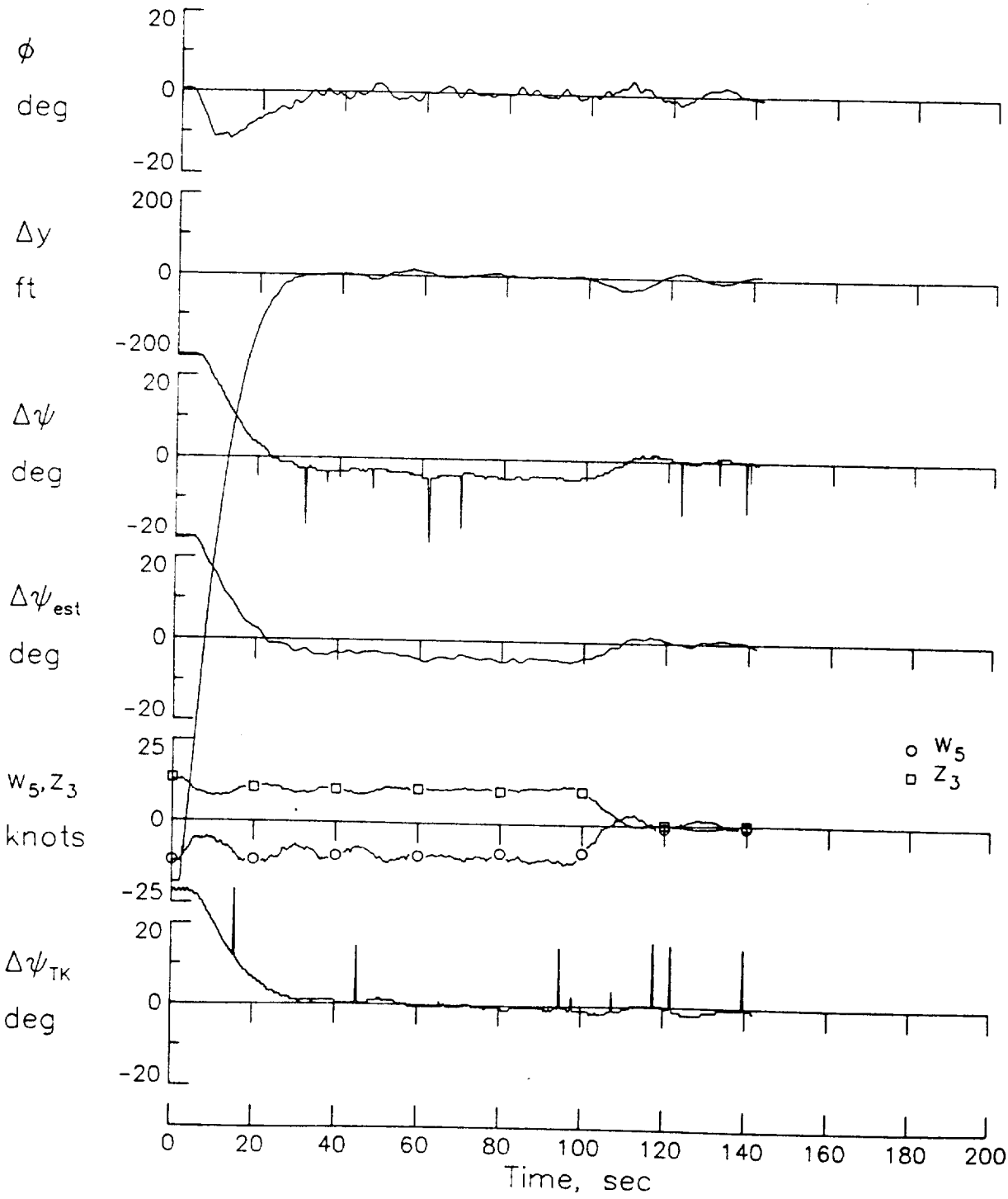

Figure 5. Crosswind Capture From the Left Side of the Runway & Wind Shear Encounter

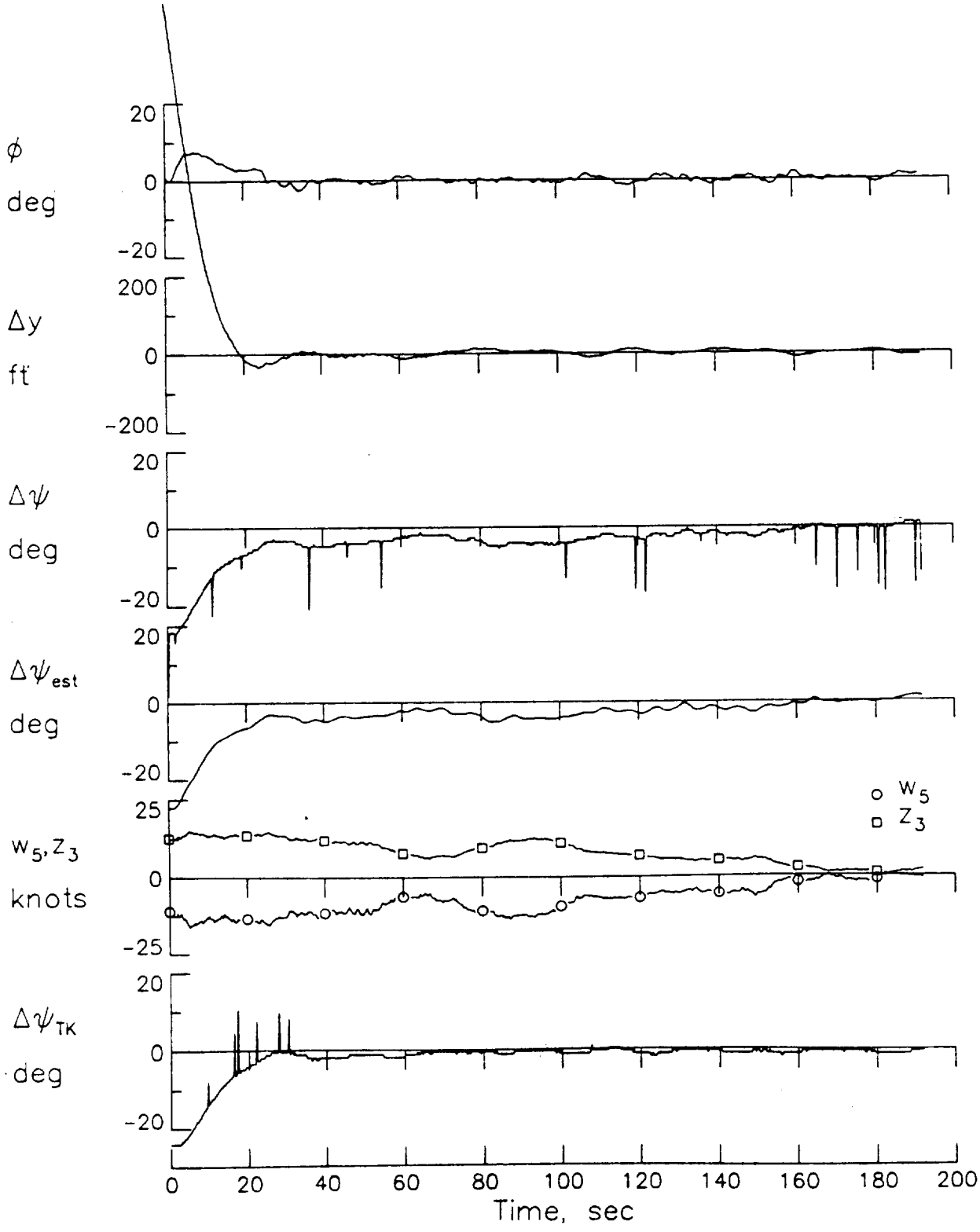

Figure 6. Crosswind Capture From Right Side of Runway

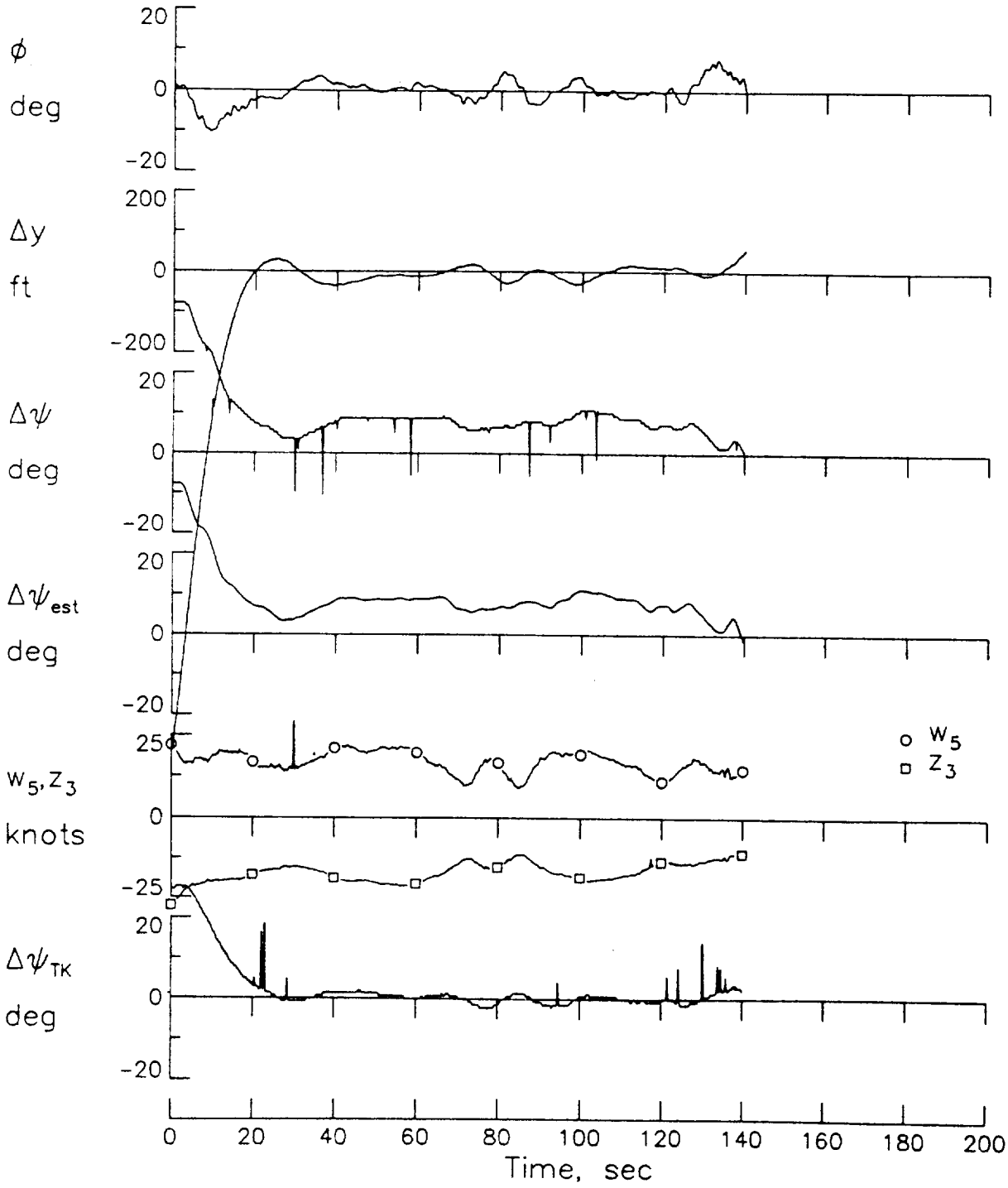

(a) Tracking Variables

Figure 7. Localizer Tracking in High Crosswinds and Gust Conditions

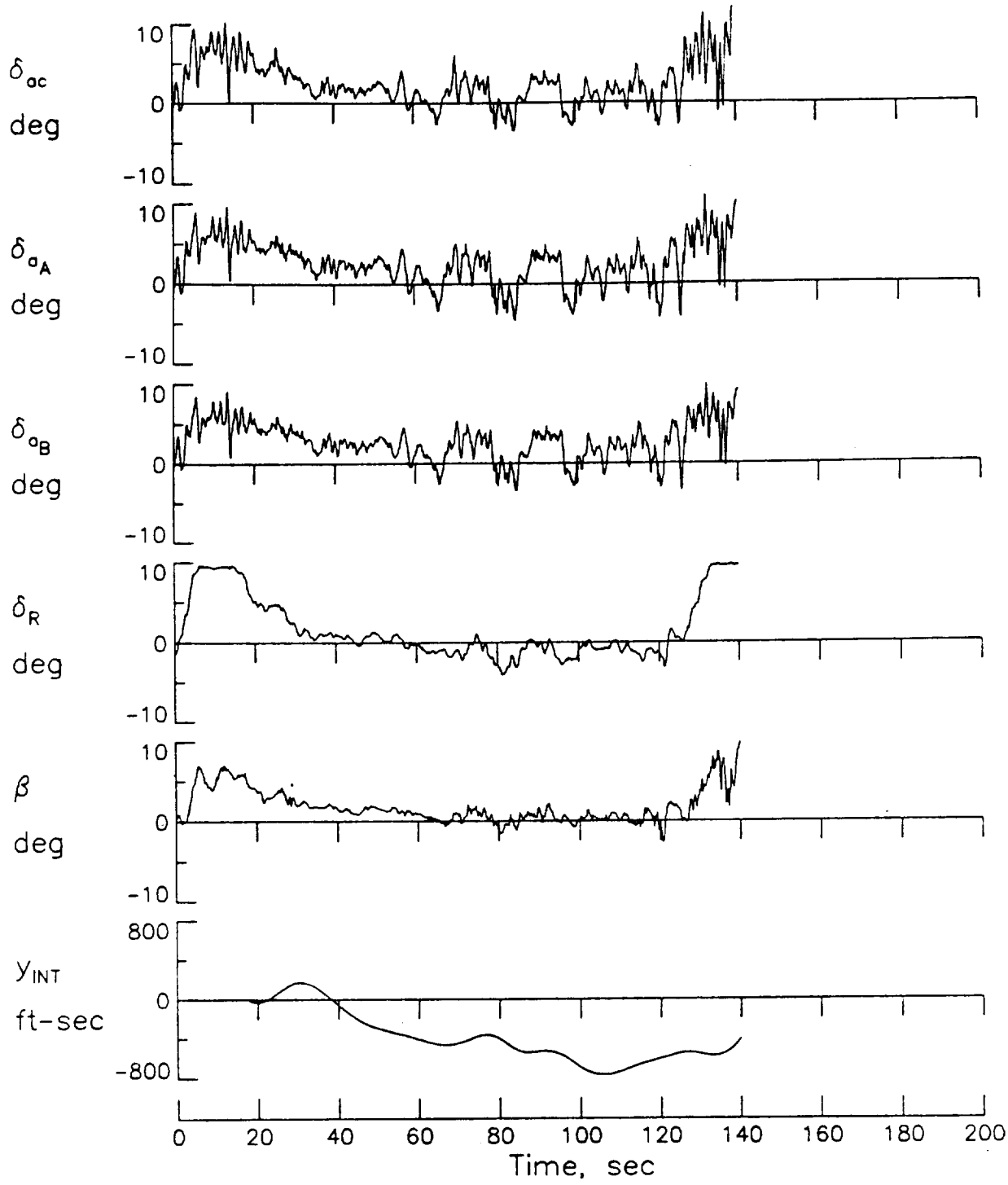

(b) Control & Tracking Variables

Figure 7. Concluded

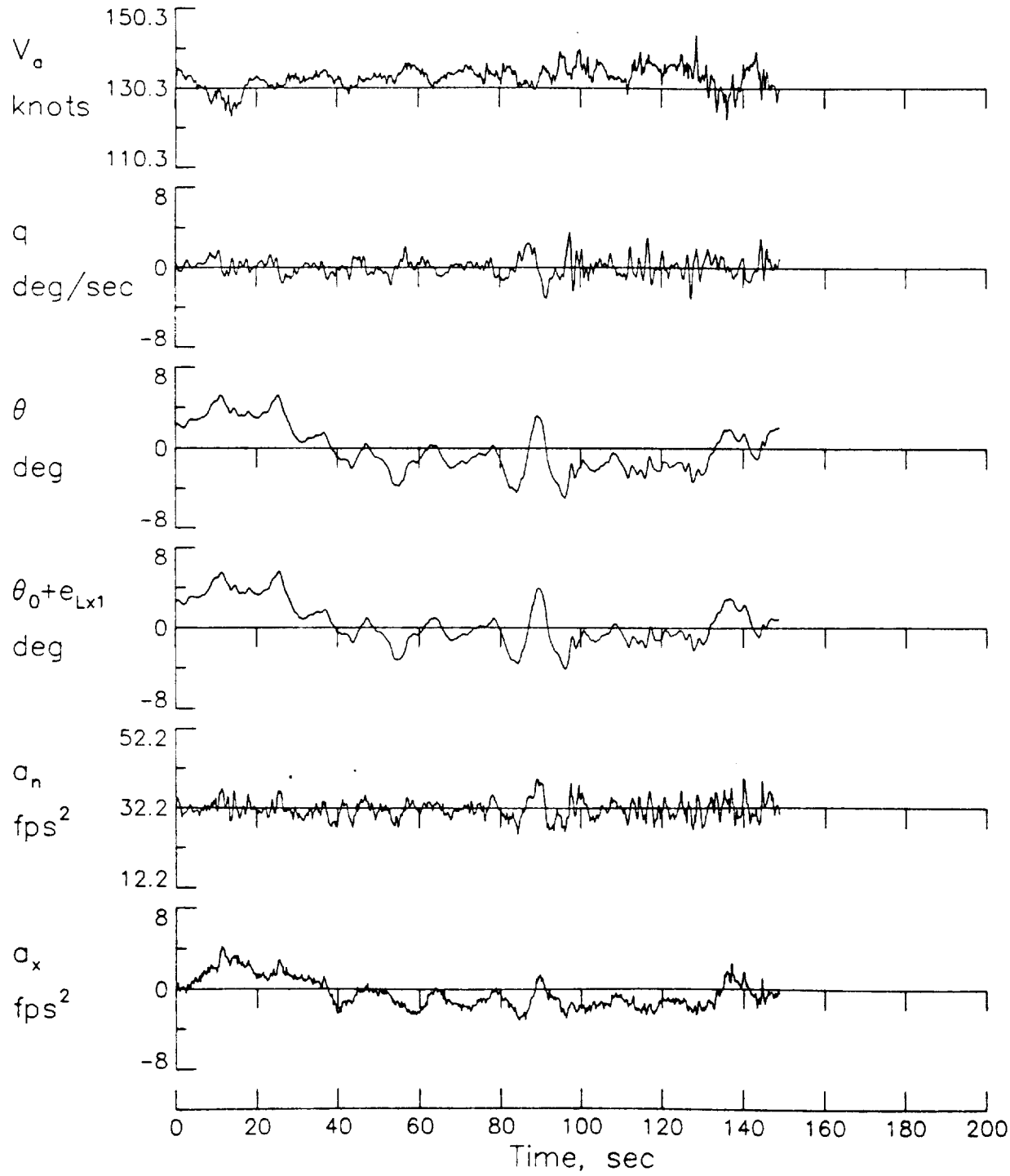

(a) Measurement Variables

Figure 8. 3^{o} Glideslope Capture, Track, and Flare

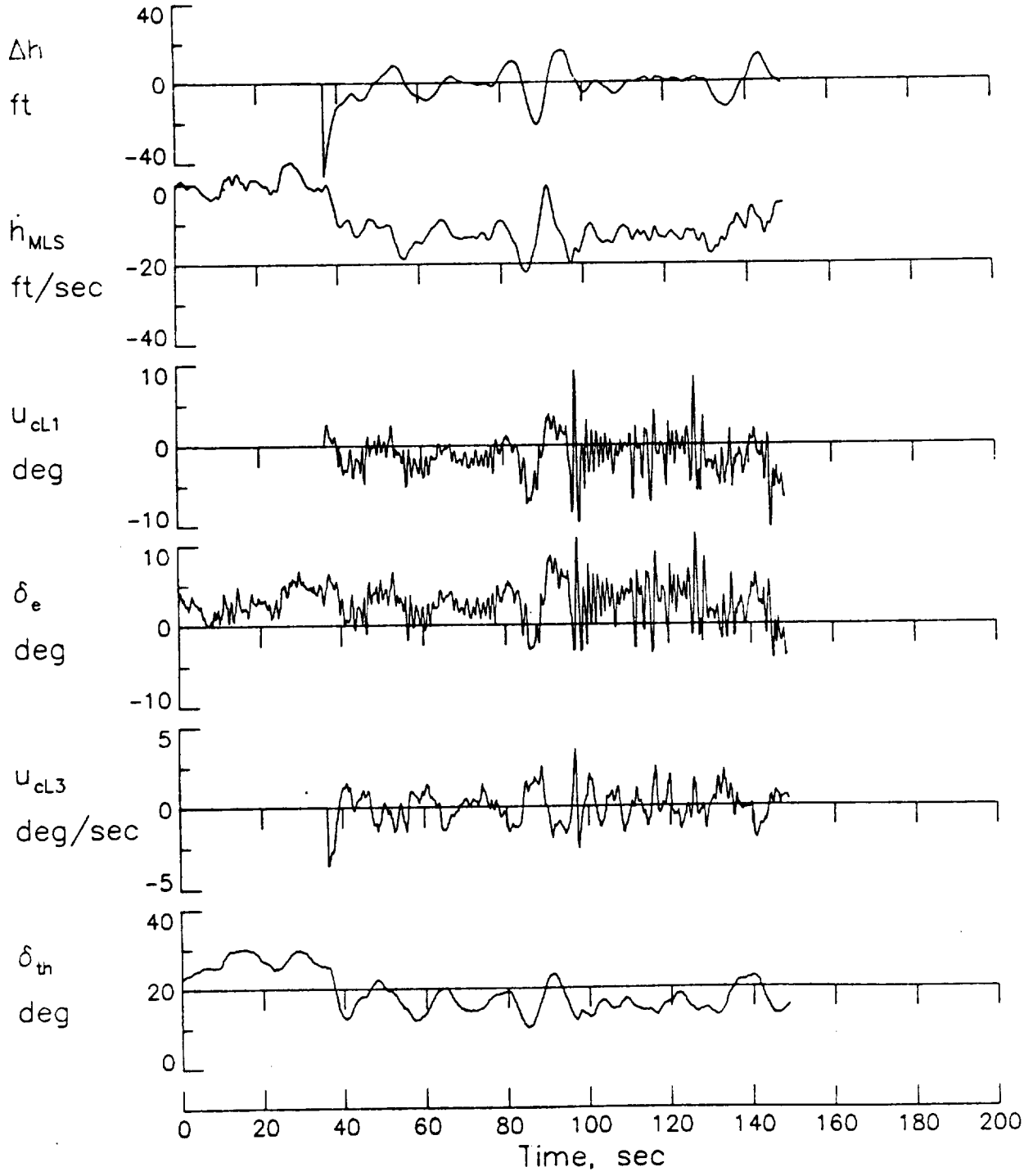

(b) Path and Control Variables

Figure 8. Concluded

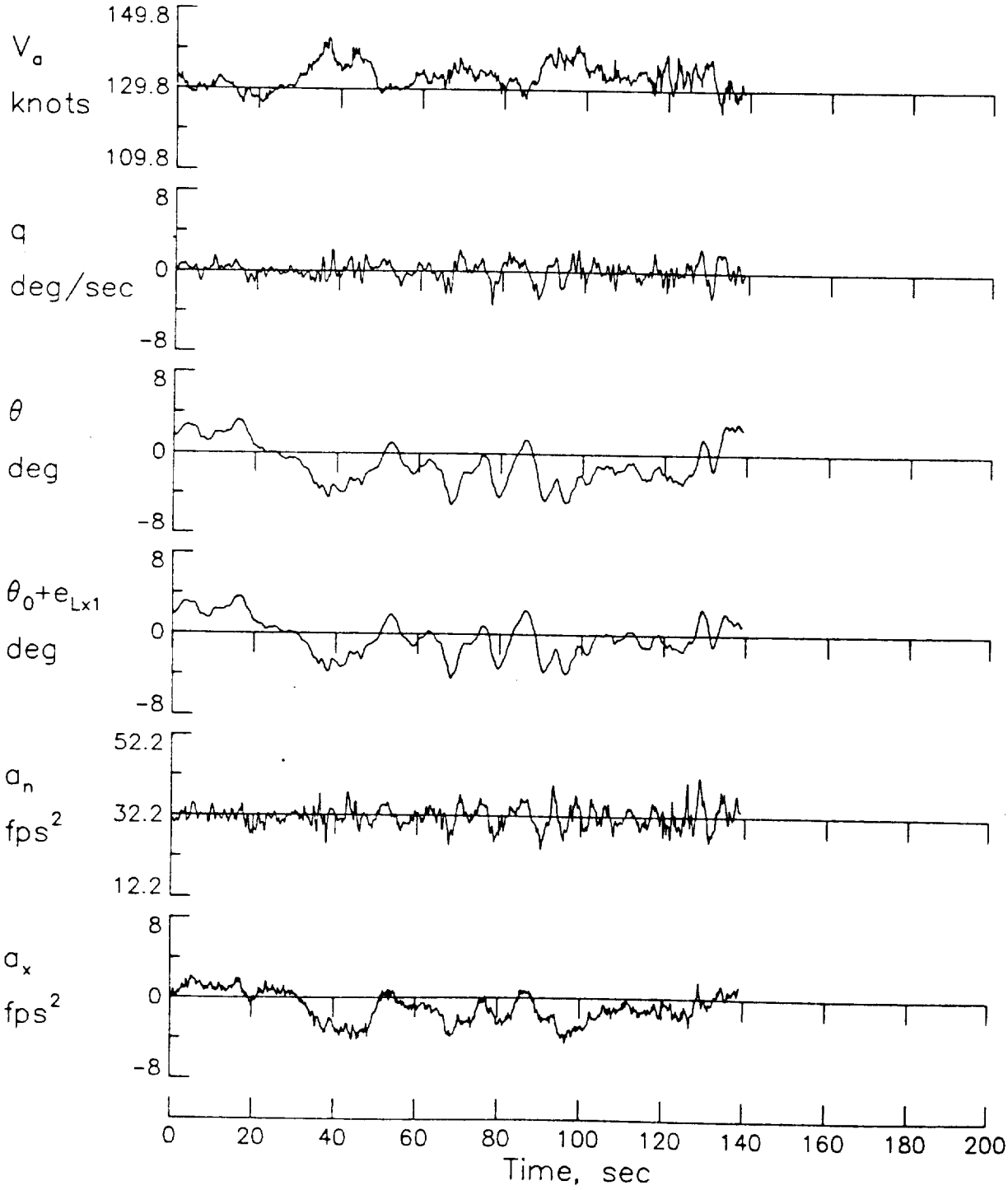

(a) Measurement Variables

Figure 9. 4^{o} Glideslope Capture, Track, and Flare

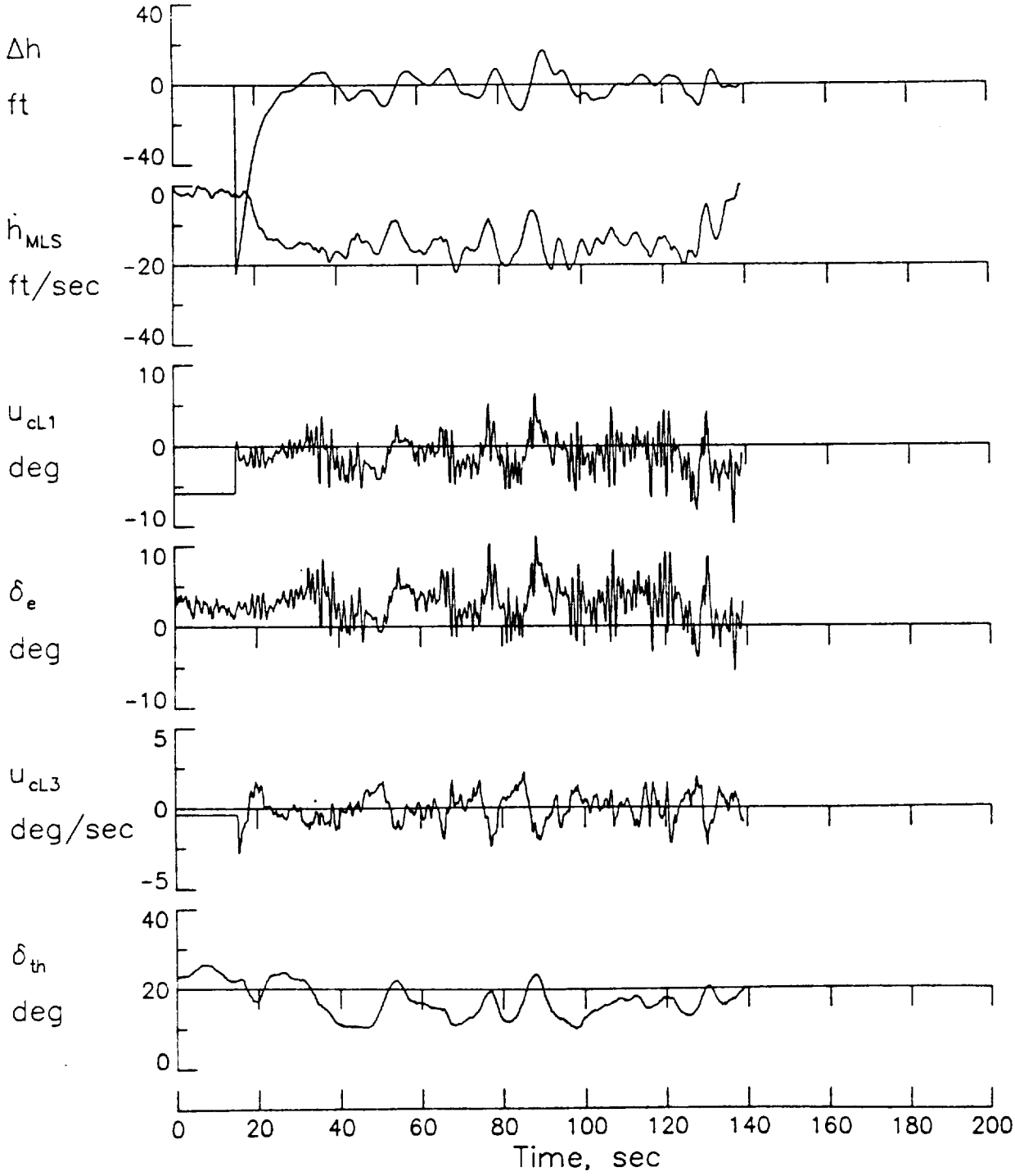

(b) Path and Control Variables

Figure 9. Concluded

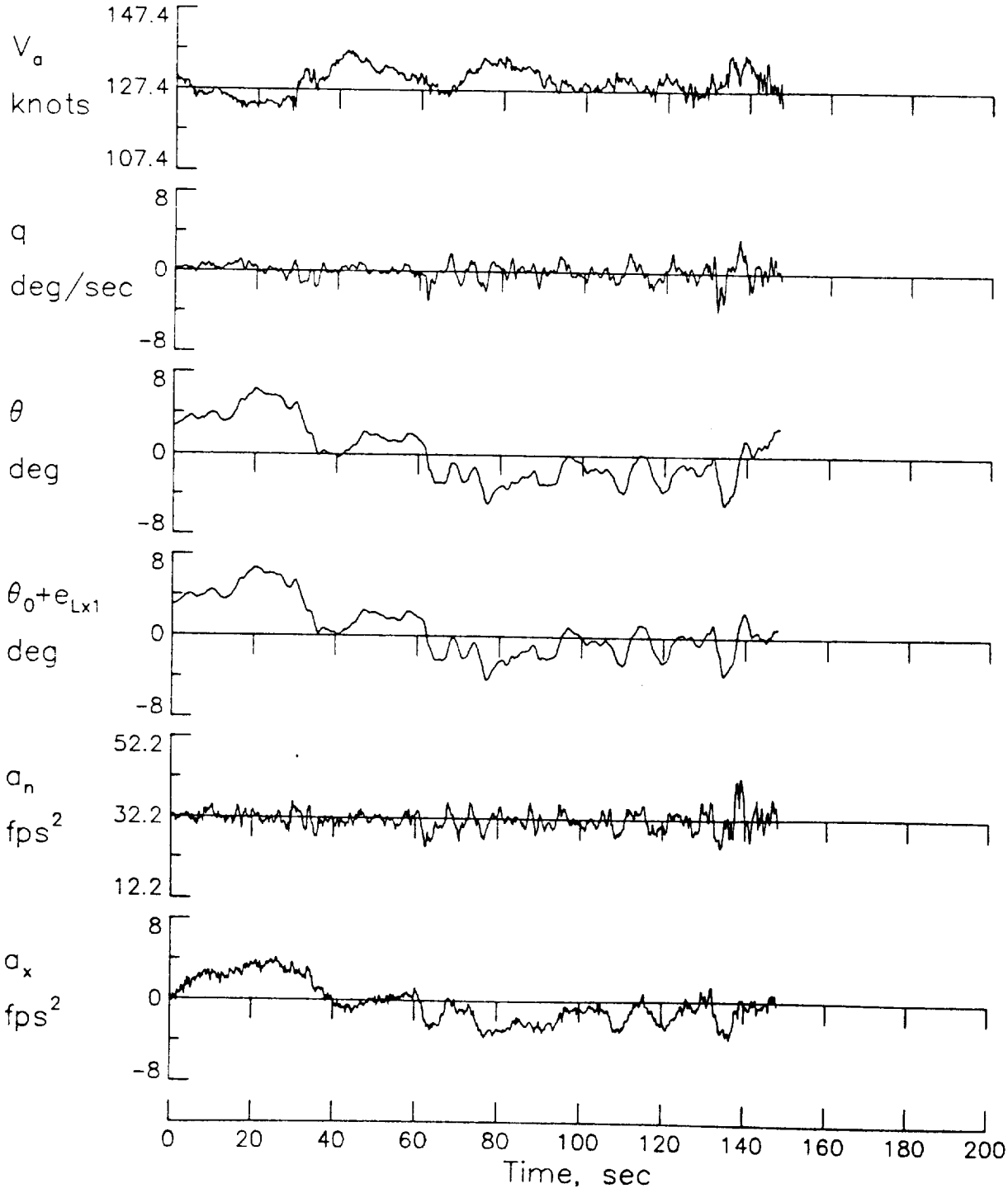

(a) Measurement Variables

Figure 10. 4.5^{o} Glideslope Capture, Track, and Flare

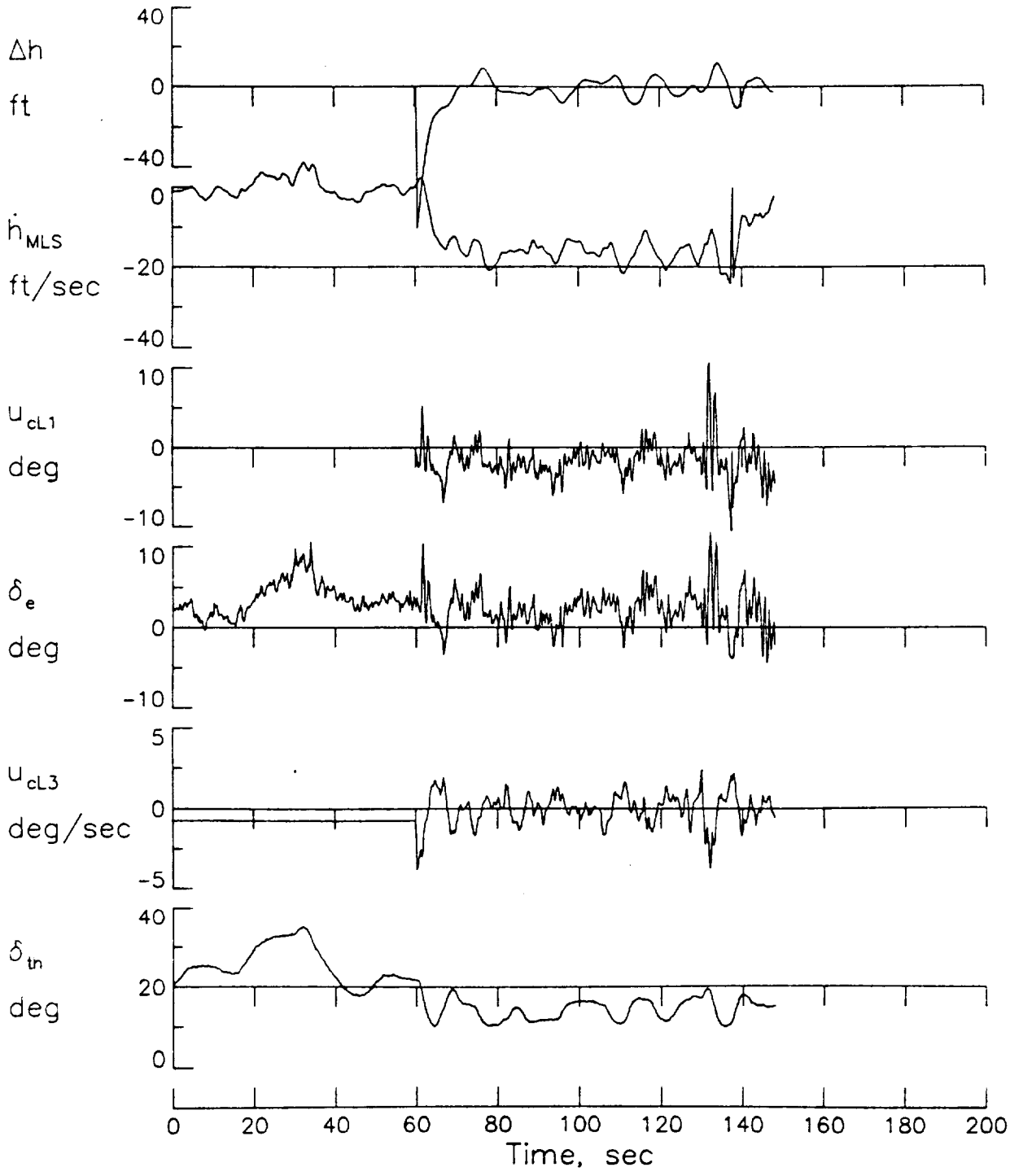

(b) Path and Control Variables

Figure 10. Concluded

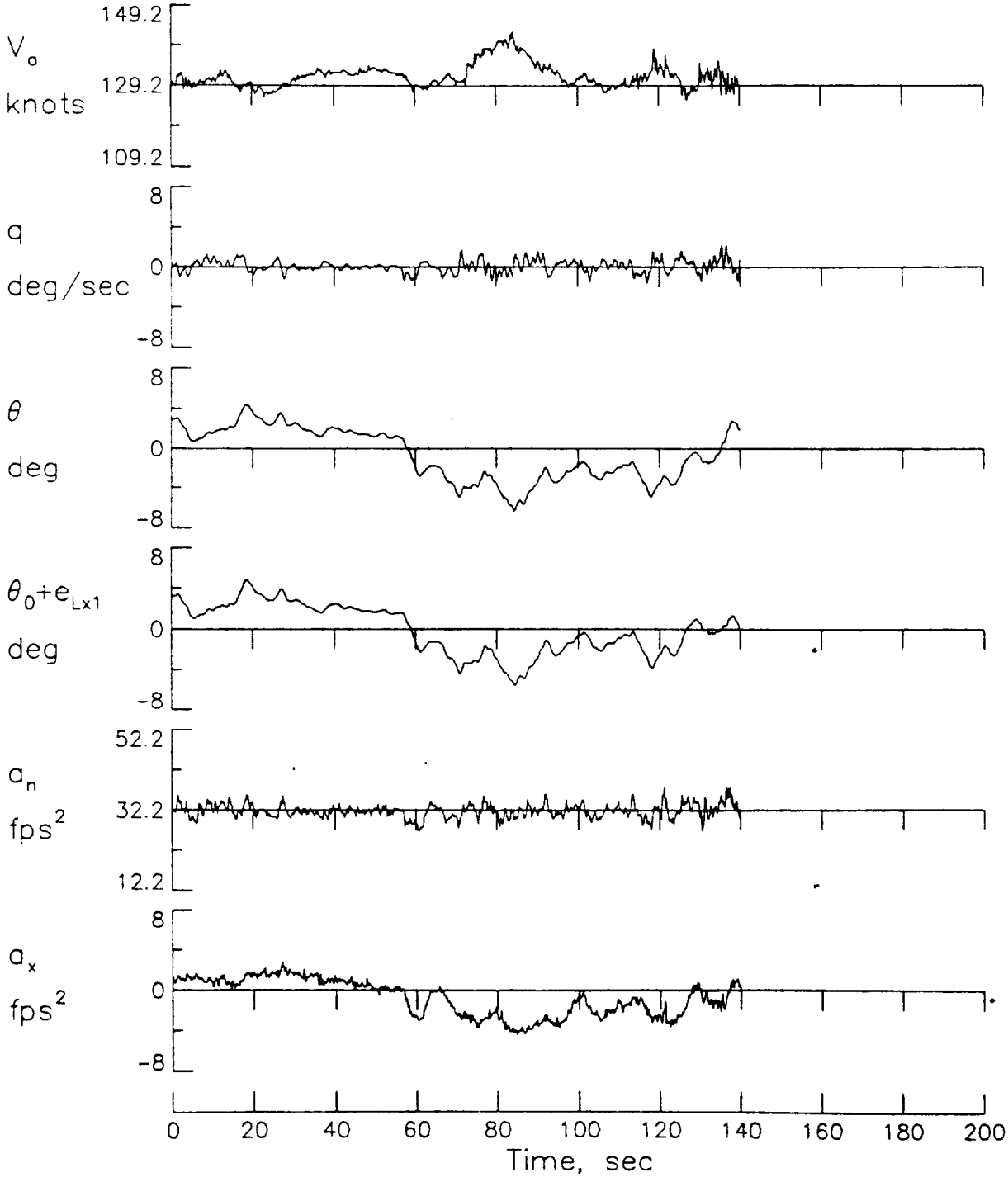

(a) Measurement Variables

Figure 11. 5^o Glideslope Capture, Track, and Flare

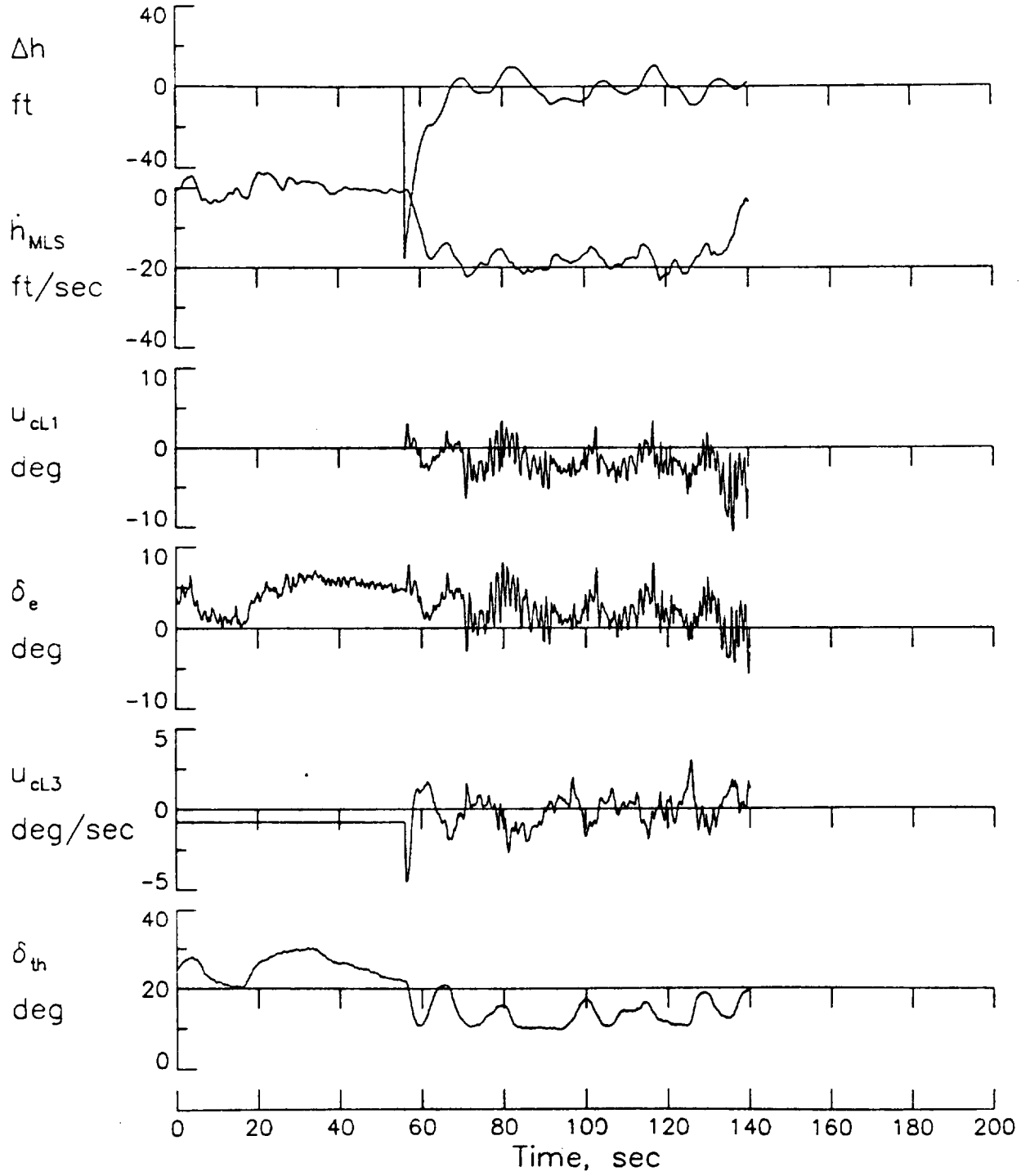

(b) Path and Control Variables

Figure 11. Continued

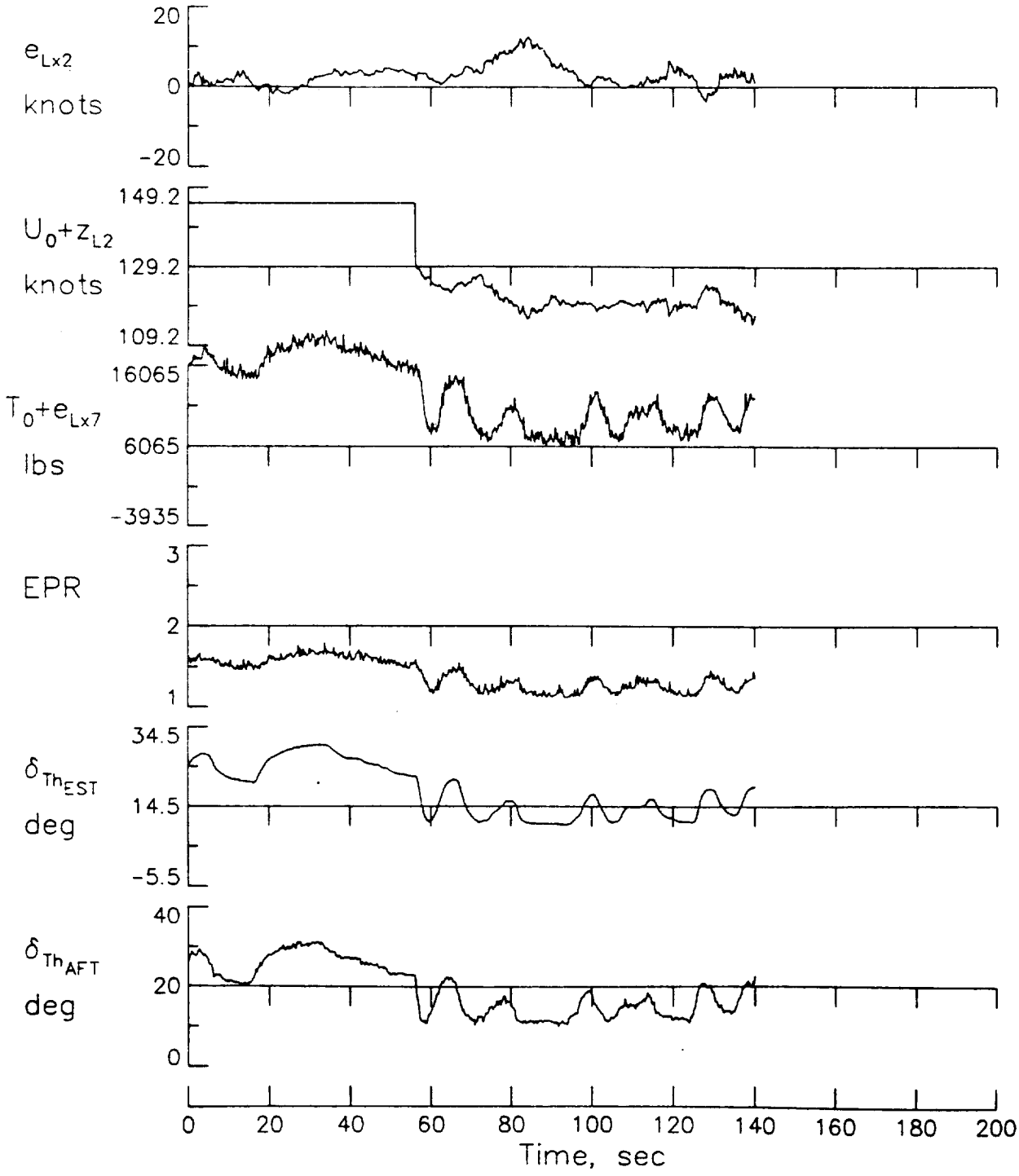

(c) Thrust and Throttle Variables

Figure 11. Concluded

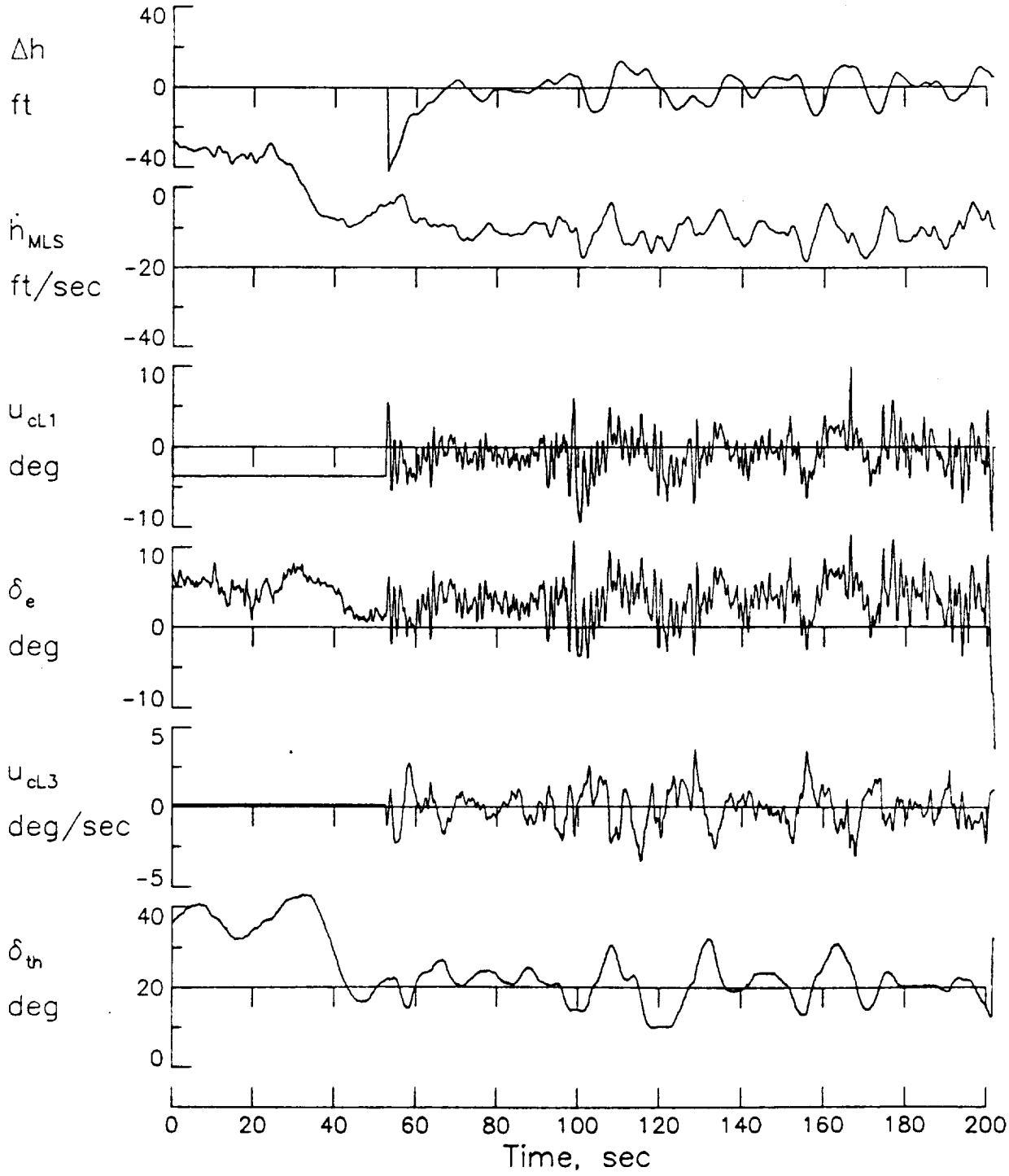

Figure 12. 3^{o} Glideslope Capture for Aircraft Descending at Capture

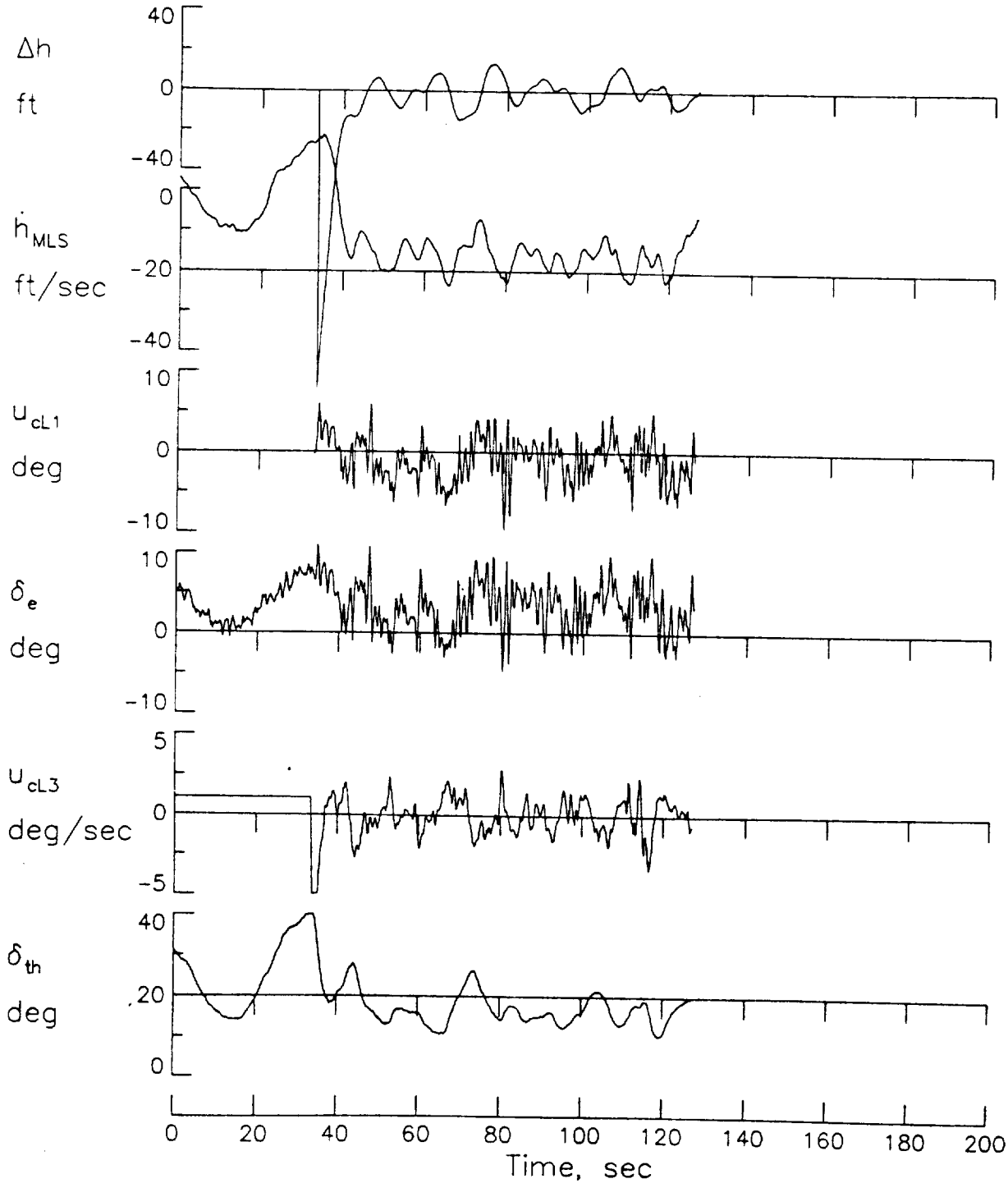

Figure 13. 4.5° Glideslope Capture for Aircraft Climbing at Capture

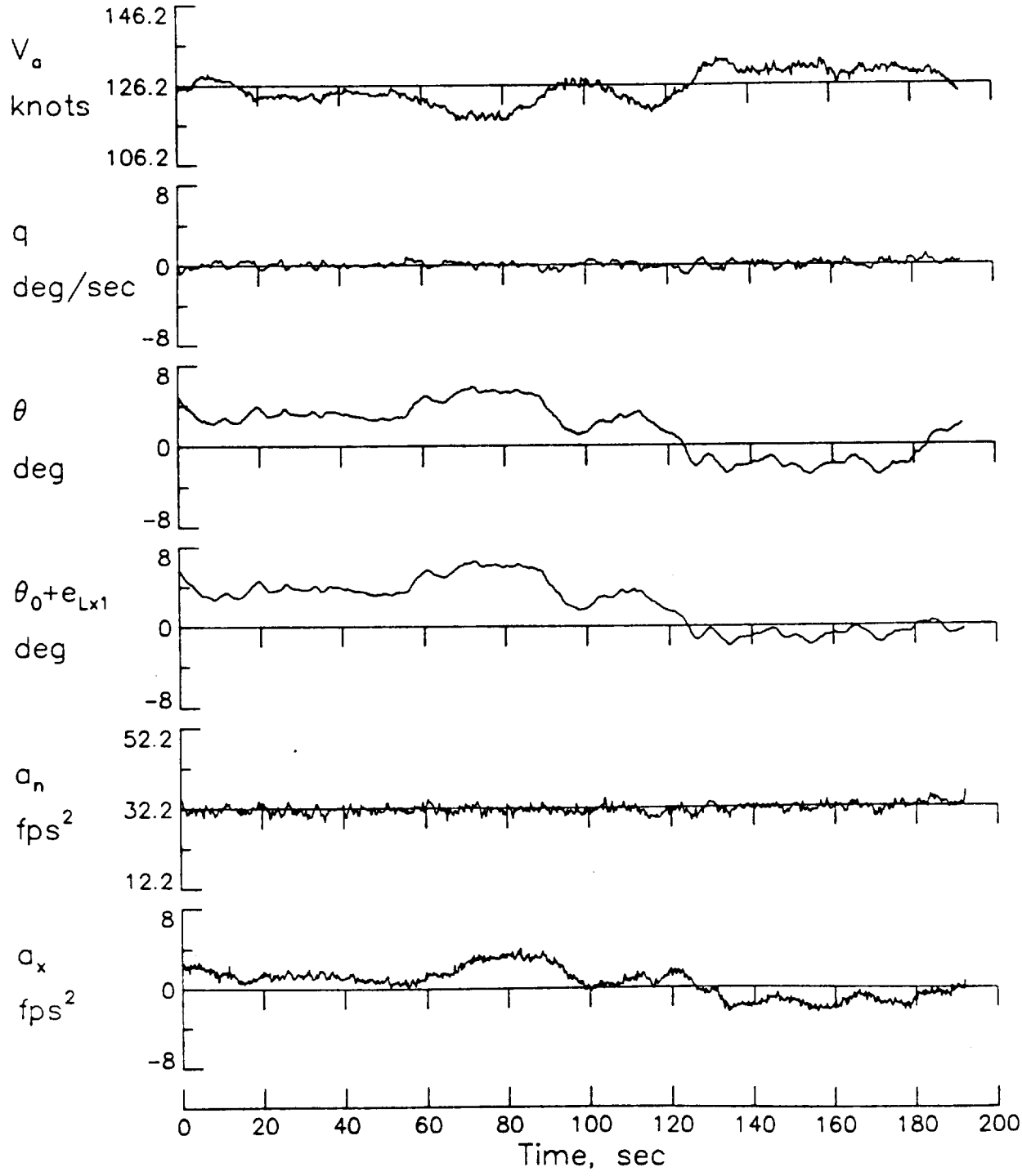

(a) Measurement Variables

Figure 14. 4.5° Glideslope Capture, Track, & Flare for Mild Winds

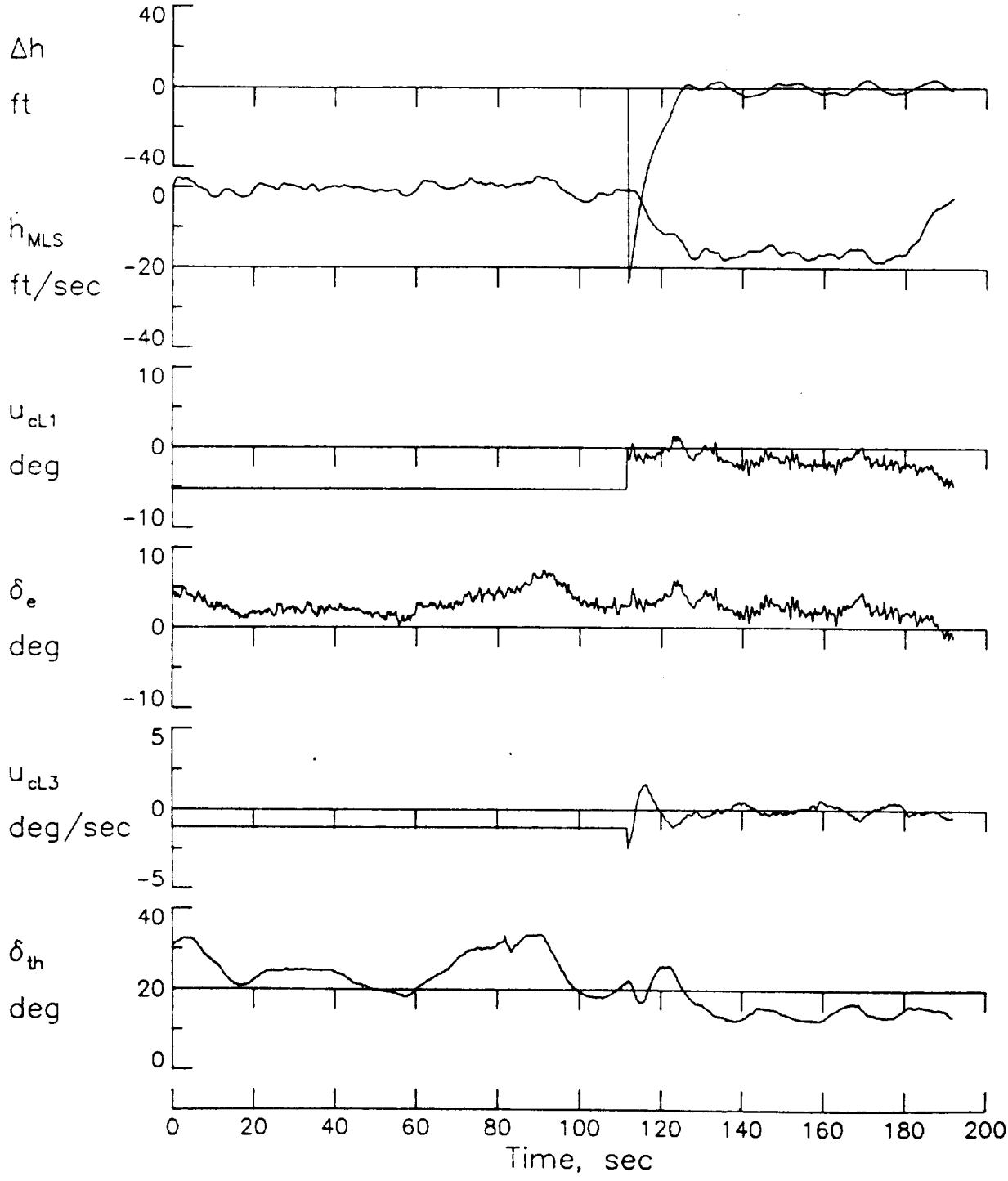

(b) Path and Control Variables

Figure 14. Continued

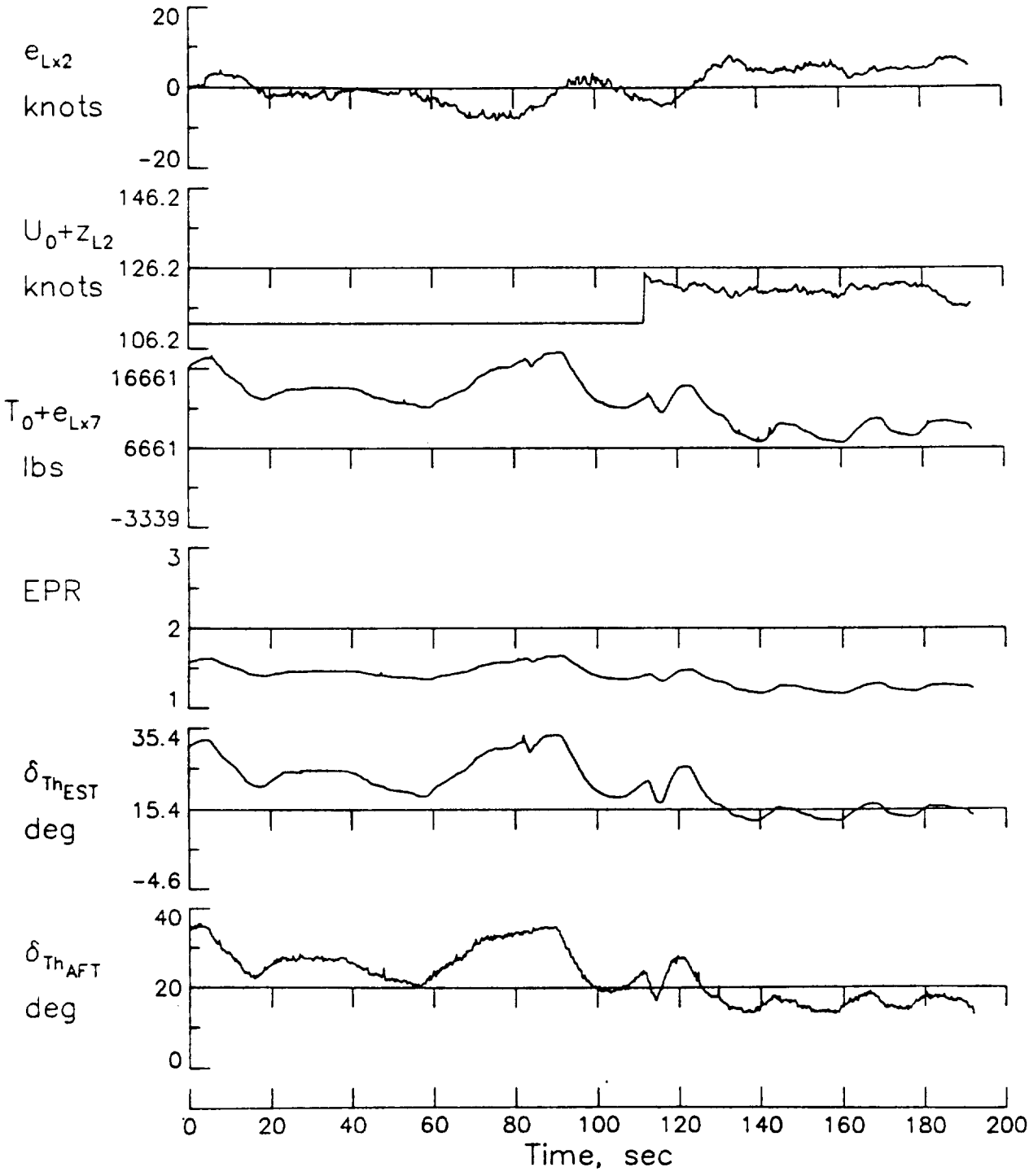

(c) Thrust and Throttle Variables

Figure 14. Concluded

1. Report No.	2. Government Accession No.	3. Recipient's Catalog No.
NASA TM-87632, Part 1		

4. Title and Subtitle	5. Report Date
Implementation and Flight Tests for the Digital Integrated Automatic Landing System (DIALS), Part 1--Flight Software Equations, Flight Test Description, and Selected Flight Test Data	July 1986
	6. Performing Organization Code: *505-66-41-04*
7. Author(s): *Richard M. Hueschen*	8. Performing Organization Report No.
9. Performing Organization Name and Address: *NASA/Langley Research Center, Hampton, VA 23665* N87-10491	10. Work Unit No.
	11. Contract or Grant No.
12. Sponsoring Agency Name and Address: *National Aeronautics and Space Administration, Washington, DC 20546*	13. Type of Report and Period Covered: *Technical Memorandum*
	14. Sponsoring Agency Code

15. Supplementary Notes

Mrs. Jessie Yeager of PRC-Kentron provided programming support.

16. Abstract

Five flight tests of the Digital Automated Landing System (DIALS) were conducted on the Advanced Transport Operating Systems (ATOPS) Transportation Research Vehicle (TSRV)--a modified Boeing 737 Aircraft for advanced controls and displays research. These flight tests were conducted at NASA's Wallops Flight Center using the Microwave Landing System (MLS) installation on Runway 22. This report describes the flight software equations of the DIALS which was designed using Modern Control Theory direct-digital design methods and employed a constant gain Kalman Filter. Selected flight test performance data is presented for localizer (runway centerline) capture and track at various intercept angles, for glideslope capture and track of 3, 4.5, and 5 degree glideslopes, for the decrab maneuver, and for the flare maneuver. Data is also presented to illustrate the system performance in the presence of cross, gust, and shear winds. The mean and standard deviation of the peak position errors for localizer capture were, respectively, 24 feet and 26 feet. For mild wind conditions, glideslope and localizer tracking position errors did not exceed, respectively, 5 and 20 feet. For gusty wind conditions (8 to 10 knots), these errors were, respectively, 10 and 30 feet. Ten "hands off" automatic landings were performed. The standard deviation of the touchdown position and velocity errors from the mean values were, respectively, 244 feet and 0.7 feet/sec.

17. Key Words (Suggested by Author(s))	18. Distribution Statement
Automatic Flight Controls *Digital Controls* *Autoland Systems* *Aircraft Flight Tests*	*Unclassified - Unlimited* Subject Category 08

19. Security Classif. (of this report)	20. Security Classif. (of this page)	21. No. of Pages	22. Price
Unclassified	*Unclassified*	134	A07

N-305

For sale by the National Technical Information Service, Springfield, Virginia 22161